MASSACHUSETTS INSTITUTE OF TECHNOLOGY

A COMPARISON OF WASHOUT FILTERS USING A HUMAN DYNAMIC ORIENTATION MODEL

SUSAN A. RIEDEL

M.S. THESIS SEPTEMBER 1977

(NASA-CR-154581) A COMPARISON OF WASHOUT FILTERS USING A HUMAN DYNAMIC ORIENTATION MODEL M.S. Thesis (Massachusetts Inst. of Tech.) 146 p HC A07/MF A01 CSCL 05E N78-11713
G3/54 Unclas 52826

MAN-VEHICLE LABORATORY
DEPARTMENT OF AERONAUTICS AND ASTRONAUTICS
CENTER FOR SPACE RESEARCH
MASSACHUSETTS INSTITUTE OF TECHNOLOGY
CAMBRIDGE, MASSACHUSETTS 02139

A COMPARISON OF WASHOUT FILTERS USING A HUMAN DYNAMIC ORIENTATION MODEL

by

Susan A. Riedel

B.S., Massachusetts Institute of Technology

(1976)

SUBMITTED IN PARTIAL FULFILLMENT

OF THE REQUIREMENTS FOR THE

DEGREE OF MASTER OF SCIENCE

at the

MASSACHUSETTS INSTITUTE OF TECHNOLOGY

September, 1977

Signature of Author Susan A. Riedel

Department of Aeronautics and Astronautics
August 24, 1977

Certified by

Thesis Supervisor

Accepted by

Chairman, Departmental Graduate Committee

A COMPARISON OF WASHOUT FILTERS USING A HUMAN DYNAMIC ORIENTATION MODEL

by

Susan A. Riedel

Submitted to the Department of Aeronautics and Astronautics on August 24, 1977, in partial fulfillment of the requirements for the degree of Master of Science.

ABSTRACT

The Ormsby model of human dynamic orientation, a discrete time computer program, has been used to provide a vestibular explanation for observed differences between two washout schemes. These washout schemes, a linear washout and a nonlinear washout, were subjectively evaluated by Parrish and Martin. They found that the linear washout presented false rate cues, causing pilots to rate the simulation fidelity of the linear scheme much lower than the nonlinear scheme. By inputting the motion histories from the Parrish and Martin study into the Ormsby model, it was shown that the linear filter causes discontinuities in the pilot's perceived angular velocity, resulting in the sensation of an anomalous rate cue. This phenomenon does not occur with the use of the nonlinear filter.

In addition, the suitability of the Ormsby model as a simulator design tool was investigated. It was found to be a useful tool in predicting behavior of simulator motion bases, even when the mechanical motion base is replaced by a computer simulation. Further investigation of the model could provide simulation designers with a tool to predict the behavior of motion bases still in the drawing board stage.

ORIGINAL PAGE IS
OF POOR QUALITY

Thesis Supervisor: Dr. Laurence R. Young
Professor of Aeronautics
and Astronautics

ACKNOWLEDGEMENTS

I wish to express my heartfelt thanks to Professor Laurence R. Young, whose guidance and teaching were a constant source of encouragement throughout this work.

I would also like to thank Russell Parrish and Dennis Martin, Jr., whose preliminary work on the washout schemes at Langley set the stage for this thesis.

This work would not have been possible without Dr. Charles Ormsby, the person responsible for the physiological model used for the analysis of the washout schemes.

Additional thanks go to Josh Borah, whose documentation of the Ormsby model is the basis for the appendix to this thesis; to Ginny Spears at Lincoln Laboratory and Mike Hutchins at Draper Laboratory who provided invaluable assistance in preparing the data for use on the Man-Vehicle Laboratory computer; and to my friends who read and commented on the manuscript at various stages of completion.

Finally, I would like to dedicate this thesis to my family. The loving and supportive environment which they provided allowed me to come this far, and to know I can go further.

This thesis was supported by NASA grants NGR 22-009-701 and NSG 1416.

TABLE OF CONTENTS

CHAPTER NUMBER			PAGE
I		Introduction	14
	1.1	The Physiology of Motion Simulation	16
	1.2	The Use of Washout and Visual Cues in Simulation	17
	1.3	Thesis Objectives and Organization	18
II		The Washout Filters	20
	2.1	The Linear Washout	21
	2.2	The Nonlinear Washout	26
	2.3	A Comparison of Washout Schemes	28
	2.4	Empirical Comparison of Washout Filters	33
III		The Physiological Model	44
	3.1	The Human Vestibular System	45
	3.2	The Ormsby Model	51
IV		Data and Results	63
	4.1	Data Description	63
	4.2	Aileron Roll Cues	68
	4.3	Aileron Yaw Cues	73
	4.4	Rudder Roll Cues	77
	4.5	Rudder Yaw Cues	81
	4.6	Results	85

V	Conclusions	89
5.1	The Vestibular Explanation Question	90
5.2	The Suitability as a Design Tool Question	94
5.3	Suggestions for Further Research	98
APPENDIX		100
A.1	Human Dynamic Orientation Model	100
A.2	Subroutine STIM	113
A.3	Subroutine DOWN	118
A.4	Subroutine Library	123
A.5	Kalman Gains Subroutines	133
A.6	Kalman Gains Subroutine Library	138
REFERENCES		142

TABLE OF FIGURES

FIGURE NUMBER		PAGE
2.1	Block diagram for Schmidt and Conrad washout scheme.	23
2.2	Block diagram for Langley linear washout scheme.	25
2.3	Block diagram for Langley nonlinear washout scheme.	27
2.4	Design concept for digital controller.	29
2.5	Amplitude and phase plots fot three types of washout filters.	31
2.6	First-order linear and nonlinear adaptive washout response to a pulse input.	32
2.7	Time histories for throttle inputs.	35
2.8	Time histories for column inputs.	37
2.9	Time histories of roll cues for aileron inputs.	38
2.10	Time histories of yaw cues for aileron inputs.	40
2.11	Time histories of roll cues for rudder inputs.	41
2.12	Time histories of yaw cues for rudder inputs.	42

3.1	Horizontal semicircular canal.	46
3.2	Orientation of semicircular canals.	47
3.3	Cross section of otolith.	49
3.4	Orientation of otoliths.	50
3.5	Afferent model of semicircular canals.	52
3.6	Afferent model of otolith system.	53
3.7	DOWN estimator.	57
3.8	Angular velocity estimator.	59
3.9	Overview of Ormsby model.	61
4.1	Commanded inputs to simulation.	66
4.2	Perceived angular velocity for simulated linear aileron roll cue input.	69
4.3	Perceived angular velocity for simulated nonlinear aileron roll cue input.	70
4.4	Perceived angular velocity for commanded aileron roll cue input.	71
4.5	Perceived angular velocity for simulated linear aileron yaw cue input.	74
4.6	Perceived angular velocity for simulated nonlinear aileron yaw cue input.	75
4.7	Perceived angular velocity for commanded aileron yaw cue input.	76
4.8	Perceived angular velocity for simulated linear rudder roll cue input.	78

4.9	Perceived angular velocity for simulated nonlinear rudder roll cue input.	79
4.10	Perceived angular velocity for commanded rudder roll cue input.	80
4.11	Perceived angular velocity for simulated linear rudder yaw cue input.	82
4.12	Perceived angular velocity for simulated nonlinear rudder yaw cue input.	83
4.13	Perceived angular velocity for commanded rudder yaw cue input.	84
5.1	Perceived angular velocity for three aileron yaw cue inputs.	91
5.2	Perceived angular velocity for three rudder yaw cue inputs.	92
5.3	Perceived angular velocity for three aileron roll cue inputs.	95
5.4	Perceived angular velocity for three rudder roll cue inputs.	96

TABLES

2.1	Pilot evaluation of motion cues for linear and nonlinear washout schemes.	34
4.1	Variables recorded during simulation runs.	64
4.2	Data used as input to Ormsby model.	67
A.1	Variables used in main program.	108
A.2	Variables output from model.	112
A.3	Twelve test cases used in STIM.	115
A.4	Variables used in STIM.	116
A.5	STIM variables and printout variables.	117
A.6	Variables used in DOWN.	121
A.7	Otolith state equations.	130
A.8	Canal state equations.	131
A.9	Variables used in Kalman gains program.	137

LIST OF PARAMETERS

a	translational acceleration
A	acceleration vector
<u>DOWN</u>	perceived vertical vector
f	specific force
F	specific force vector
FR	firing rate
g	gravity vector
G	gravity vector
n	afferent noise
p	roll rate
q	pitch rate
r	yaw rate
R	rotation vector
<u>SF</u>	specific force vector
SFR	spontaneous firing rate
x	longitudinal axis
y	lateral axis
z	vertical axis
δ	change in setting
θ	pitch angle
ϕ	yaw angle
ψ	roll angle
ω	angular velocity

LIST OF SUBSCRIPTS AND SUPERSCRIPTS

a	aircraft
c	centroid coordinate system
d	washed out variable
e	elevator
H	high frequency component
HD	head coordinate system
i	inertial coordinate system
L	low frequency component
oto	otolith
r	rudder
ssc	semicircular canals
T	throttle
tot	total
x	longitudinal axis
y	lateral axis
z	vertical axis

CHAPTER I

INTRODUCTION

For many applications it is often desirable to simulate a particular vehicle motion without using the actual vehicle:

- The Federal Highway Department sponsors many drunk driver studies. In order to insure the safety of the driver, the vehicle and the experimenters, these experiments are often carried out in a moving base simulation of an automobile.
- The U.S. Navy has commissioned studies of the habitability of large high-speed surface-effect-ships. It is necessary to understand to what extent crews will be able to function on these ships even before a prototype is built. This research is carried out on a motion generator, which simulates the expected range of motion of these ships [7].
- The U.S. Air Force makes extensive use of both stationary and moving base aircraft simulators

in pilot training programs. Simulators present no risk to the pilot, and avoid the costs of fuel and repair or possible loss of an aircraft.

The above examples illustrate three of the many possible uses of simulators - to carry out driver-vehicle studies without using an actual vehicle, to predict crew habitability on board a ship not yet built, and to train aircraft pilots without risking the pilot or the plane. As vehicles become increasingly complicated, and costs continue to rise, motion simulation takes on a new importance.

There are many types of cues a person uses to sense motion. The basic inputs are specific force and angular acceleration, which can influence the vestibular system in the inner ear, the tactile sensors at points of contact with the vehicle, and the proprioceptive sensors as muscles are stretched and compressed. In a simulator, it is not always possible to reproduce a particular motion history exactly. Often, some cues can be presented only at the expense of neglecting other cues. The basic goal in motion simulation is to arrive at a compromise in presenting the cues, in order to best represent the desired motion.

1.1 The Physiology of Motion Simulation

Simulation technology now makes heavy use of digital computers to present as much of the motion cue as possible. High speed processing allows the use of very complex linear filters,and recently, of nonlinear adaptive filters. Microprocessor technology has also made much of the slower electrical circuitry obsolete.

But the goal of simulation has not really changed - try to present as many of the specific force and angular acceleration cues as possible, without exceeding the constraints of the simulator [18]. This has always been the most straightforward approach, since it is the specific force and angular acceleration cues which are most readily available.

Once a good understanding of the physiological aspects of motion simulation is attained, a physiological model of the human operator will be a valuable tool in simulator design. The comparison of actual motion and simulated motion using such a model would be useful in determining the realism of the simulation in a quantitative way. This model would also be helpful in comparing two different simulation schemes, providing a quantitative measure of their differences.

1.2 The Use of Washout and Visual Cues in Simulation

Constraints in position, velocity and acceleration of a simulator limit the capability of producing a desired motion exactly. The problem is to present the sensations of a wide range of motion, and to do this in a very limited space. This problem is solved with the use of washout filters in each axis of motion, in order to attenuate the desired motion until it falls within the constraints of the simulator.

An important aspect of motion simulation has not yet been mentioned - the visual cues available to detect motion. Peripheral visual cues seem to be most important in presenting the sensation of motion. The peripheral field may be stimulated by a moving pattern of stripes or dots, or by an actual "out - the - window" cockpit view [2,5].

Taken together, washout filters and visual stimulation perform the function of simulation in which motions seem to go beyond the constraints of the simulator. The motion is duplicated to the point of constraint in a given axis. Then the washout filter takes over and attenuates the motion to meet the constraint. Meanwhile, the visual field is stimulated so as to give the impression of continued motion, motion beyond the capabilities of the simulator. In this way, a wide range of motions can be simulated using a very restricted motion base.

1.3 Thesis Objectives and Organization

It is obvious from the previous discussion that the washout filters in a simulator are critical to the fidelity of the simulation. The research leading to this thesis compares two different types of washout filters currently in use, in order to quantify the differences between them. The means of comparison is a physiological model of human dynamic orientation, based largely on the known physiology of the vestibular system. This work attempts to answer a specific question and a general question:

- Can the observed differences in simulation fidelity between the two filters be explained using a physiological model of human dynamic orientation?
- What are the implications for this model as a drawing board tool in simulator design?

Chapter II presents the two washout filters in detail, and discusses the previous work which led to the research presented in this thesis.

Chapter III describes the human vestibular system and the model of human dynamic orientation developed by Ormsby.

Chapter IV describes the data in this work, as input to the model, and then presents the perceived angular velocities as output from the model.

Finally, Chapter V presents the conclusions which can be drawn from the results presented in Chapter IV, in light of the questions posed in the above section. Also included are suggestions for further research in this area.

CHAPTER II

THE WASHOUT FILTERS

The two washout filters of interest in this comparitive study are the following:

- A linear filter, essentially a Schmidt and Conrad coordinated washout [16,17].
- A nonlinear filter, coordinated adaptive washout.

Basically, the two filters are versions of Schmidt and Conrad's coordinated washout. This scheme uses washout filters in the three translational axes, and only indirectly washes out the angular motion. The primary difference between the linear and nonlinear schemes is in the type of translational washout filters employed. The linear scheme uses second-order classical washout filters in the three axes, while the nonlinear scheme uses coordinated adaptive filters for longitudinal and lateral washout and digital controllers for vertical washout. These schemes differ in their presentation of the rate cues, for a pulse input. The linear scheme presents an anomalous rate cue when the pulse returns to zero. This behavior is not observed with the nonlinear scheme.

The next two sections discuss the filters in greater detail. The final sections present the differences between the filters and the results of a previous subjective analysis of the washout schemes.

2.1 The Linear Washout

The purpose of washout circuitry is to present translational accelerations and rotational rates of the simulated aircraft. It is necessary to obtain coordination between translational and rotational cues in order to accomplish certain motion simulations:

- A sustained horizontal translational cue can be represented by tilting the pilot. The gravity vector is then used to present the cue. But in order to make this process believable, the rotation necessary to obtain the tilt angle must be below the pilot's ability to perceive rotation. The solution is to start the cue with actual translational motion of the simulator until the necessary tilt angle is obtained. In this manner, the pilot will sense only translational motion, long after such motion has actually ceased.
- In a similar sense, it can be seen that a desired roll or pitch cue cannot be represented

by means of rotation alone. This would result in a false translational cue, because the gravity vector is misaligned. In order to present a rotational cue, translational motion must be used at the start, to offset the false translational motion cue induced by the rotation.

The two cases above clearly illustrate the need for coordination in translational and rotational motion. Schmidt and Conrad's coordinated washout scheme fulfills this need. Figure 2.1 presents a block diagram illustrating the basic concepts.

The desired motions of the simulated aircraft are transformed from the center of gravity of the aircraft to the centroid of the motion base. This transformation provides the desired motion at the pilot's seat. The motions of the base are based on the desired motions of the centroid.

Vertical specific force is transformed to vertical acceleration $\ddot{z}_d$ by use of a second-order classical washout filter. The longitudinal and lateral accelerations are also obtained from the longitudinal and lateral specific forces. First, these specific forces are separated into steady-state and transient parts. The steady-state part of the cue is obtained from a tilt angle to align the gravity vector. The transient part of the cue is transformed into the longitudinal acceleration, $\ddot{x}_d$, and the lateral acceleration, $\ddot{y}_d$, by a second-order classical

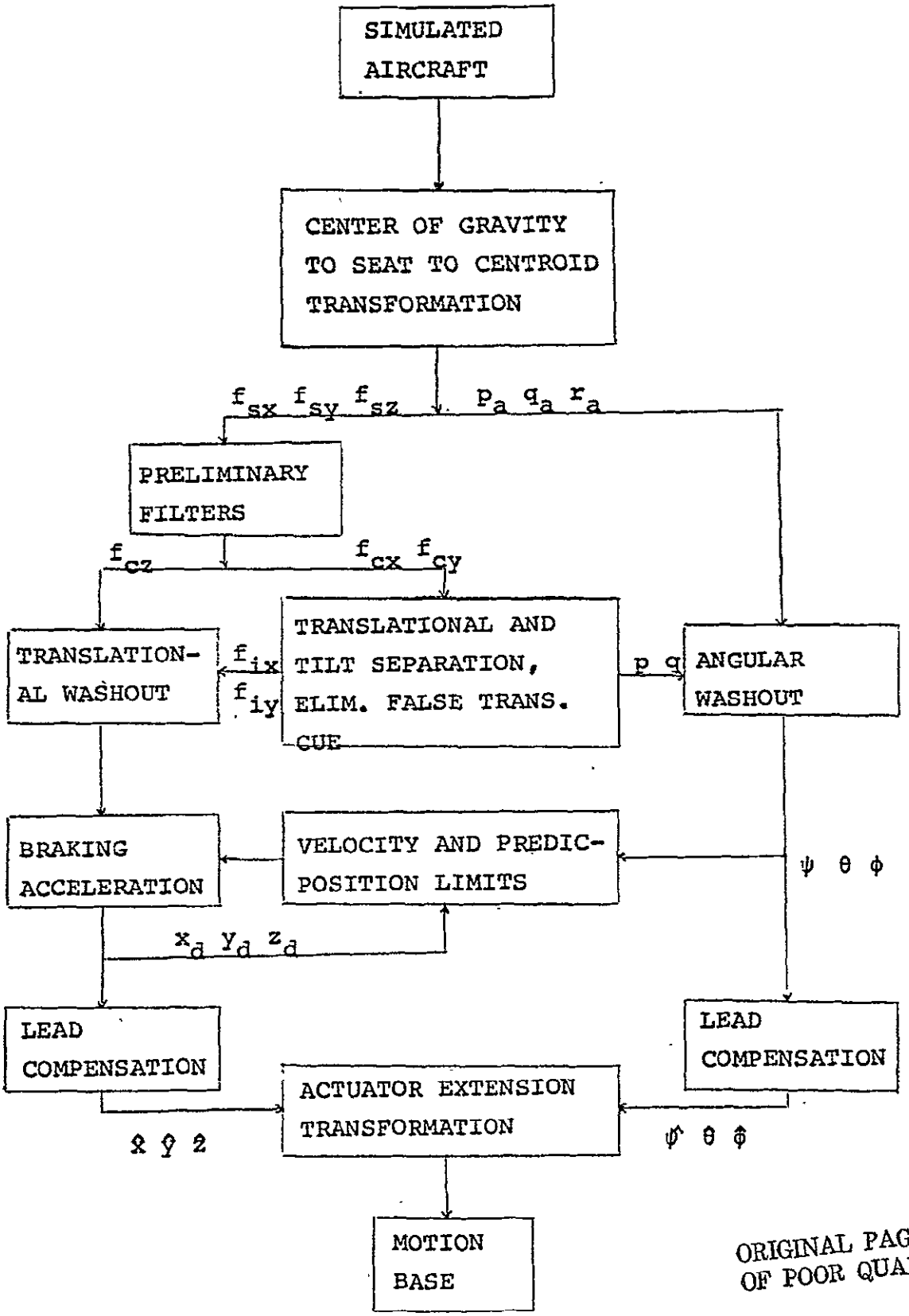

ORIGINAL PAGE IS OF POOR QUALITY

Figure 2.1 Block diagram for Schmidt and Conrad washout scheme [17]

washout filter.

Braking acceleration is then used to keep the motion within the prescribed position, velocity and acceleration limits of the motion base.

The rotational degrees of freedom are only indirectly washed out through elimination of false g cues. Rotational rate cues are represented by angular and translational motion, just as longitudinal or lateral cues. But in this case, the translational motion is used only to eliminate the false g cue induced by rotational movement, and thereby makes no direct contribution to the rotational cue.

After the six position commands $(x_d, y_d, z_d, \psi, \theta, \phi)$ are obtained from the washout circuitry, lead compensation is provided to compensate for servo lag of the base. The actuator extension transformation is then used to obtain the correct actuator lengths used to drive the motion base.

The actual filter evaluated in this work is a Schmidt and Conrad coordinated washout, adapted by Langley Research Center [14]. The major difference is that the Langley washout is carried out in the inertial reference frame, rather than the body axis system. A block diagram of this filter is shown in Figure 2.2.

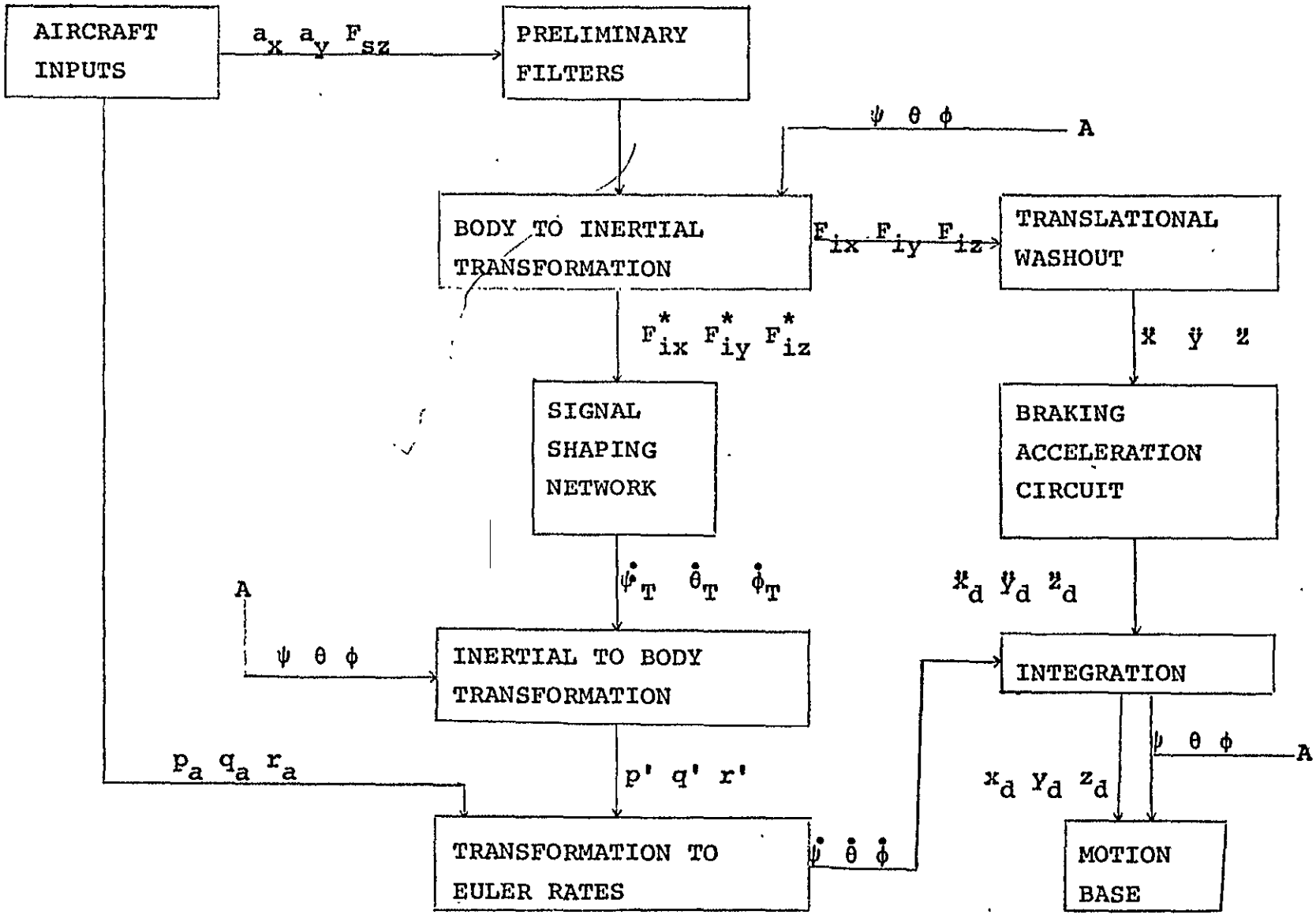

Figure 2.2 Block diagram for Langley linear washout scheme [13]

ORIGINAL PAGE IS OF POOR QUALITY

2.2 The Nonlinear Washout

The nonlinear filter of interest here is again essentially a Schmidt and Conrad coordinated washout. The difference between the nonlinear Langley filter and the Schmidt and Conrad filter are that the Langley filter uses the inertial reference frame rather than the body axis system, and nonlinear filters are used for the washout rather than the linear filters used by Schmidt and Conrad. Hence, the designation "nonlinear washout" is used.

Figure 2.3 presents a block diagram for this nonlinear scheme. It is seen that two different types of nonlinear filters are used - coordinated adaptive filters for longitudinal and lateral cues, and digital controllers for vertical cues. These two types of filters will be discussed in turn.

Coordinated adaptive filters [11] are based on the principle of continuous steepest descent. They are used in this washout scheme to coordinate surge and pitch in presenting the longitudinal cues, and sway and roll in presenting the lateral cues. Derivation of these filters can be found in the literature [11,12]. Basically, they perform the same functions as the second-order classical filters used by Schmidt and Conrad by providing translational specific force cues and rotational rate cues.

Digital controllers, the second type of nonlinear filters, are used to provide the uncoordinated heave and yaw cues. A

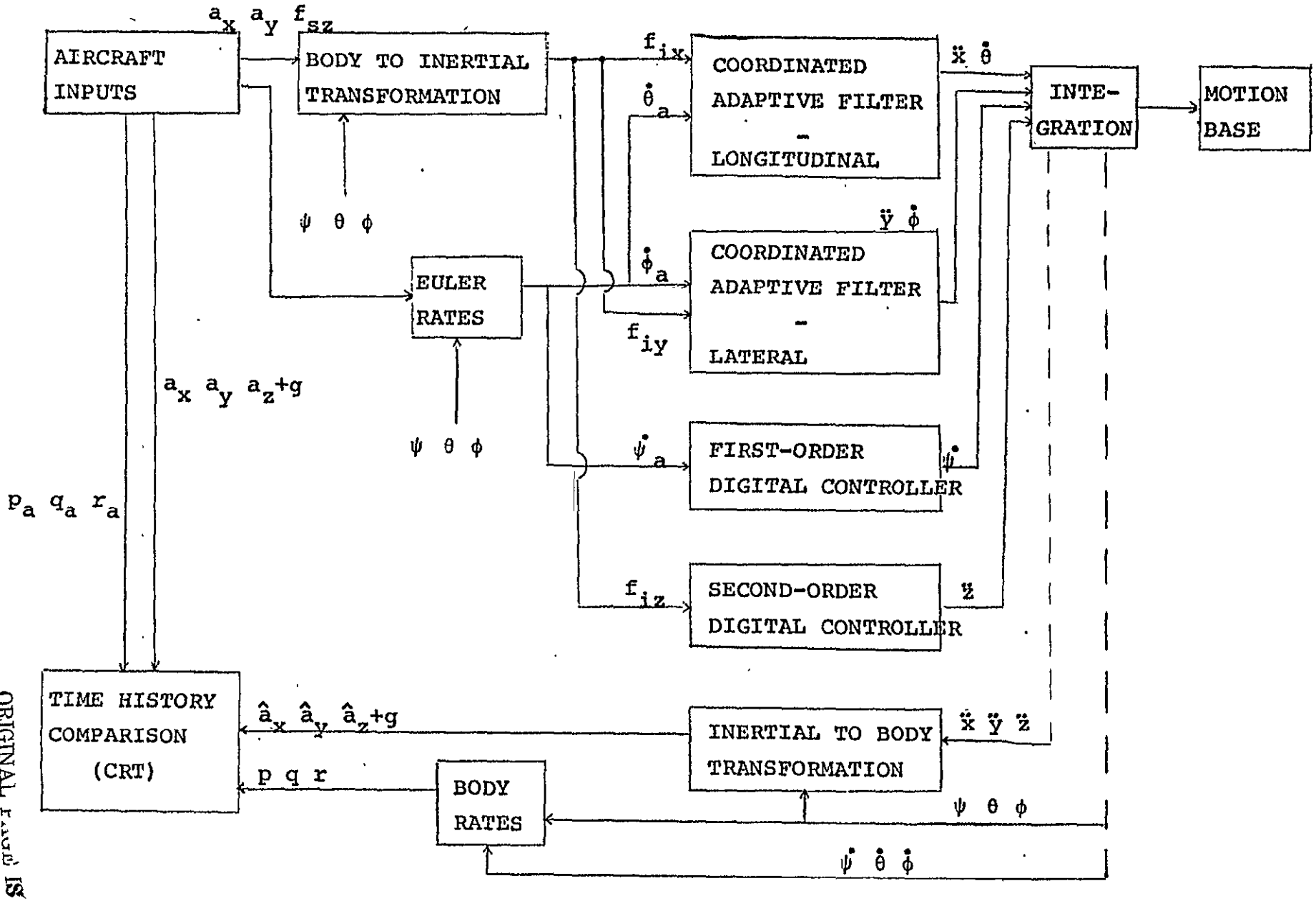

Figure 2.3 Block diagram for Langley nonlinear washout scheme [13]

ORIGINAL PAGE IS OF POOR QUALITY

first-order digital controller provides the yaw rate cue, while a second-order controller provides the vertical specific force cue. These filters are designed to present as much of the onset cue as possible before switching to the washout logic.

Figure 2.4 illustrates the design concept for a first-order digital controller. From 0 to τ_1 the controller presents a scaled version of the commanded input. At τ_1 a linear decay is applied to reduce the command to the motion base constraint value, B. Washout then occurs at the constrained value, unless another input is commanded, as at τ_2.

The second-order digital controller used for the vertical specific force is similar, although mathematically more complex.

2.3 A Comparison of Washout Schemes

Essentially, the two washout schemes of interest are Schmidt and Conrad washouts. The so-called linear washout contains second-order classical washout filters which transform the specific forces in each axis to translational accelerations in each axis. The Langley washout performs these transformations in the inertial frame rather than the body axis frame used by Schmidt and Conrad.

The nonlinear washout scheme uses two types of nonlinear filters to provide the translational acceleration cues. A coordinated adaptive filter is used to coordinate surge and

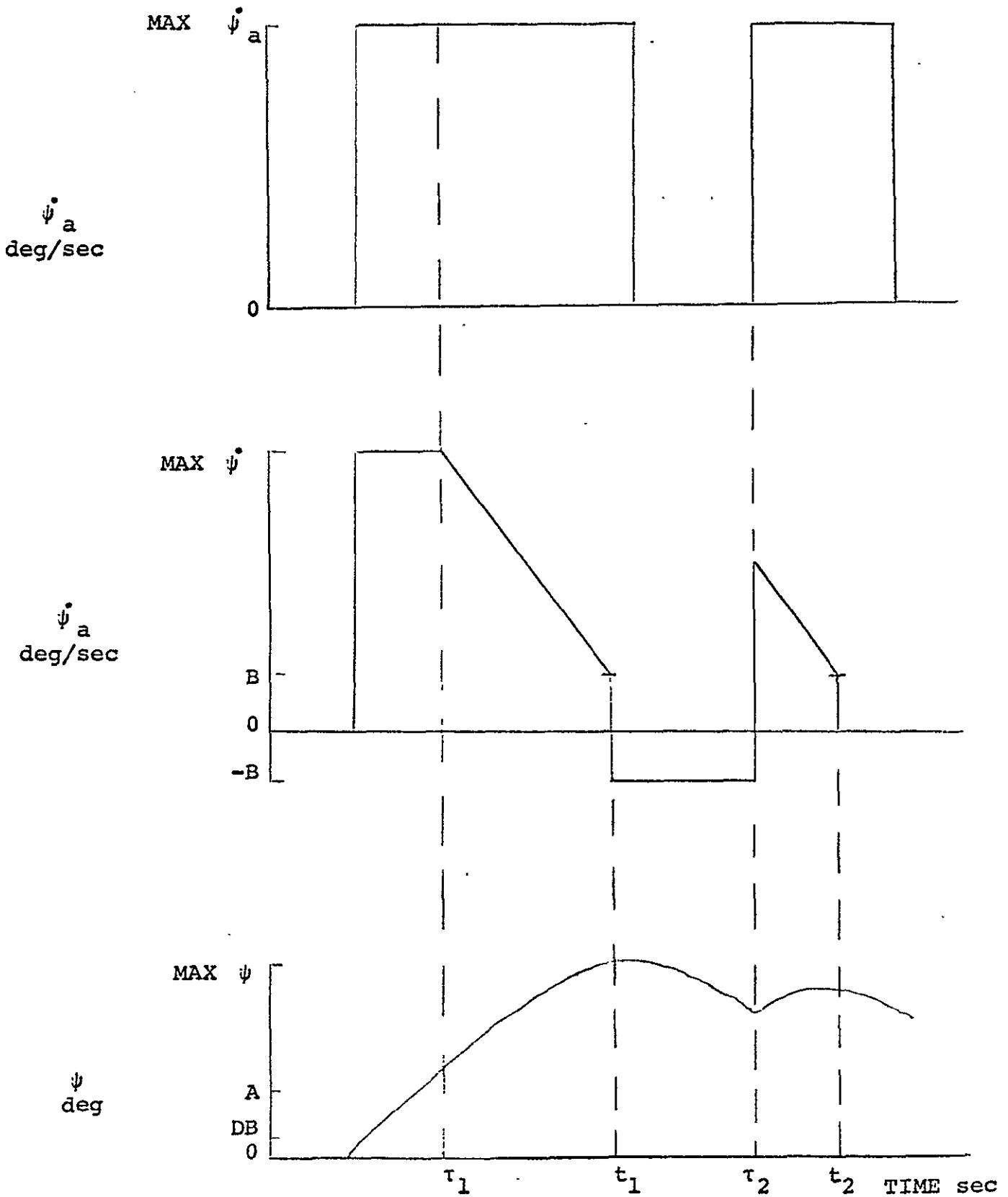

Figure 2.4 Design concept for digital controller [11]

ORIGINAL PAGE IS
OF POOR QUALITY

pitch for longitudinal cues, and sway and roll for lateral cues. A digital controller is used for the uncoordinated heave and yaw motions. Again, the Langley nonlinear scheme washes out in the inertial frame.

In Figure 2.5, amplitude and phase versus frequency is shown for the three types of washout filters - linear, adaptive and digital controller. Both the first-order and second-order cases are shown. The motion base characteristics are the same in all cases. Since the amplitude and phase response of the nonlinear adaptive filter changes with the magnitude of the input, the worst case for the nonlinear filter is presented here. As is shown, the digital controller has the best response characteristics, and the adaptive filter is better than the linear filter. This holds true for both the first- and second-order cases.

In terms of motion cues, there is a fundamental difference between the linear filter and nonlinear filter for the first-order case. Figure 2.6 shows the response of the two filters to a pulse input. The difference between the filters is the anomalous rate cue presented by the linear filter as the pulse input returns to zero. This false cue is most noticeable for pulse-type inputs, and disappears as the input becomes sinusoidal. Since the differences between the linear and nonlinear filters vary with input, performance of a given filter is dependent on pilot input and simulator responsiveness in each axis.

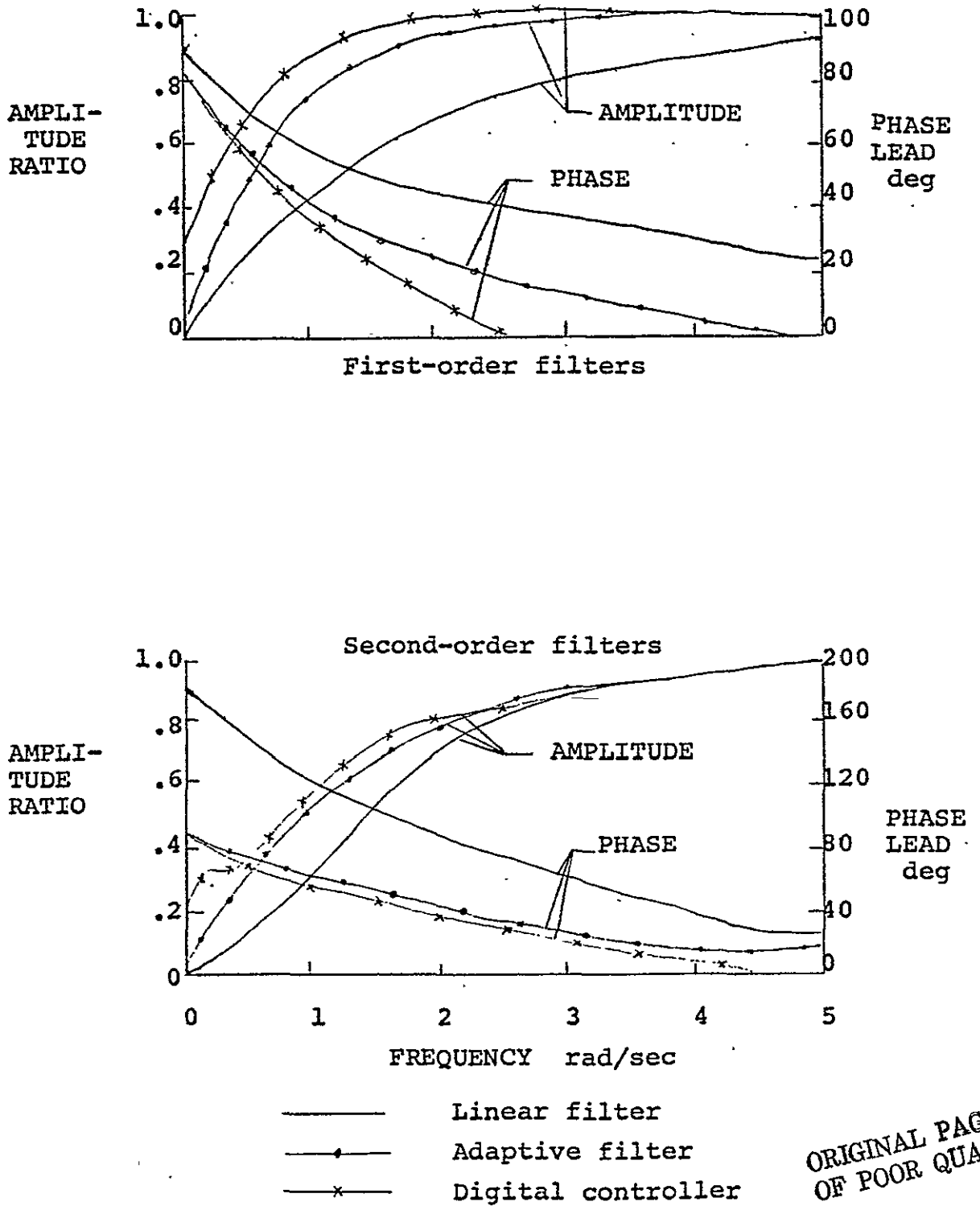

ORIGINAL PAGE IS
OF POOR QUALITY

Figure 2.5 Amplitude and phase plots for three types of filters [1]

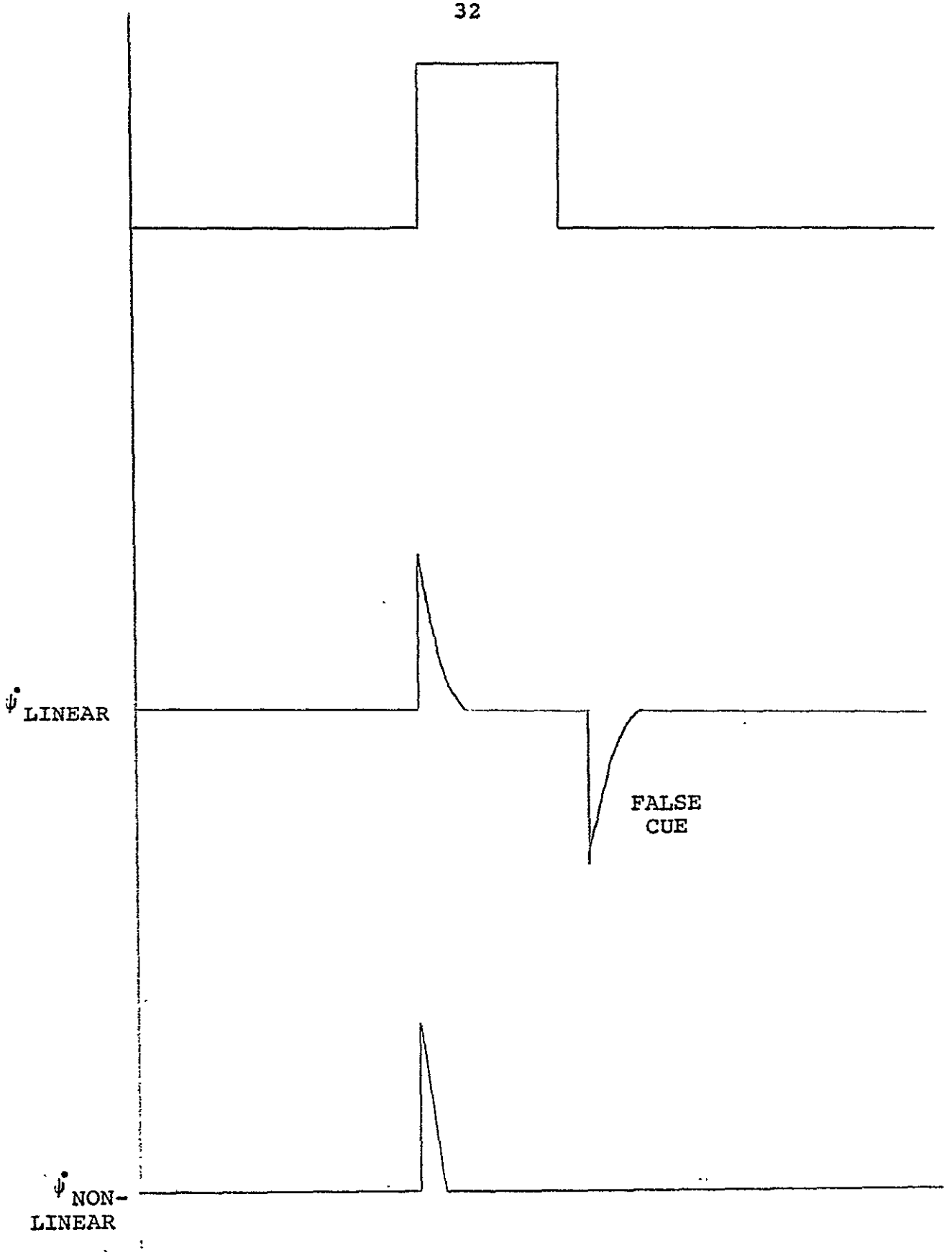

Figure 2.6 First-order linear and nonlinear adaptive response to a pulse input [13]

2.4 Empirical Comparison of Washout Filters

Parrish and Martin, the major investigators of these two washout schemes at Langley, devised a subjective test to determine the differences between the two filters in actual simulation [13]. Seven pilots flew a six-degree-of-freedom simulator equipped with both linear and nonlinear washout schemes. The pilots were asked to rate the motion cues presented by each scheme for throttle, column, wheel and pedal inputs about a straight-and-level condition during a landing approach.

The results of this evaluation process are presented in Table 2.1. Each pilot determined his own criteria for evaluation. In addition to rating the cues for each input, the pilots were asked to rate the overall airplane feel - that is, how successful the overall motion was in representing the actual airplane. In the table, the open symbols represent the rating of the linear method, while the solid symbols represent the rating of the nonlinear method. The washout methods were applied to a 737 CTOL aircraft simulation, and four of the pilots (represented by the triangular symbols) had previous 737 cockpit experience.

The pilot ratings for the throttle input are the same for each method, as shown in Table 2.1. Even given the methods back to back for comparison, the pilots could not detect that a change had been made. Figure 2.7 shows the time histories for such a change in throttle setting. Longitudinal accelera-

RATING / INPUT		EXC.	HALF - WAY	GOOD	HALF - WAY	FAIR	HALF - WAY	POOR	HALF - WAY	UN-ACCEP-TABLE
THROTTLE				▷ △ ▽ □ ⬡ ○		◁				
				▶ ▲ ▼ ■ ⬢ ●		◀				
COLUMN		△	⬡	◁ ▷ ▽	○	□				
		▲	◀ ⬢	▶ ▼ ● ■						
WHEEL AND PEDAL	ROLL	●	▶ ◀ ▲ ▼ ⬢	■	▷	◁ ○		△ ▽ ⬡ □		
	YAW		▼ ●	▶ ◀ ▲ ■ ⬢	○	◁ ▽		▷ △ ⬡ □		
OVERALL AIRPLANE FEEL		●	▶ ◀ ▲	▼ ⬢ ■	○	▷ ◁	⬡	△ ▽ □		

PILOT NO.	LINEAR WASHOUT	NONLINEAR WASHOUT
1	△	▲
2	▽	▼
3	▷	▶
4	◁	◀
5	□	■
6	⬡	⬢
7	○	●

ORIGINAL PAGE IS
OF POOR QUALITY

Table 2.1 Pilot rating of motion cues for two washout filters [13]

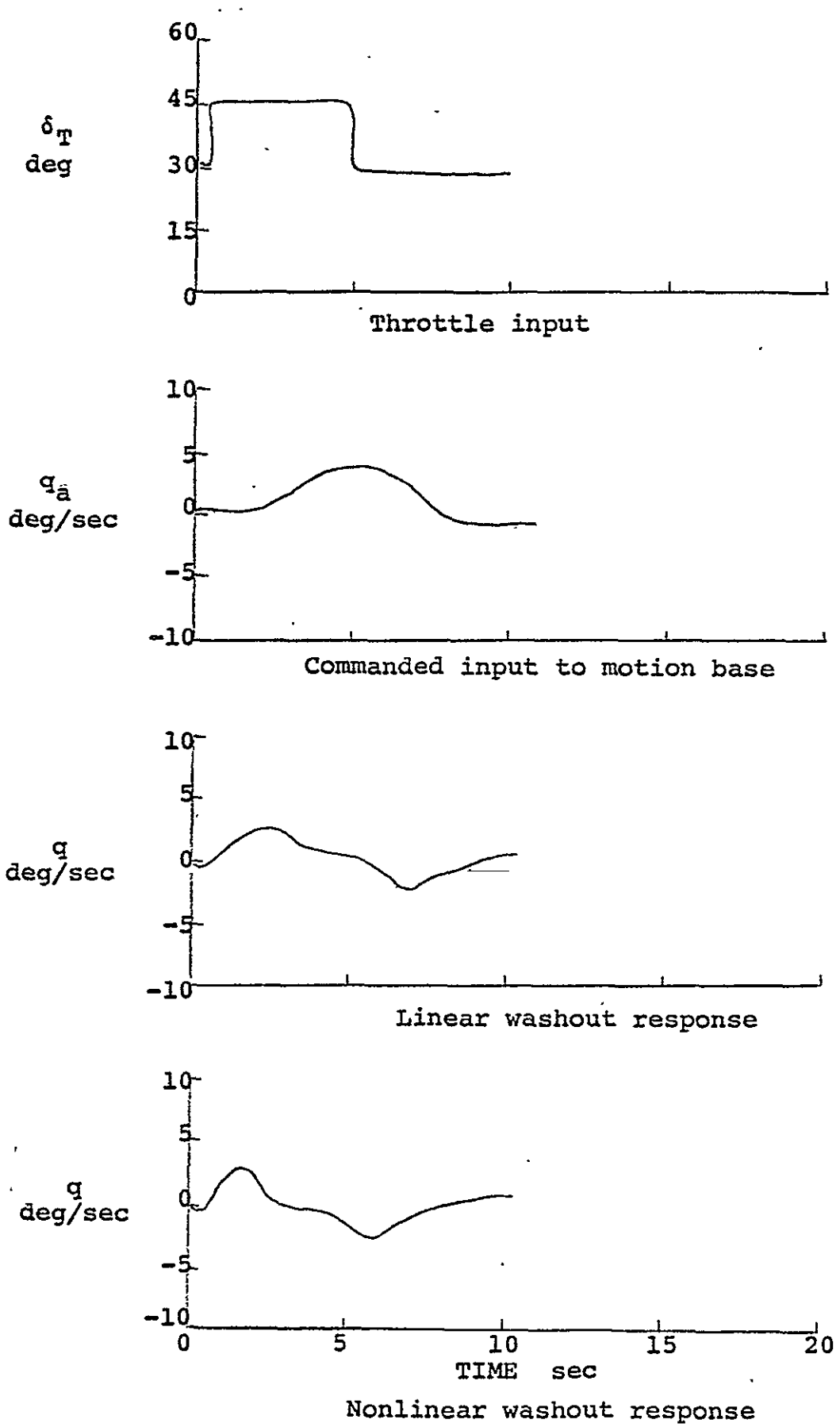

Figure 2.7 Time histories for throttle input

tion and pitch rate are the inputs to the washouts from the simulated aircraft for such a maneuver. The figure shows very little difference between the washout schemes, as the pilot ratings indicated. The fundamental difference between the two pitch rate filters is obscured in order to correctly represent the decrease in longitudinal acceleration at six seconds.

An elevator doublet was input to rate the motion cues for a column input. Again, the pilots found little difference between the linear and nonlinear washout schemes, as shown in Table 2.1. Four pilots rated the filters the same, while the other three rated the nonlinear filter slightly higher. The time histories for the elevator inputs are shown in Figure 2.8. As in the throttle input case, the fundamental difference between the pitch rate filters is not apparent, due to the coordination between pitch rate and longitudinal acceleration. In addition, the pitch response of the 737 is not at all pulse-like, which lessens the difference in performance of the filters.

Wheel inputs were evaluated using ailerons to bank the simulator 20° for a 30° heading change with a return to straight-and-level flight. The pilots preferred to separate the wheel inputs into roll cues and yaw cues to evaluate these cues individually. Figure 2.9 shows the time histories for roll cues in the maneuver described. The anomalous rate cue is present for the linear washout. This is reflected in the pilots' rating, as seen in Table 2.1. All seven pilots felt the nonlinear

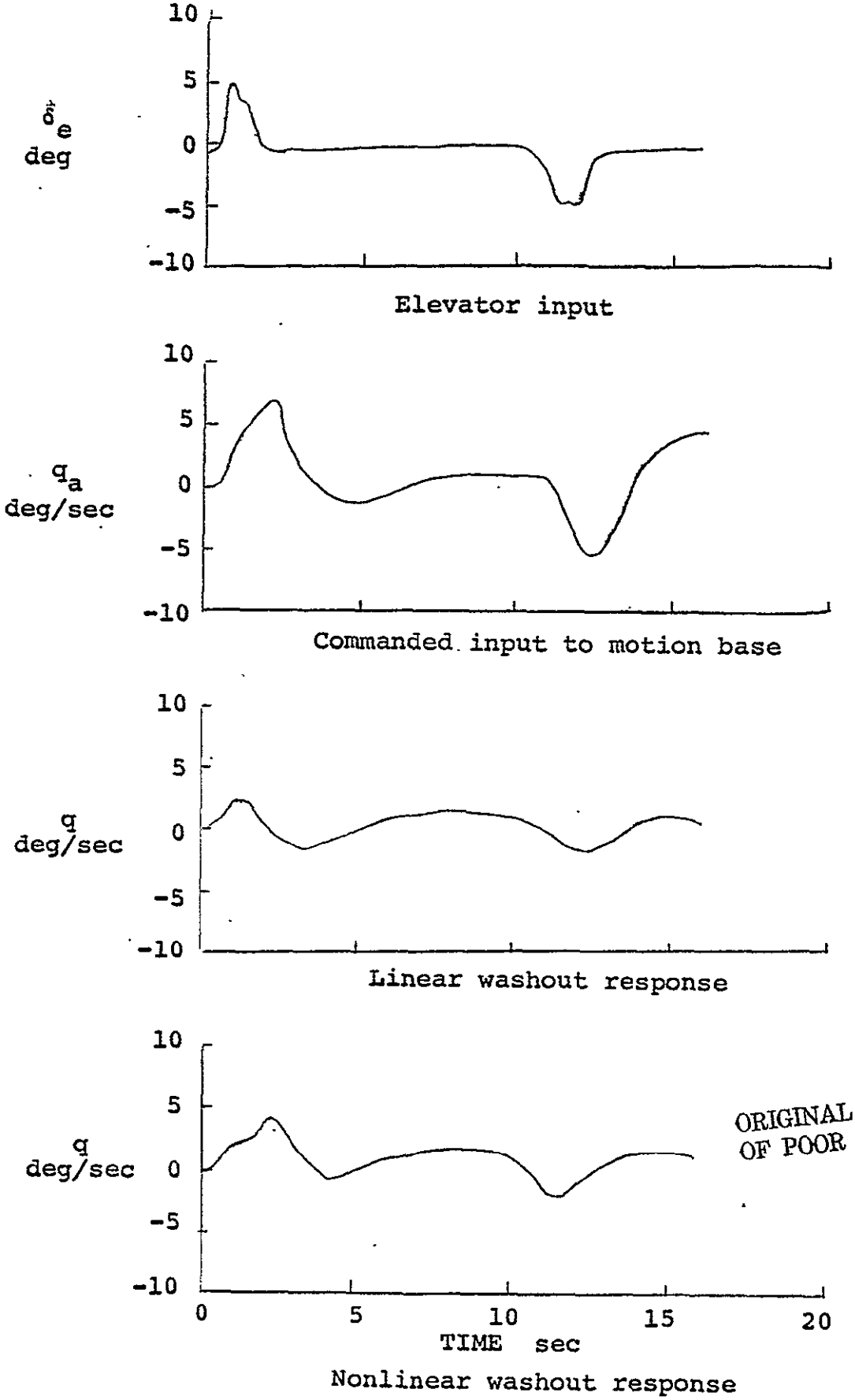

ORIGINAL PAGE IS
OF POOR QUALITY

Figure 2.8 Time histories for column input

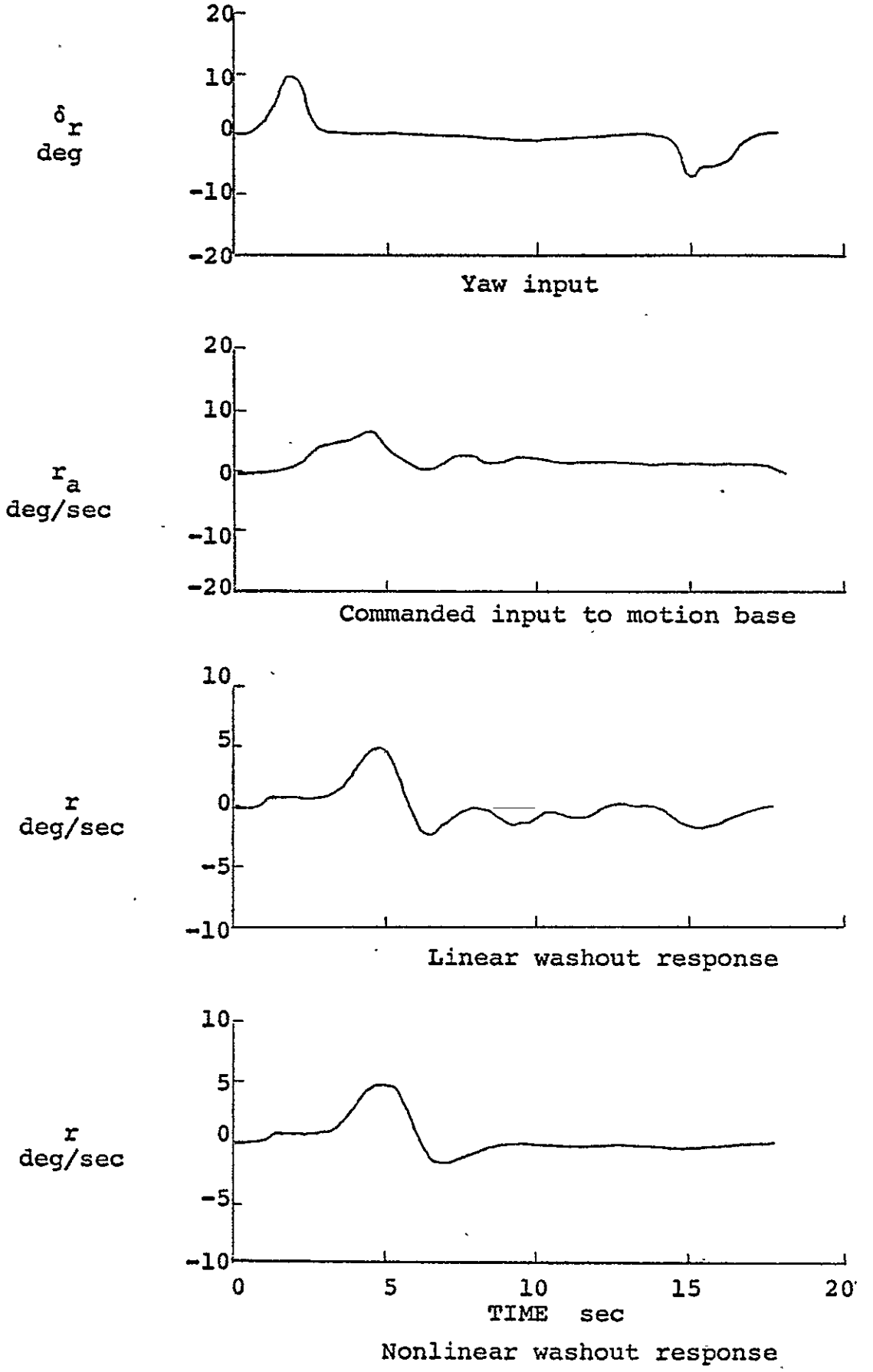

Figure 2.10 Time histories of yaw cues for aileron inputs

filter to be at least one and one-half categories higher than the linear filter.

Figure 2.10 shows the time histories for yaw cues during the same aileron maneuver. Again, the anomalous rate cue is present for the linear filter scheme. The pilots were particularly aware of a negative rate cue when the simulated aircraft rate returned to zero during maneuvers of this type. The ratings in Table 2.1 are at least one category higher for the nonlinear scheme, reflecting the unnateral feel of the linear rate cue.

Each pilot flew a set of rudder maneuvers for both washouts to evaluate roll and yaw cues. There were no changes in the ratings from those obtained using the wheel. This is reflected in the time histories for roll and yaw, shown in Figures 2.11 and 2.12, respectively.

Finally, each pilot was asked to rate the two washout schemes in terms of overall airplane feel. Table 2.1 shows the large contribution made by roll representationin the overall airplane simulation. All pilots rated the nonlinear washout at least one and one-half categories higher than the linear washout. They specifically objected to the anomalous rate cue presented by the linear filter in both roll and yaw.

From this study, Parrish and Martin concluded that the nonlinear washout scheme better represents actual airplane motions than does the linear washout method, at least in an empirical

ORIGINAL PAGE IS
OF POOR QUALITY

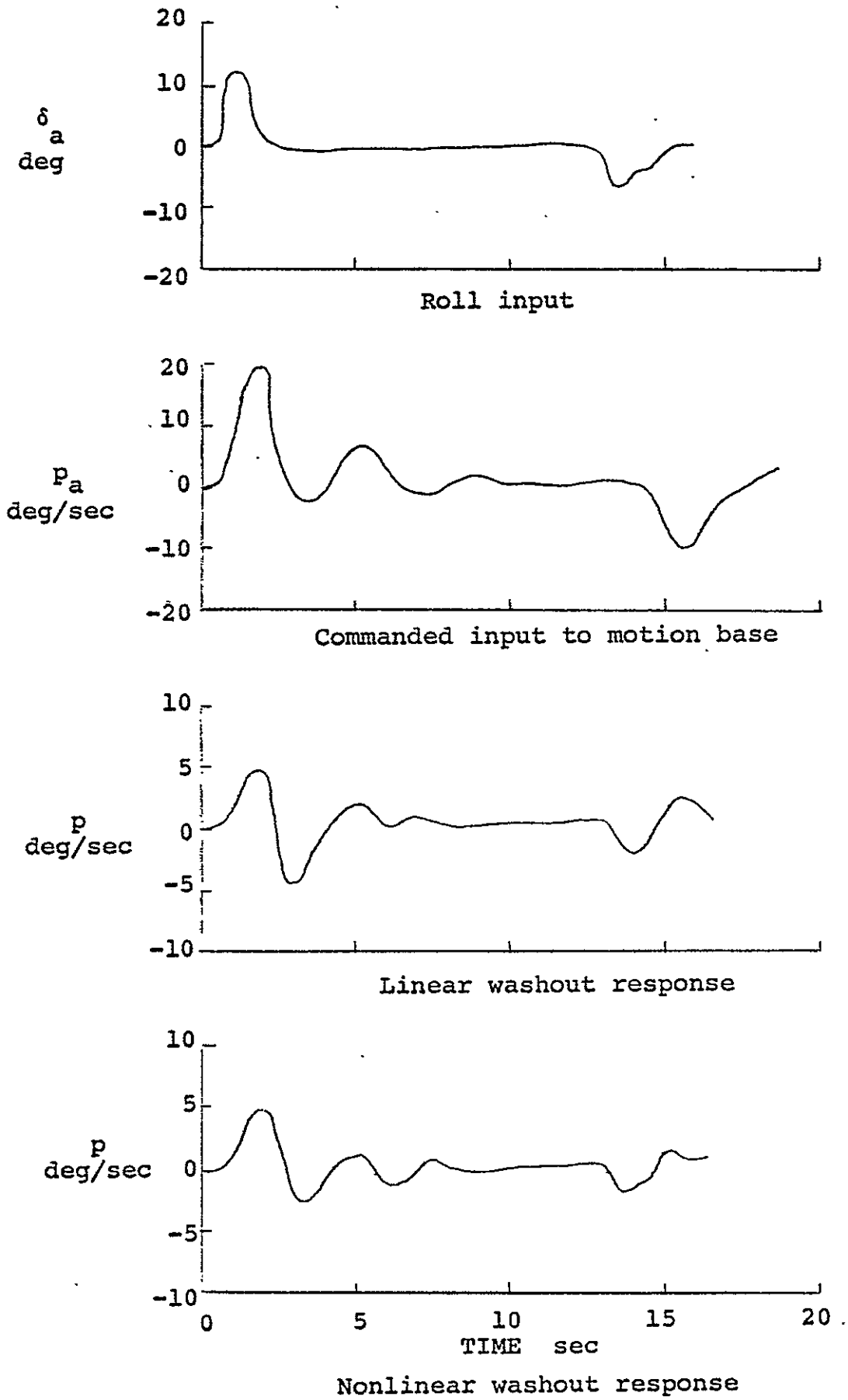

Figure 2.9 Time histories of roll cues for aileron inputs

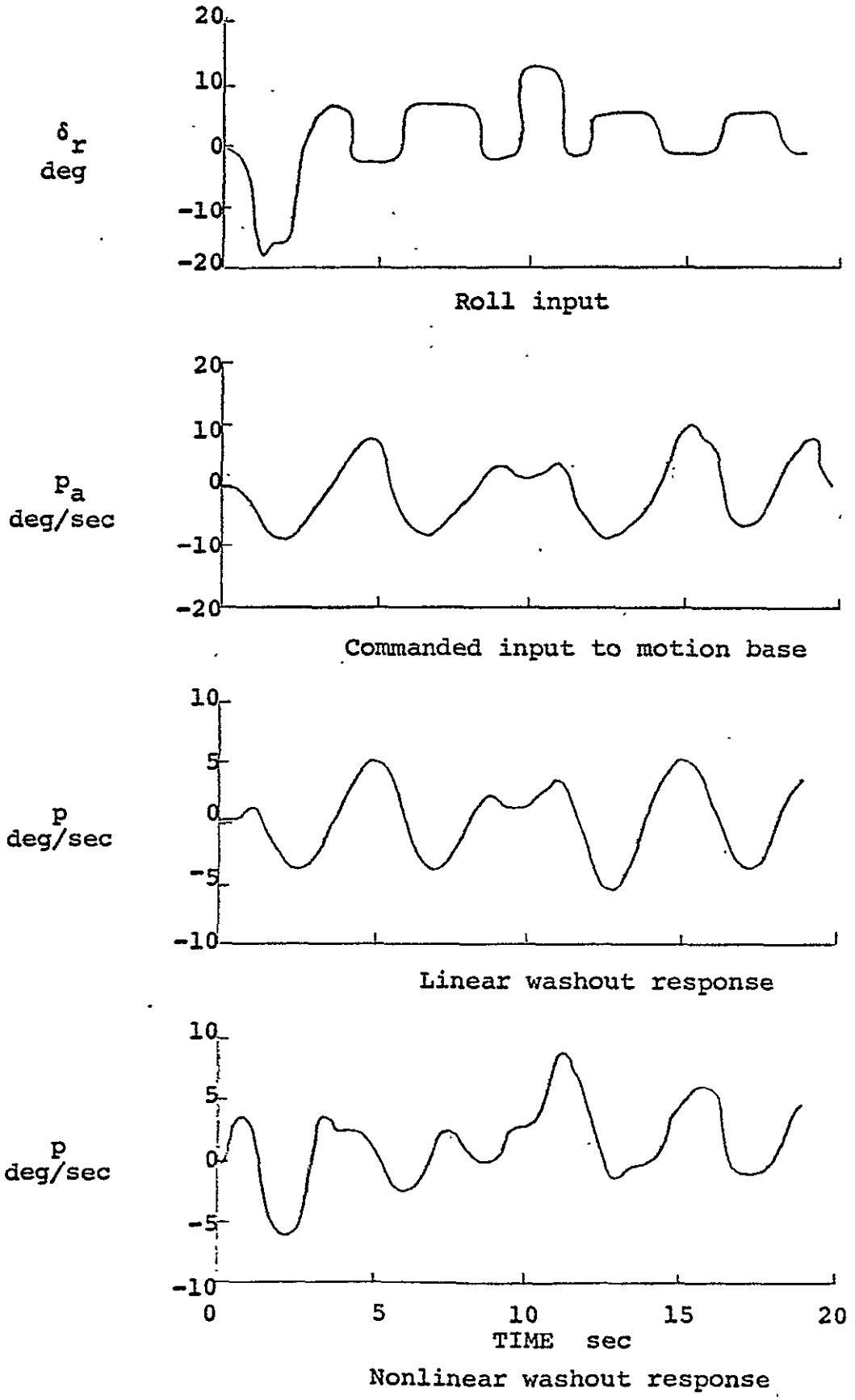

ORIGINAL PAGE IS
OF POOR QUALITY

Figure 2.11 Time histories of roll cues for rudder inputs

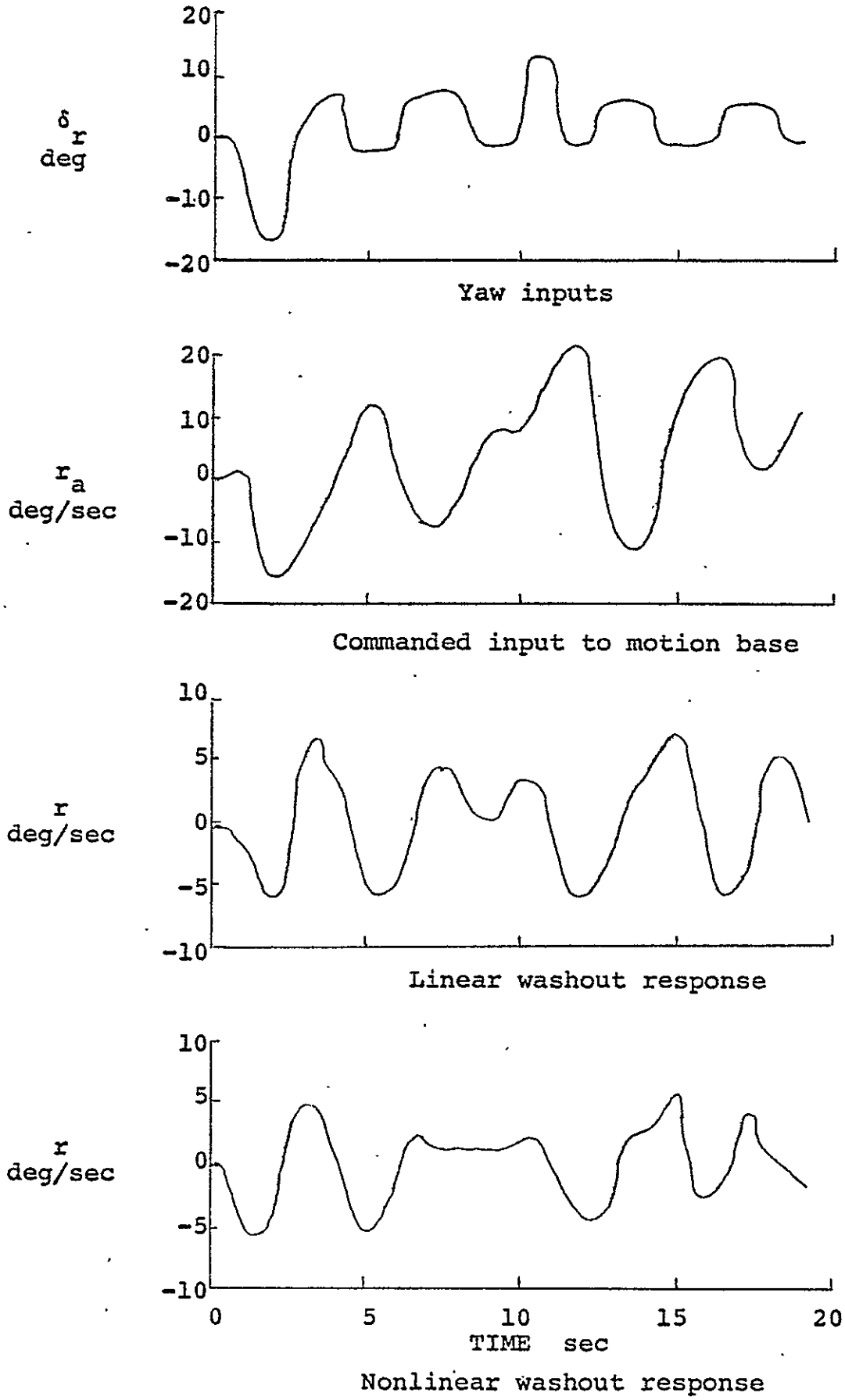

Figure 2.12 Time histories of yaw cues for rudder inputs

sense. It appears that the nonlinear scheme does not present more of the motion cue; it merely eliminates the false cue present in the use of the linear washout.

The work presented in this paper attempts to quantify the results obtained in the subjective analysis made by Parrish and Martin. In order to accomplish this, the motion histories from the Parrish and Martin study are input to a model of human dynamic orientation. The output from the model will provide a vestibular explanation for the sensation differences between the two filters. Results of this work are presented in Chapter IV.

CHAPTER III

THE PHYSIOLOGICAL MODEL

A model which predicts human perceptual response to motion stimuli has been developed at M.I.T.'s Man-Vehicle Laboratory by Ormsby [10]. The model, which exists as a FORTRAN computer program, is based on the known physiology of the vestibular system. While little is known about the processing of the specific forces and angular accelerations received from the vestibular organs, the simplifying assumptions made about this process produce a model which agrees with available neurological and physiological data.

This chapter first presents an overview of the vestibular system, and then goes on to discuss the mathematical modelling of the system which leads to the current FORTRAN model. More detailed descriptions of the vestibular system may be found in the literature [9,15,19,20]. The complete derivation of the model of human dynamic orientation is found in Ormsby. And a description of the actual FORTRAN programs and their use is available in the appendix to this thesis.

3.1 The Human Vestibular System

The vestibular system, or labyrinth, comprises the non-auditory portion of the inner ear. It is composed of three semicircular canals, one utricle and one saccule in each ear. The semicircular canals are the rotational motion sensors. They consist of three approximately orthogonal circular toroidal canals. The canals are filled with a water-like fluid called endolymph. When the head undergoes angular acceleration, the endolymph tends to lag behind the motion of the canal walls. The motion of the endolymph relative to the canal walls displaces the cupula, a gelatinous mass which completely obstructs one section of the canal called the ampulla. Sensory hair cells embedded at the base of the cupula detect its displacement. As a result, the deformation of the cupula is transformed into an afferent firing rate which provides a signal of rotational motion to the central nervous system (see Figure 3.1).

In a particular canal, all of the hair cells have the same polarization. When the flow of endolymph displaces the cupula in a single direction, the hair cells are either all excited or all inhibited. As shown in Figure 3.2, the canals on either side are essentially coplanar with the other side. Thus, they are pairwise sensitive to angular accelerations about the same axis. Since a pair of canals which are sensitive about the same axis have opposite polarities, it is assumed that the high-

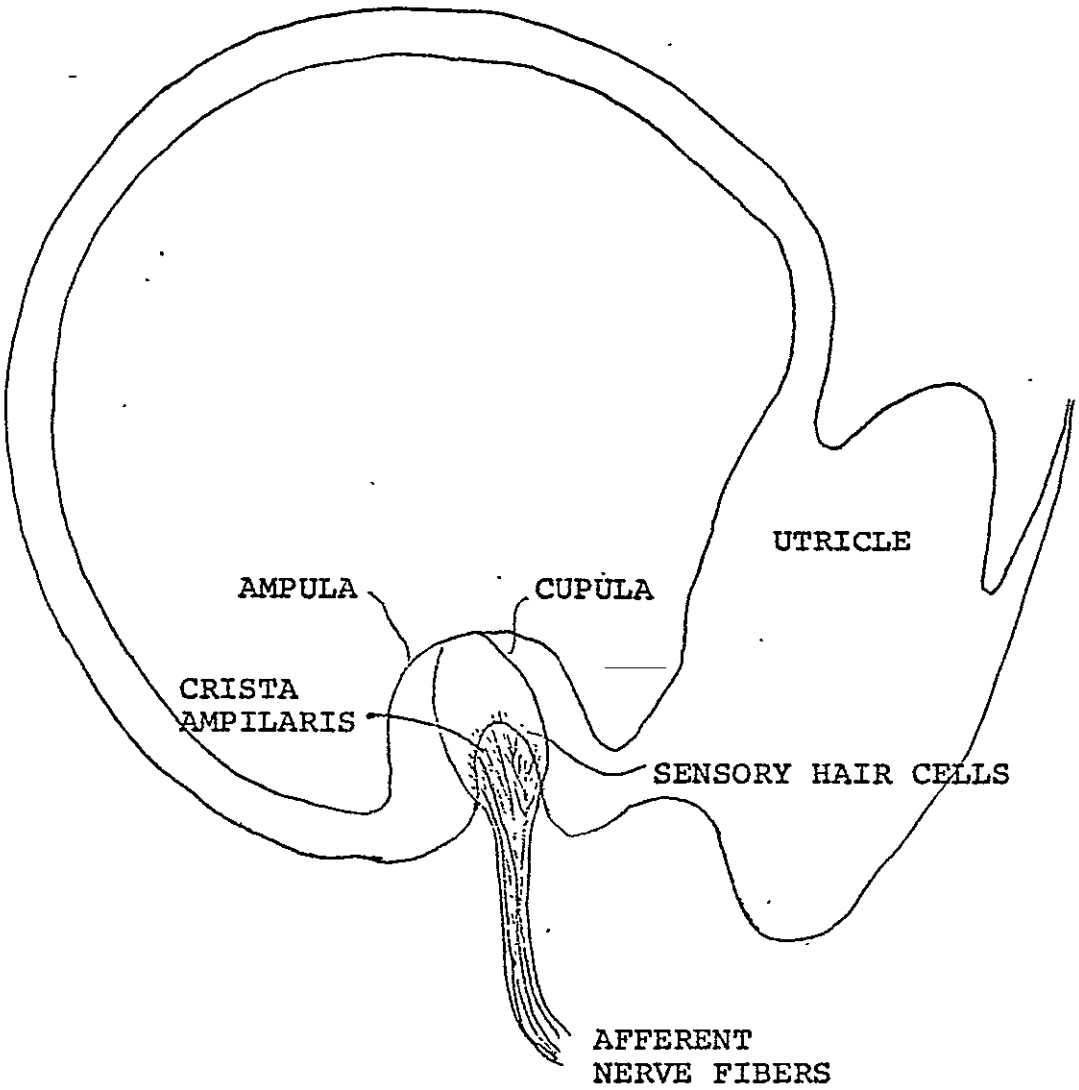

Figure 3.1 Horizontal semicircular canal [10]

ORIGINAL PAGE IS
OF POOR QUALITY

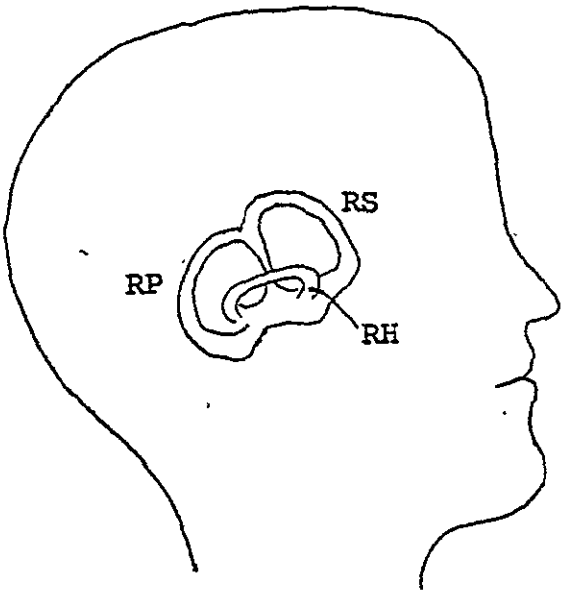

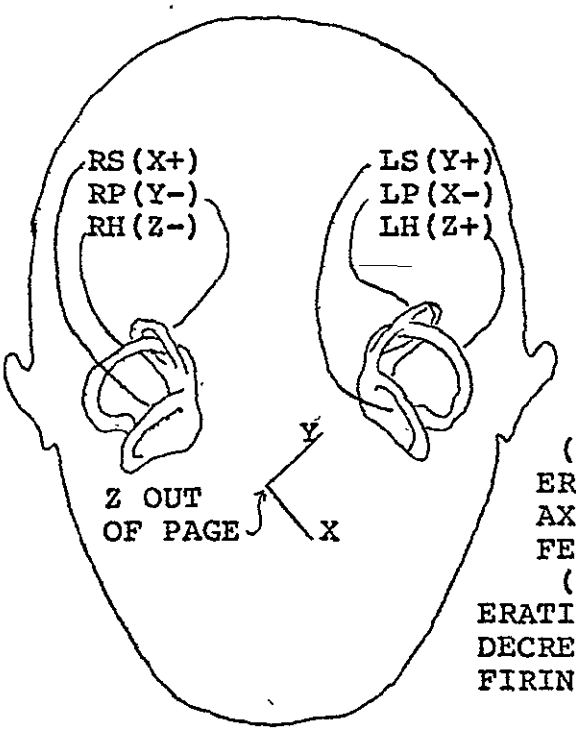

KEY

R RIGHT
L LEFT
H HORIZONTAL
P POSTERIOR
S SUPERIOR
(X+) POSITIVE ACCELERATION ABOUT THE X AXIS INCREASES THE AFFERENT FIRING RATE
(Y-) POSITIVE ACCELERATION ABOUT THE Y AXIS DECREASES THE AFFERENT FIRING RATE

Figure 3.2 Orientation of semicircular canals [10]

er processing centers respond to the difference in afferent firing rates.

Two otolith organs, consisting of a utricle and a saccule, are located in each ear. The otolith is sensitive to changes in specific force. Figure 3.3 depicts the basic structure of the otolith organs. The otolith consists of a gelatinous layer containing calcium carbonate crystals, known as otoconia. This layer is supported by a bed of sensory hair cells. An acceleration of the head shifts the otoconia relative to the surrounding endolymph, due to the higher specific gravity of the otoconia. This shifting causes the sensory hair cells to bend, sending a change in afferent firing rate through the afferent nerve fibers to the central nervous system.

As shown in Figure 3.4, the utricles are oriented such that their sensitivity is in a plane parallel to the plane of the horizontal semicircular canals. The sensitivity of the saccules is in a plane perpendicular to the horizontal canals. The hair cells in the utricle are sensitive in all directions parallel to its plane of orientation, while the hair cells in the saccule make it predominantly sensitive to accelerations perpendicular to the utricular plane.

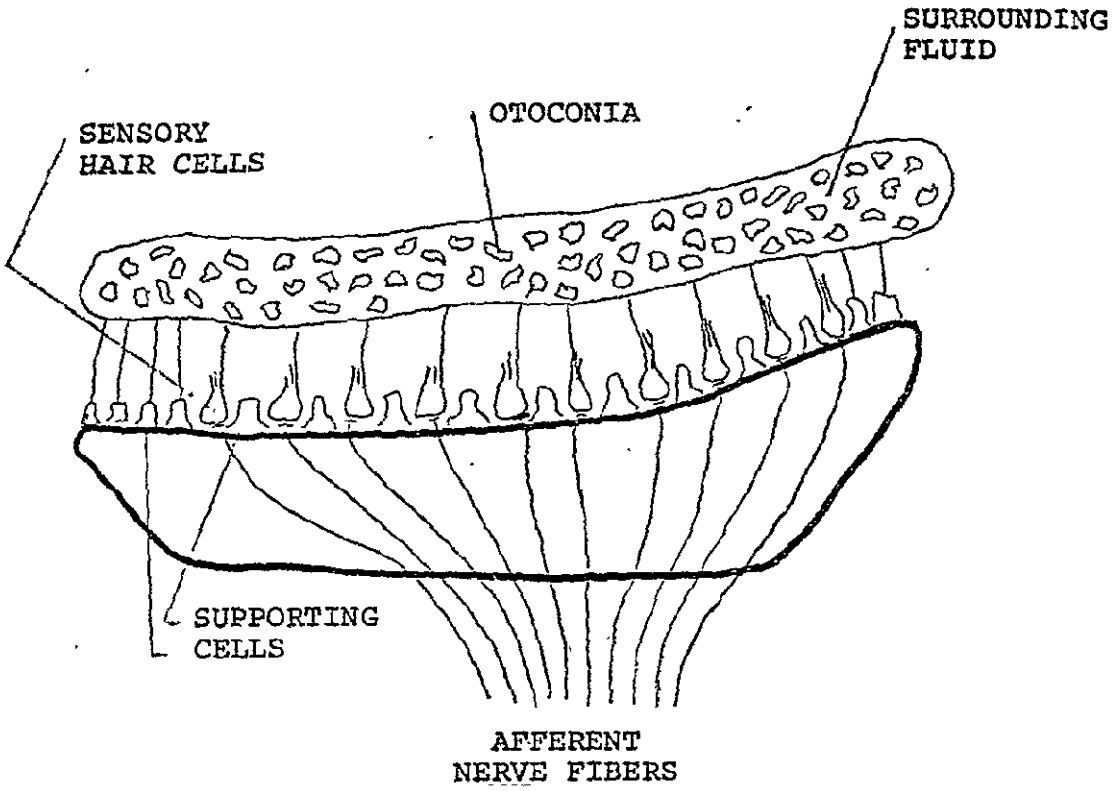

Figure 3.3 Cross section of otolith [10]

ORIGINAL PAGE IS
OF POOR QUALITY

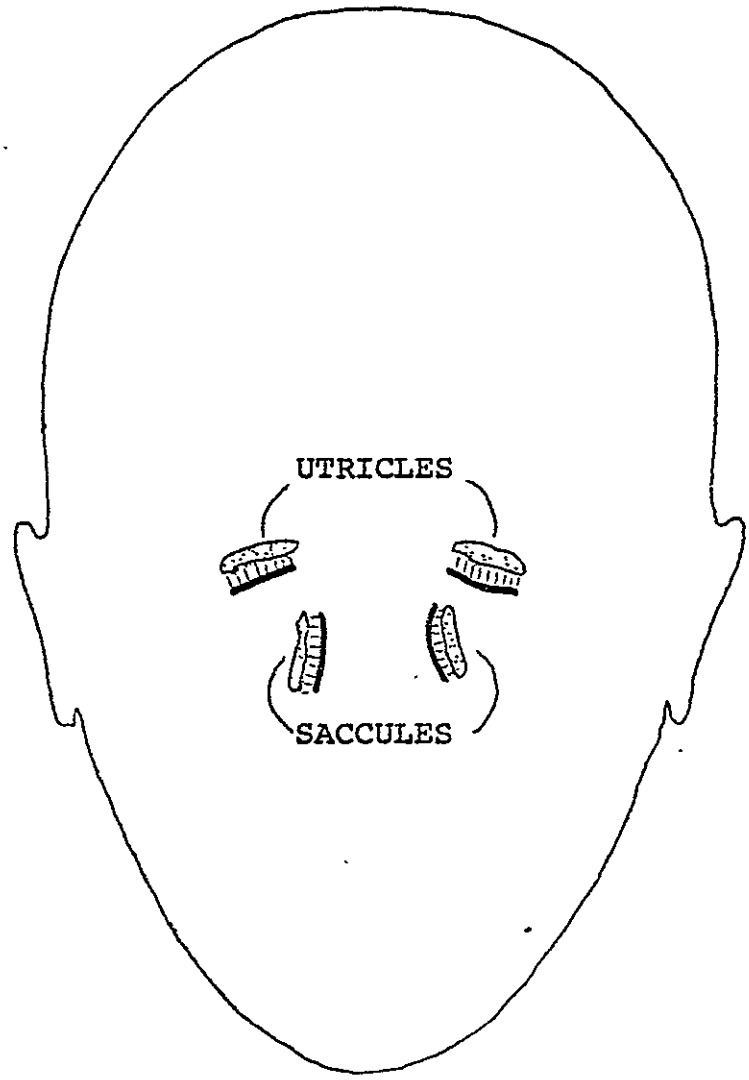

Figure 3.4 Orientation of otoliths [10]

3.2 The Ormsby Model

The mathematical model of the semicircular canals consists of several parts. The first part is the mechanical model of the cupula deflection caused by motion of the endolymph. The second part includes the interaction between the mechanical movement and the afferent firing rate. The third part concerns measurement noise, which is that portion of the afferent signal found to be independent of the mechanical stimulus input.

Figure 3.5 depicts the afferent model of the semicircular canals as arrived at by Ormsby. Observation of cupula motion led to the torsion pendulum model [9], suggesting that the overdamped system reacts to angular velocity rather than angular acceleration. The results of the model are expressed as a transfer function of the following form:

$$FR_c(s) = \frac{(57.3)(300s^2)(.01s+1)}{(18s+1)(.005s+1)(30s+1)}\,\omega(s) + \frac{SFR}{s} + n(t) \qquad (3.1)$$

The model of the otolith system is composed of two parts - the mechanical model of the otolith sensor, and the afferent response to otolith displacement. Figure 3.6 presents the afferent model of the otolith system used by Ormsby. The mechanical model of the otolith is that of a fluid-immersed mass retained by a spring. The resulting transfer function relat-

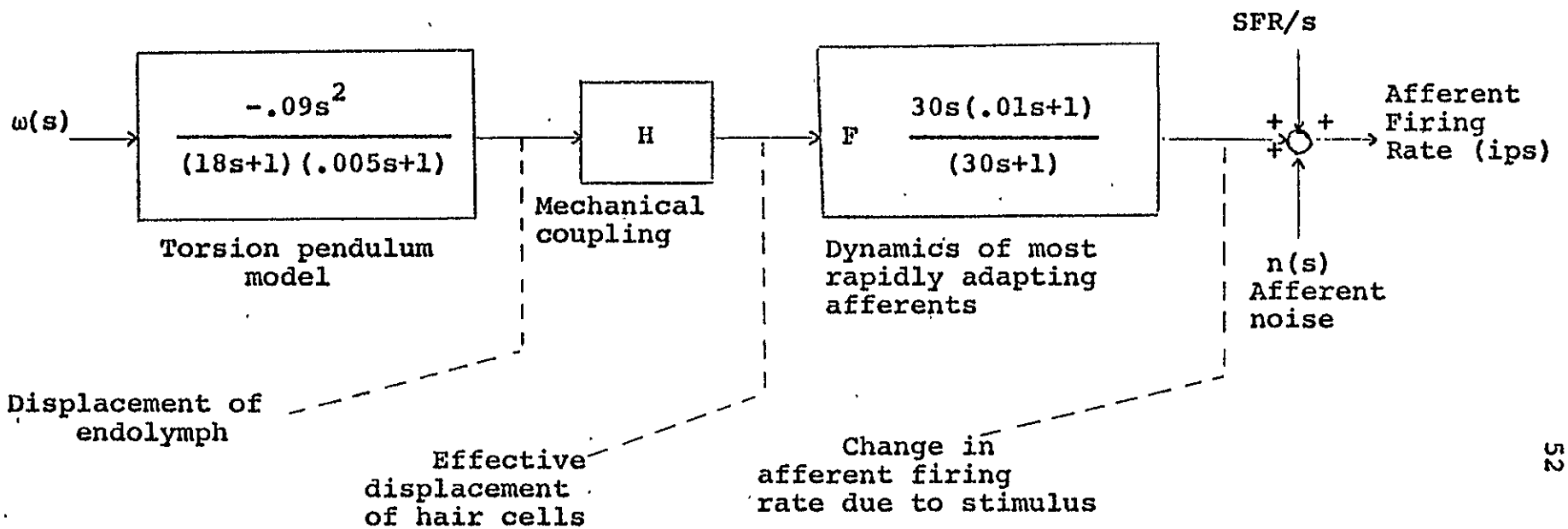

ω(s) = stimulus, angular velocity of head

H = Mechanical coupling of endolymph to effective hair cell displacement

F = Constant which relates hair cell displacement to change in firing rate

SFR = Spontaneous firing rate of typical afferent cell (90 ips)

Figure 3.5 Afferent model of semicircular canals (after Ormsby [10])

ORIGINAL PAGE IS OF POOR QUALITY

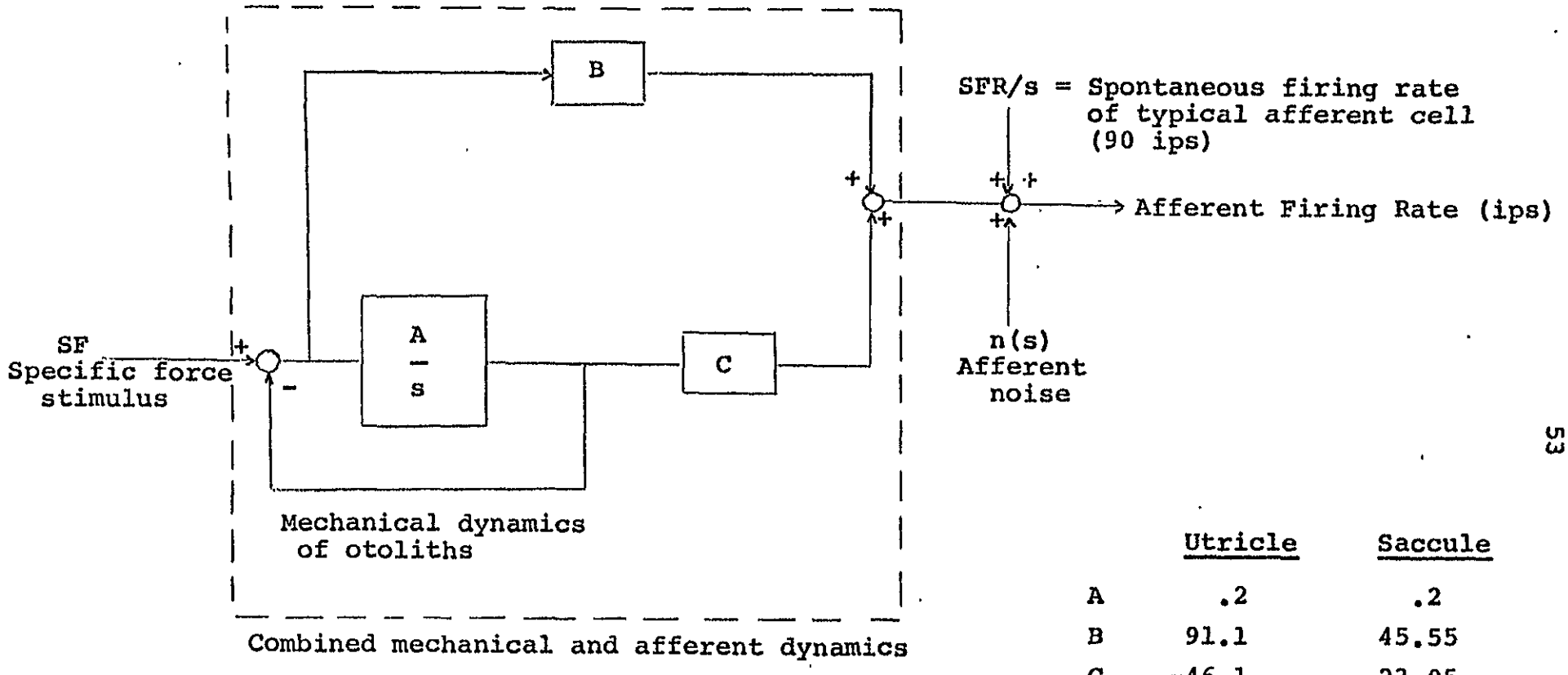

	Utricle	Saccule
A	.2	.2
B	91.1	45.55
C	-46.1	-23.05

Figure 3.6 Afferent model of otoliths (after Ormsby [10])

ing afferent firing rate to specific force is:

$$FR_o(s) = \frac{(18000)(s+.1)}{(s+.2)(s+200)} SF(s) + \frac{SFR}{s} + n(t) \qquad (3.2)$$

The input to the model consists of a stimulus composed of specific forces and angular accelerations in each axis of the head coordinate system. Each of these afferent inputs is then transformed into sensor coordinates. From this sensor stimulation, the afferent firing rates are derived, using the transfer functions presented above.

At this point, the process becomes purely guesswork. Even assuming that these afferent firing rates are available to some central processing system in the brain, the form which this processing takes is simply a guess. Ormsby guessed that the central processor performs a type of least mean squares error optimization to make an estimate of the specific force and angular velocity inputs based on the afferent firing rates output from the vestibular system sensors.

In this case, such a least mean squares estimator is a Kalman filter [4,8]. The input is unknown except for an expected range of magnitude and a frequency bandwidth, and an expected measurement noise. Also, the input and the noise statistics are time invariant, which makes the filter a steady-state Kalman (or Wiener) filter. This steady-state Kalman filter is used by the model to produce estimates of specific force

ORIGINAL PAGE IS
OF POOR QUALITY

and angular velocity from the afferent firing rates. These estimates are tuned, using the Kalman filter gains, to yield estimates which fit the available neurological and physiological data for known inputs.

The filters used for canal processing are tuned such that the estimates produced for the angular velocities are essentially unchanged from the afferent inputs. This observation is in agreement with available data, suggesting that very little central processing is performed. The otolith filters must be tuned so that a more dramatic effect by the filters on the afferent input is observed. This suggests that more central processing is required, or that the model of the afferent response is missing a term which has subsequently been attributed to the central processing mechanism in the tuning procedure. Basically, the filter acts as a low pass filter with a time constant of 0.7 seconds. The utricle and saccule differ only in the Kalman filter gains, where the saccule gains are twice the utricle gains.

Once the specific force and angular velocity estimates have been obtained from the Kalman filters, the saccule nonlinearity must be accounted for. This is done by means of a nonlinear input-output function, and allows the model to include observed attitude perception inaccuracies known as Aubert or Mueller effects [6]. The resulting specific force and angular velocity estimates are transformed back to head coor-

dinates.

These estimates must now be combined to yield new estimates of perceived position, velocity and acceleration. In the model this is accomplished by a separate scheme, known as DOWN. DOWN is a vector of length 1 g in the direction of perceived vertical; as such, it is the model's prediction of the perceived vertical. The basic assumptions used in combining the specific force and angular velocity estimates to arrive at DOWN are the following:

- The system will rely on the low frequency portion of the specific force estimates provided by the otoliths.
- The system will use that part of the canal information which is in agreement with the high frequency content of the rotational information provided by the otoliths.

This logic is presented in Figure 3.7. Block A produces the estimate of rotational rate from the input specific forces assuming SF is fixed in space. The low frequency component of this estimate is filtered out in Block B. Block C isolates the component of the low frequency angular velocity estimate which is perpendicular to SF and DOWN. This is the mechanism discussed in Chapter II, which allows cancellation of canal signals arising when prolonged rotations are stopped suddenly. The effect of the three blocks is to produce a rotational

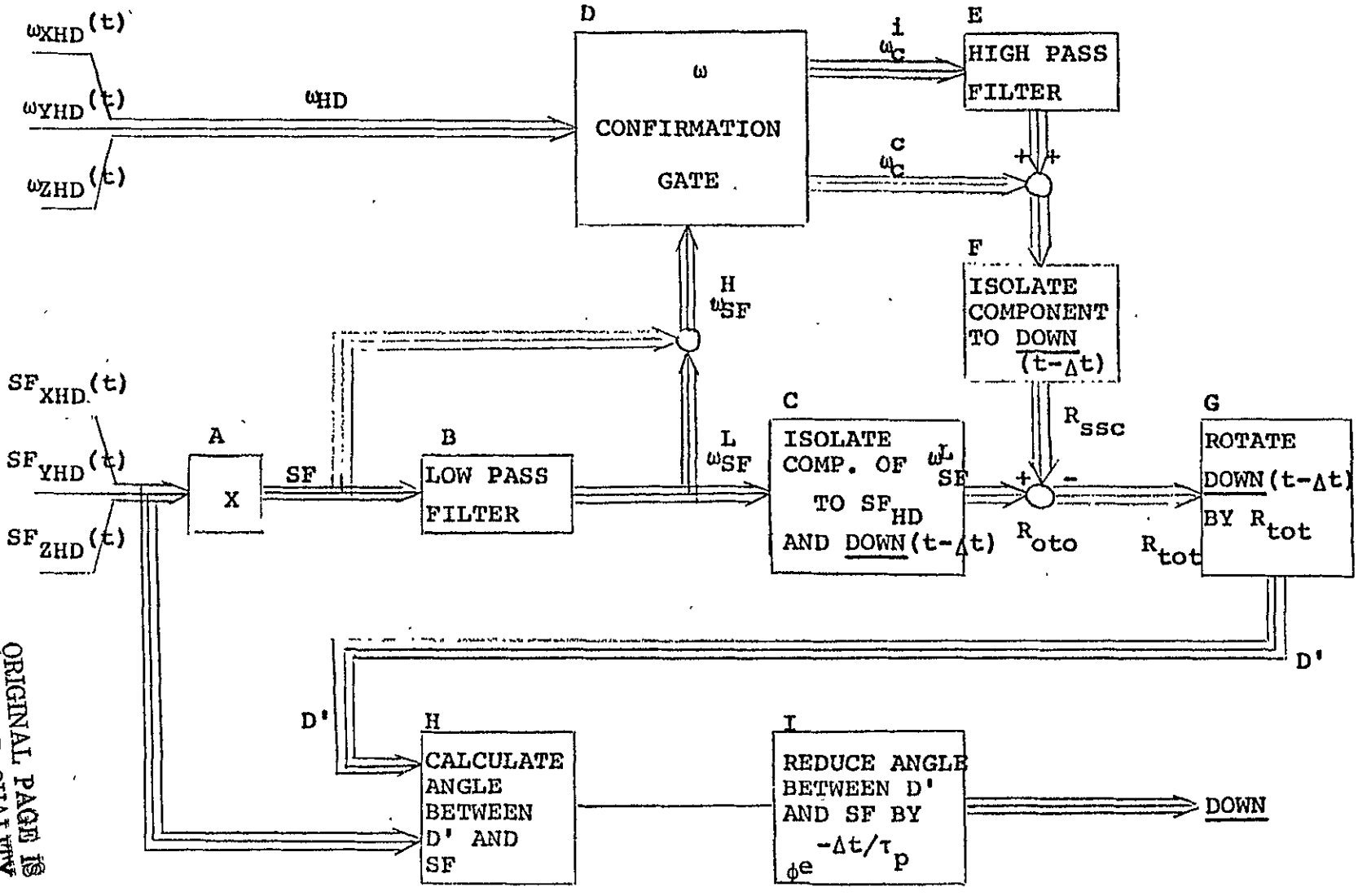

Figure 3.7 DOWN estimator [10]

ORIGINAL PAGE IS
OF POOR QUALITY

vector which represents the low frequency rotational information available from the otoliths (R_{oto}).

Block D confirms whether or not the high frequency portion of the canal rotational information is consistent with the high frequency portion of the otolith rotational information. The inconsistent part of the canal information is sent through a high pass filter (Block E) and is then combined with the consistent portion of the canal information. The component of the resulting rotation vector parallel to DOWN is then eliminated, leaving a rotational vector due to canal information (R_{ssc}). The total estimate of the rotation rate of the outside world with respect to the last estimate of DOWN, R_{tot}, is computed by subtracting R_{ssc} from R_{oto}. The net result of Blocks H and I is to produce an estimate of DOWN which is the same as the estimated specific force vector. This is accomplished by a slow reduction in the discrepancy between SF and DOWN, eliminating any accumulated errors resulting from the integration of rate information.

Figure 3.8 illustrates the model for predicting perceived rotational rate. The angular velocity vector parallel to DOWN becomes the perceived parallel angular velocity. The perpendicular angular velocity is computed in three steps:

1. Calculate the difference between the component of angular velocity perpendicular to DOWN, and the angular velocity consis-

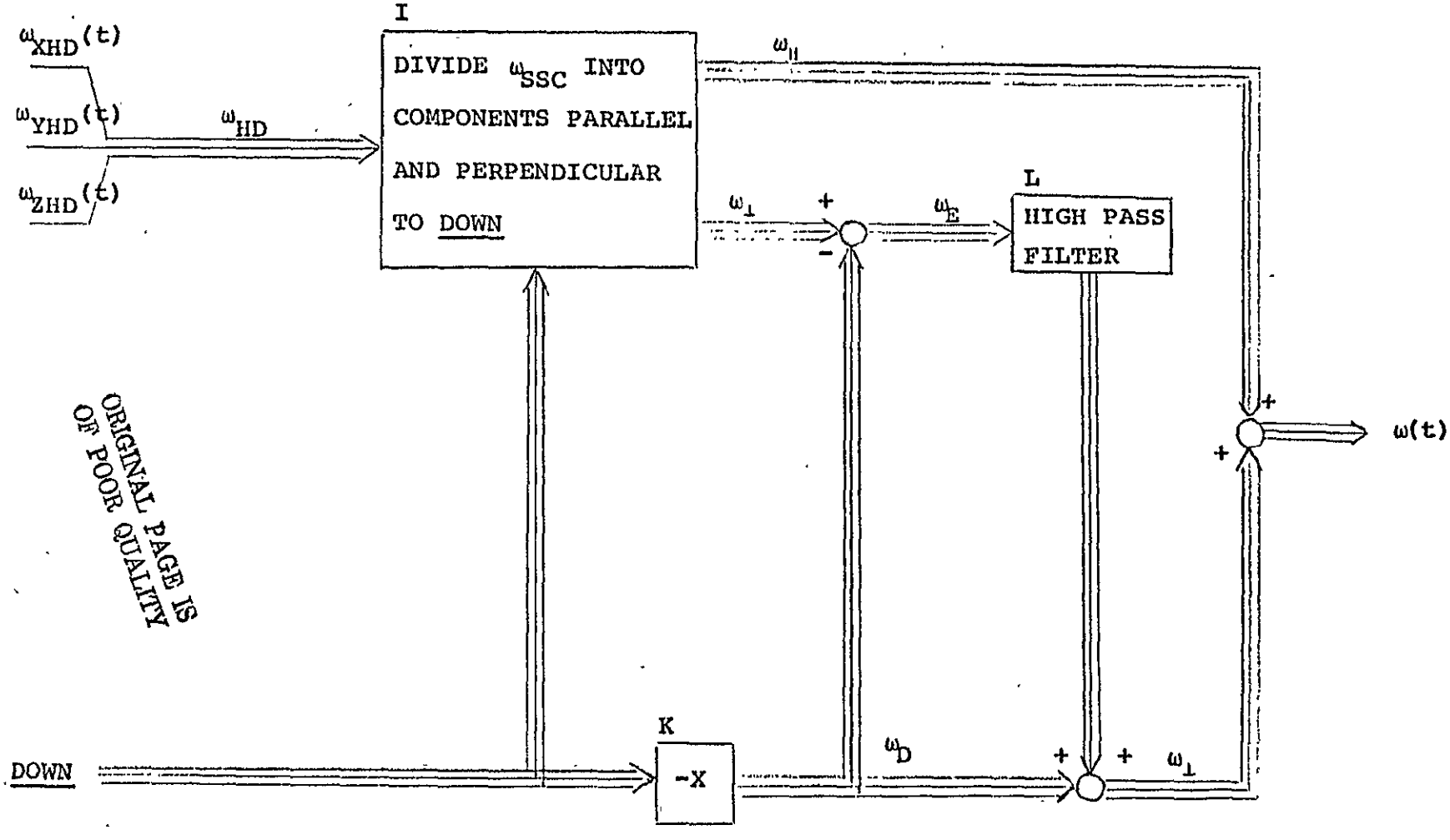

ORIGINAL PAGE IS OF POOR QUALITY

Figure 3.8 Angular velocity estimator [10]

tent with the rate of change of the direction of DOWN (Block K).

2. High pass filter this difference.

3. Combine the filtered result with the DOWN-consistent angular velocity.

This process assures that the canals provide the high frequency component of the rotational rate, while the low frequency component is the rotational rate consistent with DOWN. The total sense of rotation is thus the sum of the parallel and perpendicular components.

This completes the description of the form of the Ormsby model used in this work. A complete description of the model may be found in Ormsby's thesis. Figure 3.9 presents an overview of the entire model. At this point, a few important observations should be made:

- The Ormsby model was tuned using inputs with known outputs for a certain set of discrete time intervals - namely, an afferent update interval of 0.1 seconds and a Kalman filter estimate update interval of 1.0 seconds. In this thesis, due to the characteristics of the input data, the afferent update interval is 0.03125 seconds, and the Kalman filter estimate update interval is 0.25 seconds. In order to use these two intervals, the model had to

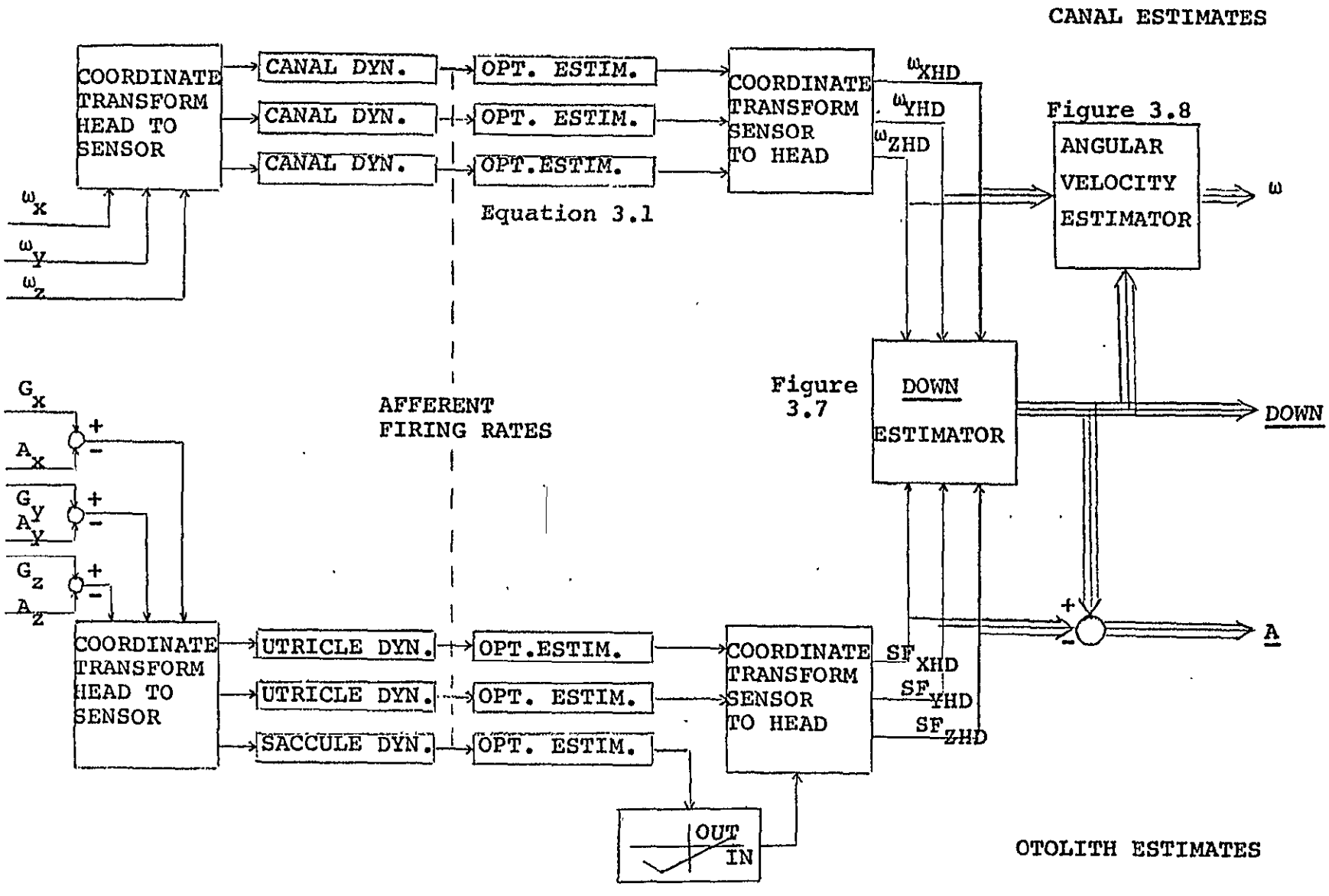

Figure 3.9 Overview of Ormsby model (after Borah [3])

ORIGINAL PAGE IS OF POOR QUALITY

be retuned by changing the Kalman gains. This process, which is necessary each time the update intervals are changed, is described in more detail in the appendix.

- One important assumption made by this model is that the inputs are unknown prior to their processing. It was noted in the introduction to this thesis that specific force and angular acceleration act on the body as a whole, providing visual, tactile and proprioceptive, as well as vestibular, cues. This model takes account of the vestibular cues only, although the tuning process may force it to consider certain aspects of the other sensory cues. Thus, when this model is applied to cases where the subject might have prior knowledge, or at least an expectation of the motion, the results must be interpreted in light of the limitations imposed by the model.

The Ormsby model of human dynamic orientation was used in this work as a FORTRAN program implemented on a PDP 11/34. The main program, as well as all associated subroutines, is documented in the appendix.

CHAPTER IV

DATA AND RESULTS

As a logical consequence of the two previous chapters, it is desirable now to evaluate the two washout schemes using the Ormsby model of human dynamic orientation. Such an evaluation could serve the purpose of quantifying the differences between the two filters which Parrish and Martin found in their subjective study. In addition, this evaluation could shed some light on the question of the model's usefulness in simulator design.

This chapter presents the data used for this study, and the results of the processing of the data by the Ormsby model.

4.1 Data Description

The data used in this work consists of four runs made with a linear or a nonlinear washout on the Langley simulator. These runs coincide with Figures 2.9, 2.10, 2.11, and 2.12. Table 4.1 lists the definitions of the variables measured during these simulation runs. Note that not only are the simulator motions recorded, but also the commanded motions of the aircraft. This allows evaluation of both the computer simula-

PRECEDING PAGE BLANK NOT FILMED

Table 4.1 Variables recorded during simulation runs

VARIABLE	DEFINITION
TIME	time
DELA	aileron deflection
DELE	elevator deflection
DELR	rudder deflection
THRIL	throttle input
PA	roll rate of airplane
PADOT	roll acceleration of airplane
QA	pitch rate of airplane
QADOT	pitch acceleration of airplane
RA	yaw rate of airplane
RADOT	yaw acceleration of airplane
AXA	longitudinal acceleration of airplane
AYA	lateral acceleration of airplane
PSIA	ψ of airplane
THEA	θ of airplane
PHIA	ϕ of airplane
P	roll rate command to simulator
Q	pitch rate command to simulator
R	yaw rate command to simulator
PDOTM	roll acceleration measured on simulator
QDOTM	pitch acceleration measured on simulator
RDOTM	yaw acceleration measured on simulator
AXCM	longitudinal acceleration measured on simulator
AYCM	lateral acceleration measured on simulator
PSIMB	ψ of simulator
THEMB	θ of simulator
PHIMB	ϕ of simulator
XDDMB	longitudinal acceleration of simulator without gravity component
YDDMB	lateral acceleration of simulator without gravity component

tion of the motion and the actual simulator motion. This data was recorded at Langley on their CDC 6600 computer.

Figure 4.1 presents the aileron and rudder inputs to the simulation schemes, as previously shown in Chapter II. Table 4.2 illustrates the four separate runs, and the data taken from each for use in the Ormsby model. Thus, there are twelve separate cases under evaluation. Both the rudder and the aileron inputs are simulated using the linear and nonlinear filters. For each of these four cases there are two simulated motion histories and one commanded motion history.

The input to the Ormsby model is a subroutine known as STIM. The input to STIM is the time in seconds into the motion history. This is computed in the main program. The output from STIM consists of three vectors - a specific force vector in g's, a unit vector in the direction of gravity in g's, and an angular velocity vector in radians/second. The particular STIM subroutine used for this work can be found in the appendix. Basically, it reads the data from a file on disk in consecutive time order and places the desired data in the correct vector location. For example, when running the linear aileron roll data, the twentieth data item in the twenty-nine item list (see Table 4.1) is read into the first location of the angular velocity vector, after transforming it from an acceleration in degrees/second^2 to a velocity in radians/second. Thus, the STIM subroutine must be changed each time the model is run, to accomodate the new data.

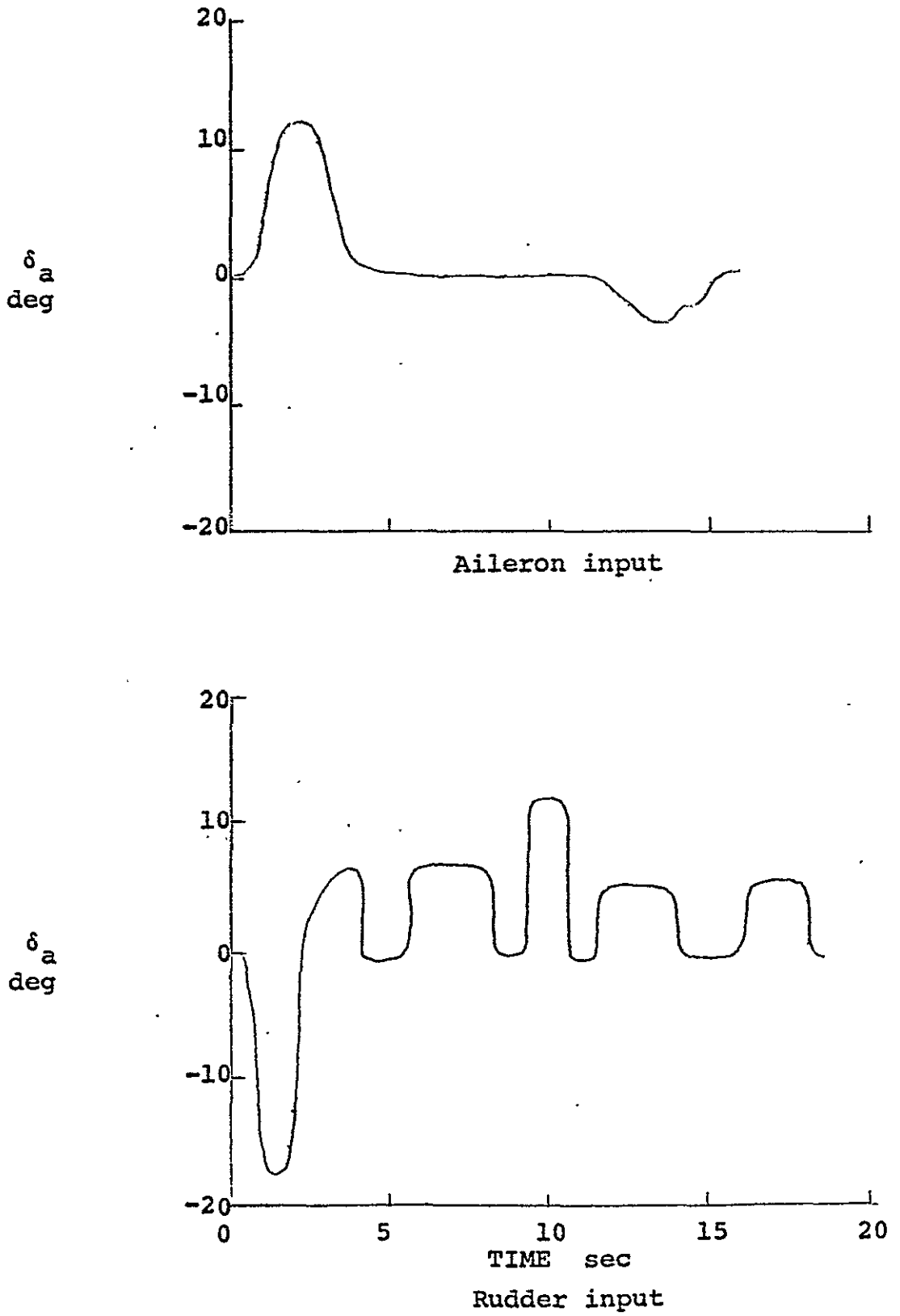

ORIGINAL PAGE IS
OF POOR QUALITY

Figure 4.1 Commanded inputs to simulation

AXIS / INPUT	ROLL		YAW	
AILERON	Linear Simulator (PDOTM)	Nonlinear Simulator (PDOTM)	Linear Simulator (RDOTM)	Nonlinear Simulator (RDOTM)
	Command (PADOT)		Command (RADOT)	
RUDDER	Linear Simulator (PDOTM)	Nonlinear Simulator (PDOTM)	Linear Simulator (RDOTM)	Nonlinear Simulator (RDOTM)
	Command (PADOT)		Command (RADOT)	

Simulator - recorded motions of the moving base simulator

Command - requested motions of the moving base simulator made by the simulation routine

Table 4.2 Data used as input to Ormsby model

The following four sections present the output of the model for the four major categories - aileron roll cues, aileron yaw cues, rudder roll cues and rudder yaw cues.

4.2 Aileron Roll Cues

Figures 4.2, 4.3 and 4.4 present the time histories of perceived angular velocity in response to aileron roll cues, using the linear and nonlinear washout schemes. In addition, the response to the commanded aileron roll is also shown. In each case, the perceived motion is approximately the same for the first thirteen seconds. The angular velocity rises gradually to a peak of .06 radians/second (3.5 degrees/second). This is consistent with the expected response to the 5°/second input roll velocity of the pulse-type aileron cue. It is after this peak perceived velocity is reached that the interesting differences occur.

But it is just at thirteen seconds when the second pulse is input. The linear and nonlinear washouts cause the perceived velocity to change direction, as indicated by the sign change. In the linear case, this change in direction does not occur until the end of the run, while in the nonlinear case it occurs at fifteen seconds. In both cases there is apparent confusion of direction. Just as there was in the first pulse, there should be a delay before the perceived angular velocity begins to return to zero. The experiment actually ends too soon, so the zero level is never reached.

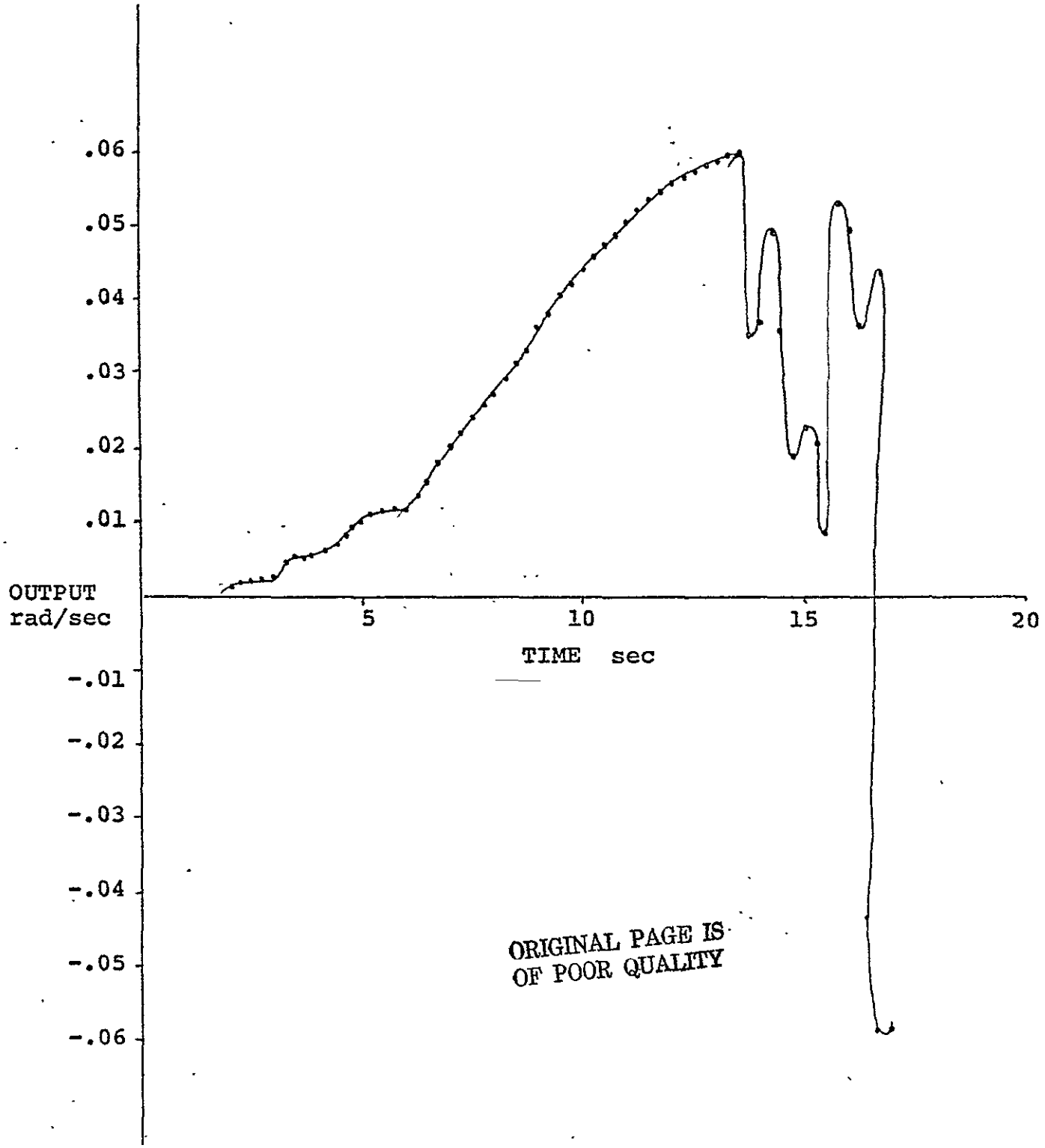

ORIGINAL PAGE IS
OF POOR QUALITY

Figure 4.2 Perceived angular velocity for simulated linear aileron roll cue input

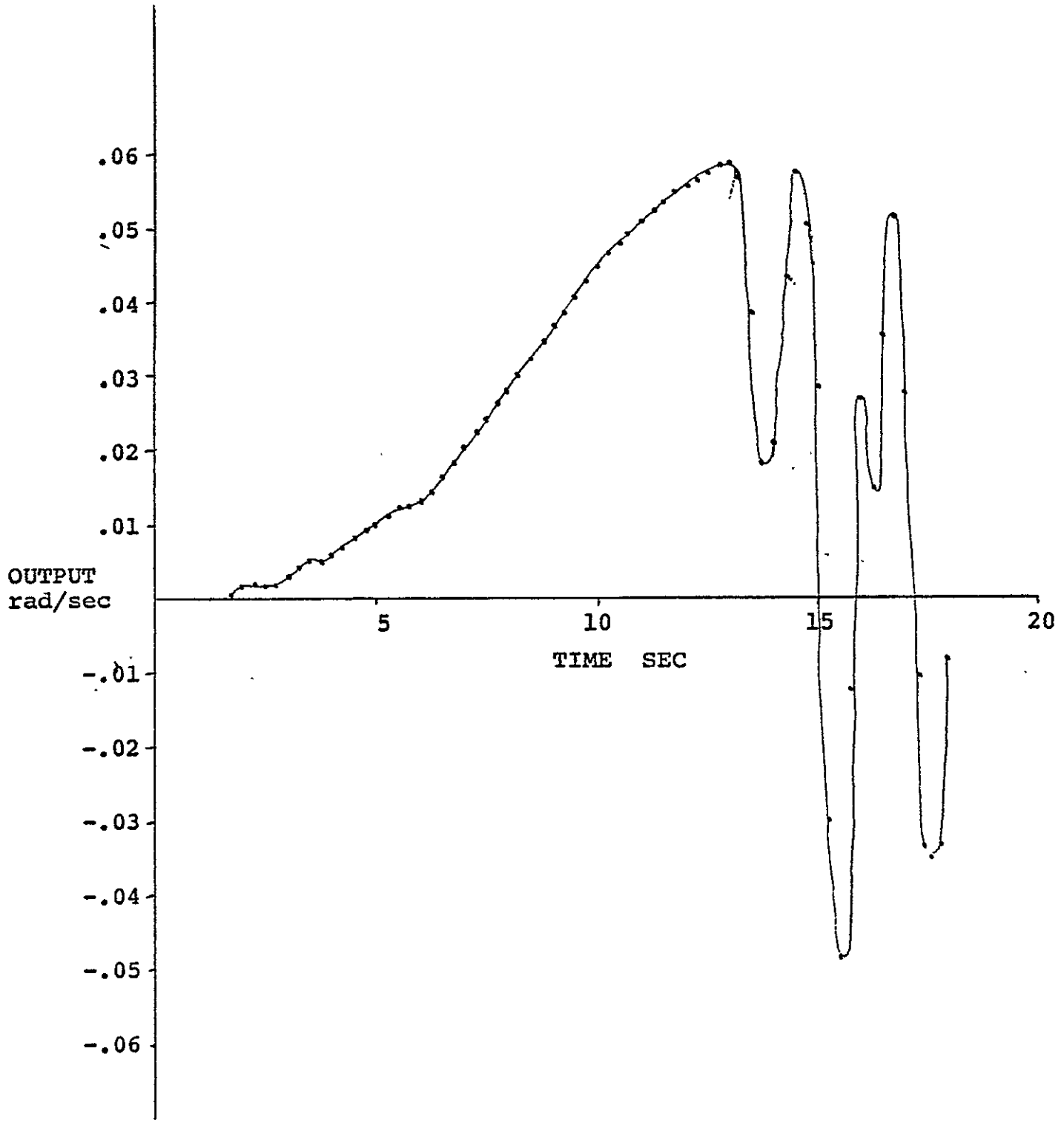

Figure 4.3 Perceived angular velocity for simulated nonlinear aileron roll cue input

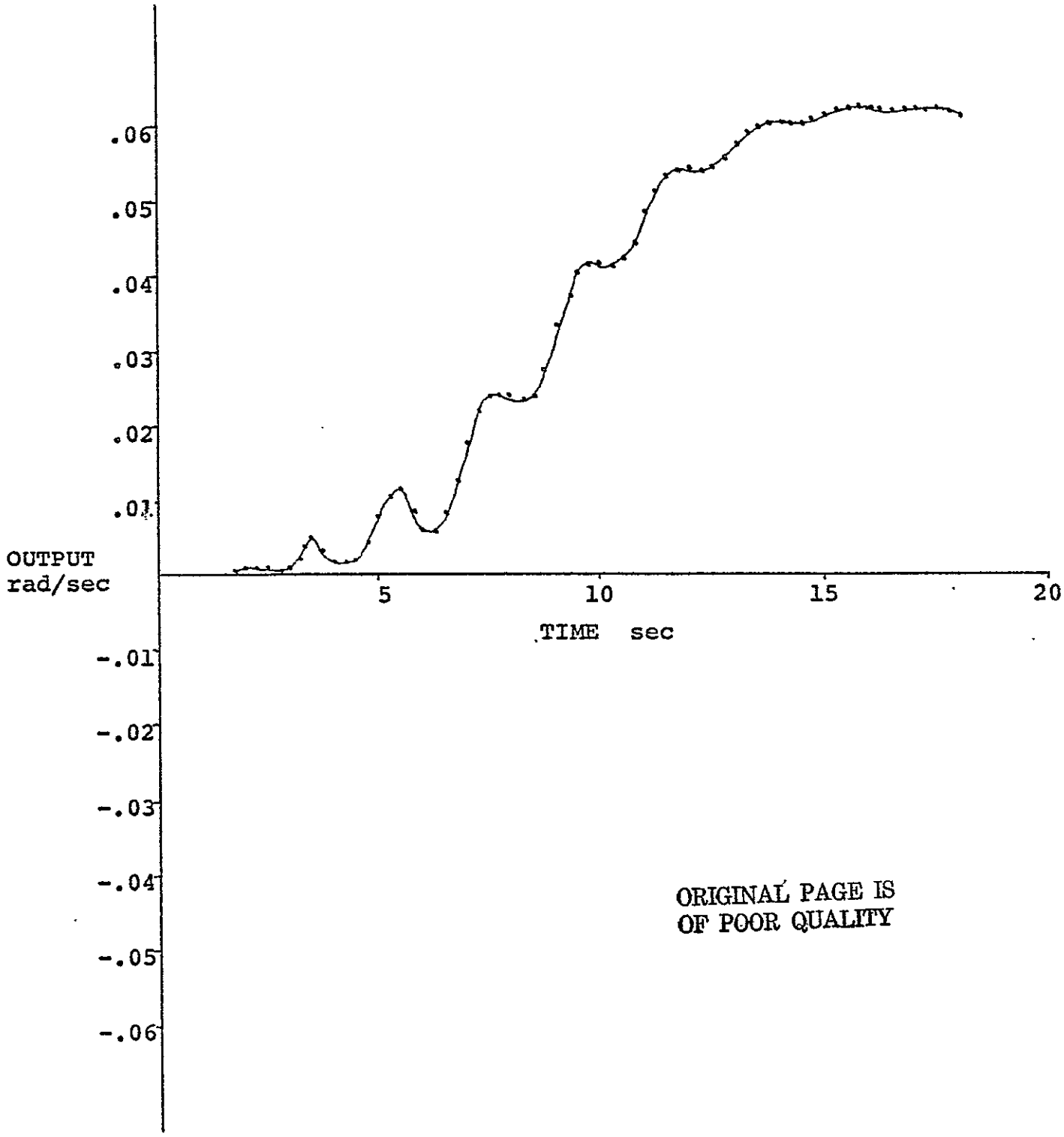

ORIGINAL PAGE IS
OF POOR QUALITY

Figure 4.4 Perceived angular velocity for commanded aileron roll cue input

A real difference can be seen in comparing the simulated cases with the commanded case. As can be seen in Figure 4.4, the commanded case behaves as predicted - there is a gradual increase to the maximum perceived angular velocity, and then a leveling off. Presumably, if the experiment had been carried past the second pulse, there would be a gradual return to zero in angular velocity

In this case, then, the nonlinear filter acts to contain the confused perception involved in transferring the second pulse to the motion base. While it performs better than the linear filter, it presents motion cues which are not quite able to duplicate the desired motion perception.

4.3 Aileron Yaw Cues

Figures 4.5, 4.6 and 4.7 present the perceived angular velocities output from the Ormsby model, for inputs of yaw cues for aileron motions. In this case, the difference between the linear and the nonlinear washouts is evident. Again, the first thirteen seconds for each case are about the same - the expected response to a pulse input is the slow rise to a maximum angular velocity, then a leveling off. This is the same response observed for the roll cues, as seen in Figures 4.2, 4.3 and 4.4.

Thirteen seconds into the motion history, the second pulse is introduced. In the case of the roll cues, the motion transferred to the simulator was rather rough. But for the yaw cues, the simulation was very close to the desired motion. This can also be seen by comparing Figure 2.9 with Figure 2.10 - notice how smooth the nonlinear response is in Figure 2.10 compared to the linear response in Figure 2.9.

As before, the commanded motion to the simulator is smooth and presents the expected response. A comparison of Figures 4.5 and 4.6 shows that the nonlinear filter presented the second pulse with very little disturbance, while the linear filter caused a noticeable discontinuity in the motion. This is the anomalous rate cue which the pilots reported on in Table 2.1.

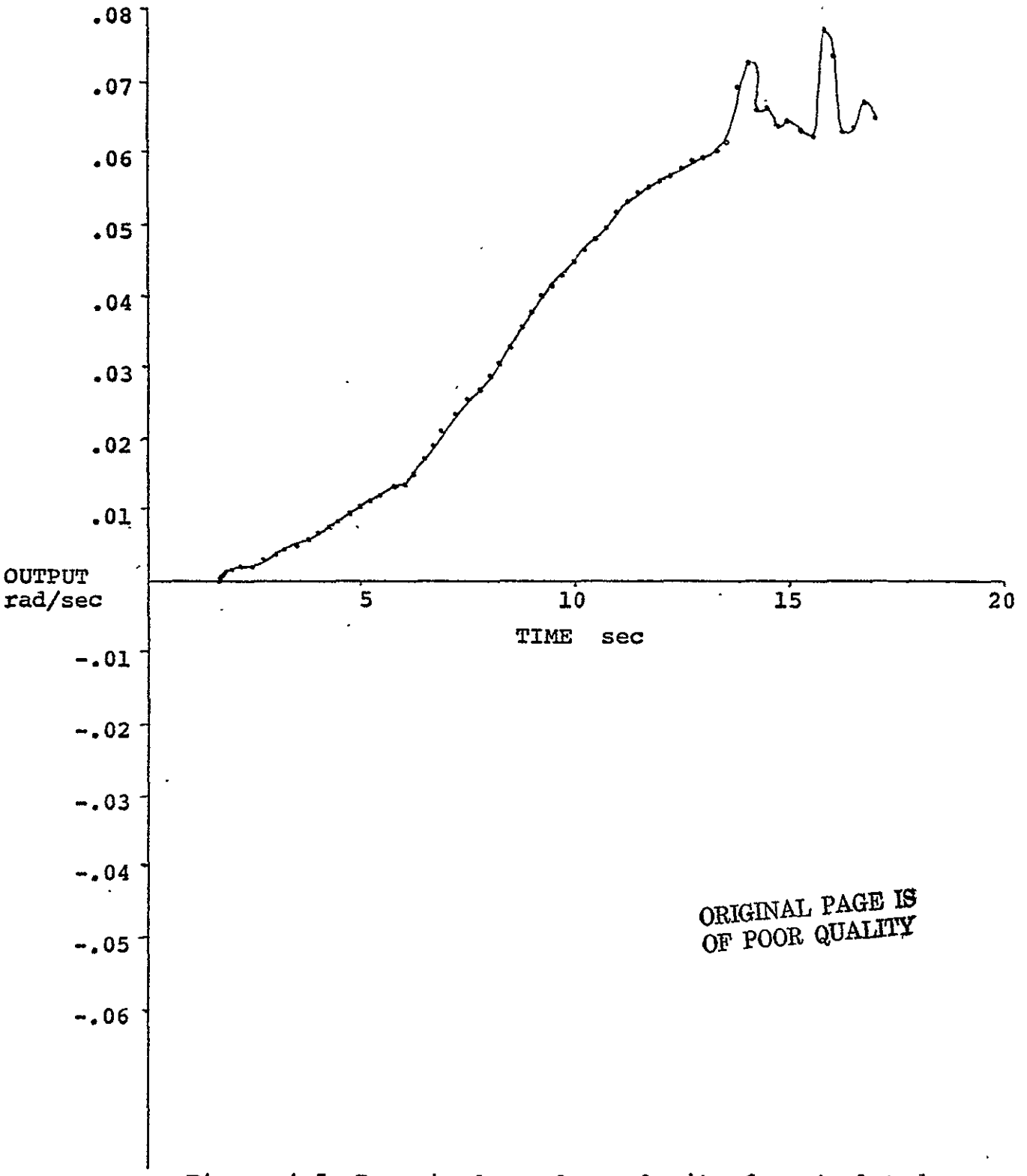

ORIGINAL PAGE IS
OF POOR QUALITY

Figure 4.5 Perceived angular velocity for simulated linear aileron yaw cue input

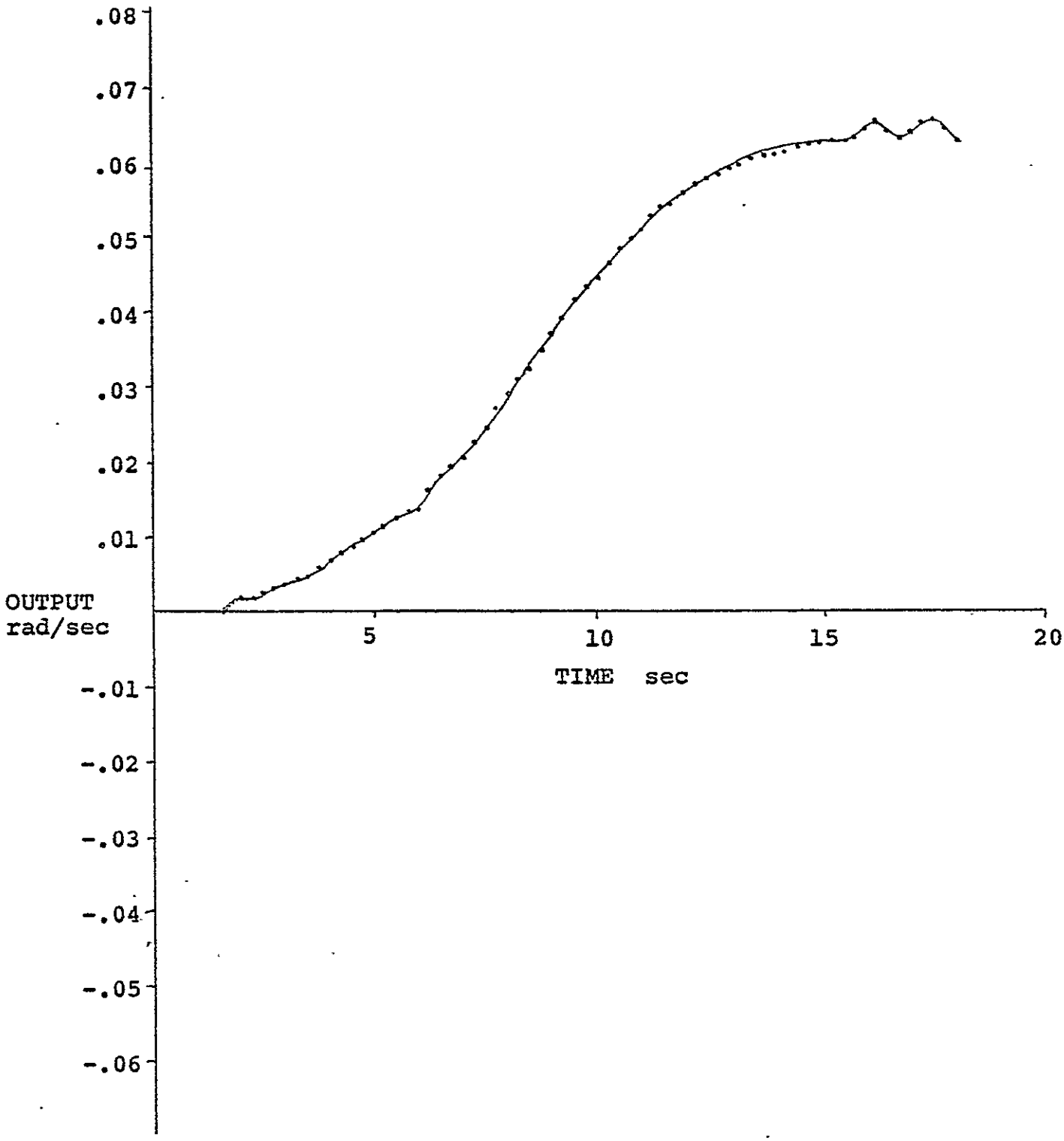

Figure 4.6 Perceived angular velocity for simulated nonlinear aileron yaw cue input

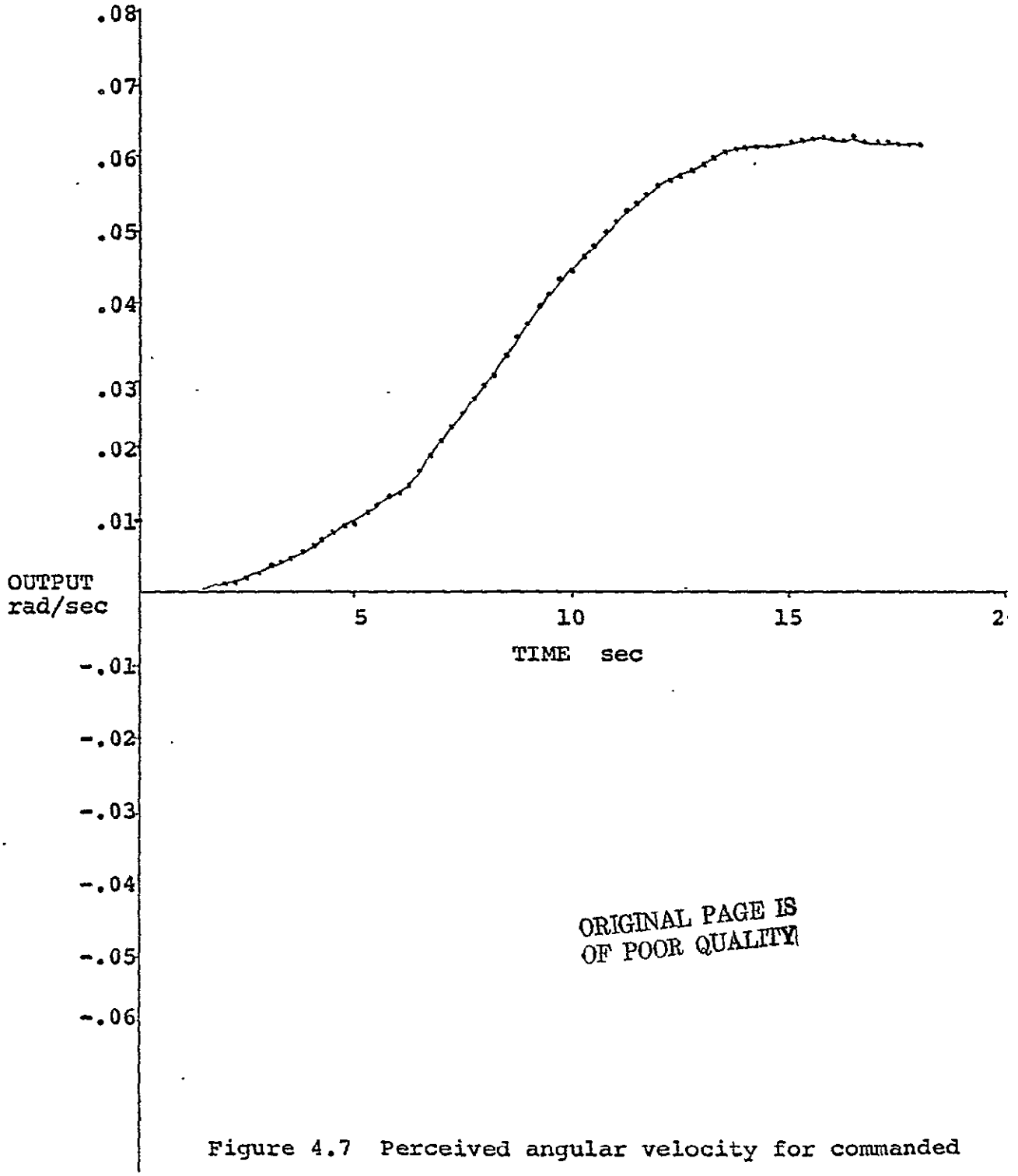

ORIGINAL PAGE IS
OF POOR QUALITY

Figure 4.7 Perceived angular velocity for commanded aileron yaw cue input

4.4 Rudder Roll Cues

Figures 4.8, 4.9 and 4.10 present the perceived angular velocities obtained from the rudder roll cue inputs. The situation here is different from the previous aileron cases, simply because the motion history in the rudder cue cases is much more complicated than in the aileron cue cases (see Figure 4.1). It is not clear that the Ormsby model is equipped to handle such a rapidly varying motion history, and this must be kept in mind during an analysis.

It does appear, however, that even in this more complex case, the nonlinear filter is able to contain the confused perceptions associated with transferring the pulse train to the motion base. Figure 4.10 shows that even the commanded input has wide motion discontinuity, which might lead to the conclusion that the Ormsby model has trouble handling this complex pulse train. Again, the perceived velocity gradually increases to a maximum, at about ten seconds. Had the experiment been continued past nineteen seconds, the zero perceived velocity level would presumably gradually be reached. While there is some room for argument that the nonlinear filter better presents the motion cues in this case, it is a tenative argument at best.

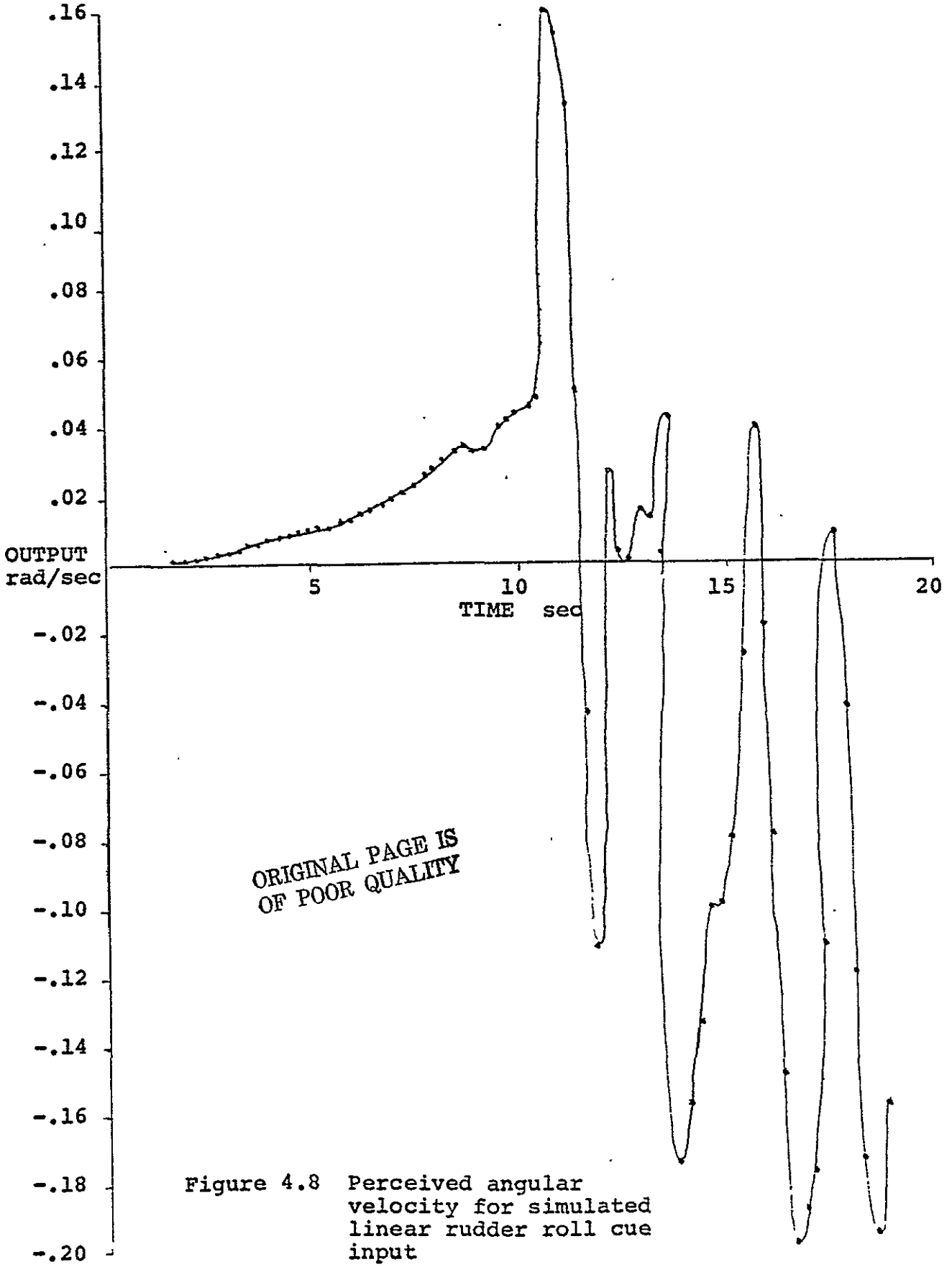

ORIGINAL PAGE IS
OF POOR QUALITY

Figure 4.8 Perceived angular velocity for simulated linear rudder roll cue input

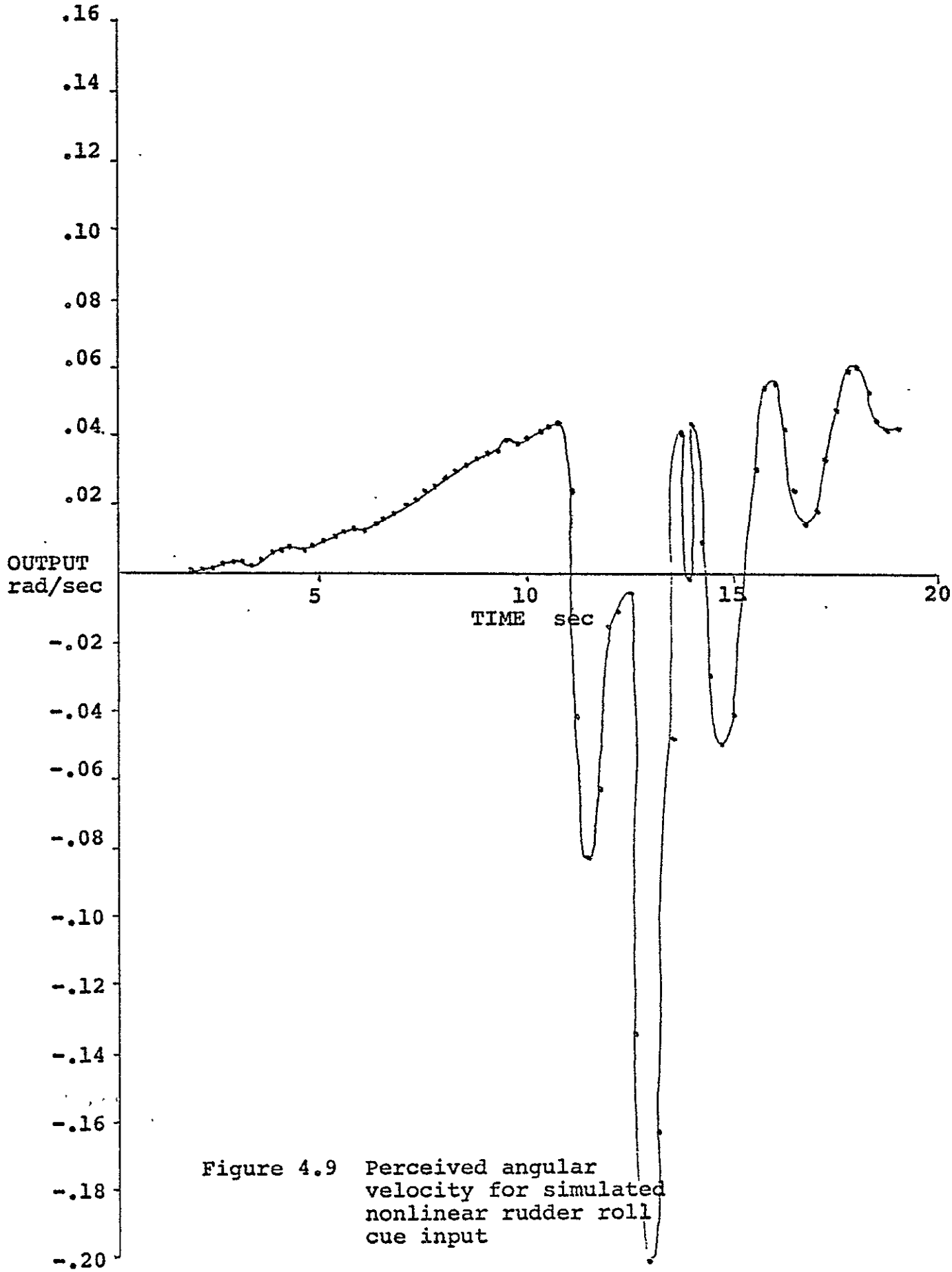

Figure 4.9 Perceived angular velocity for simulated nonlinear rudder roll cue input

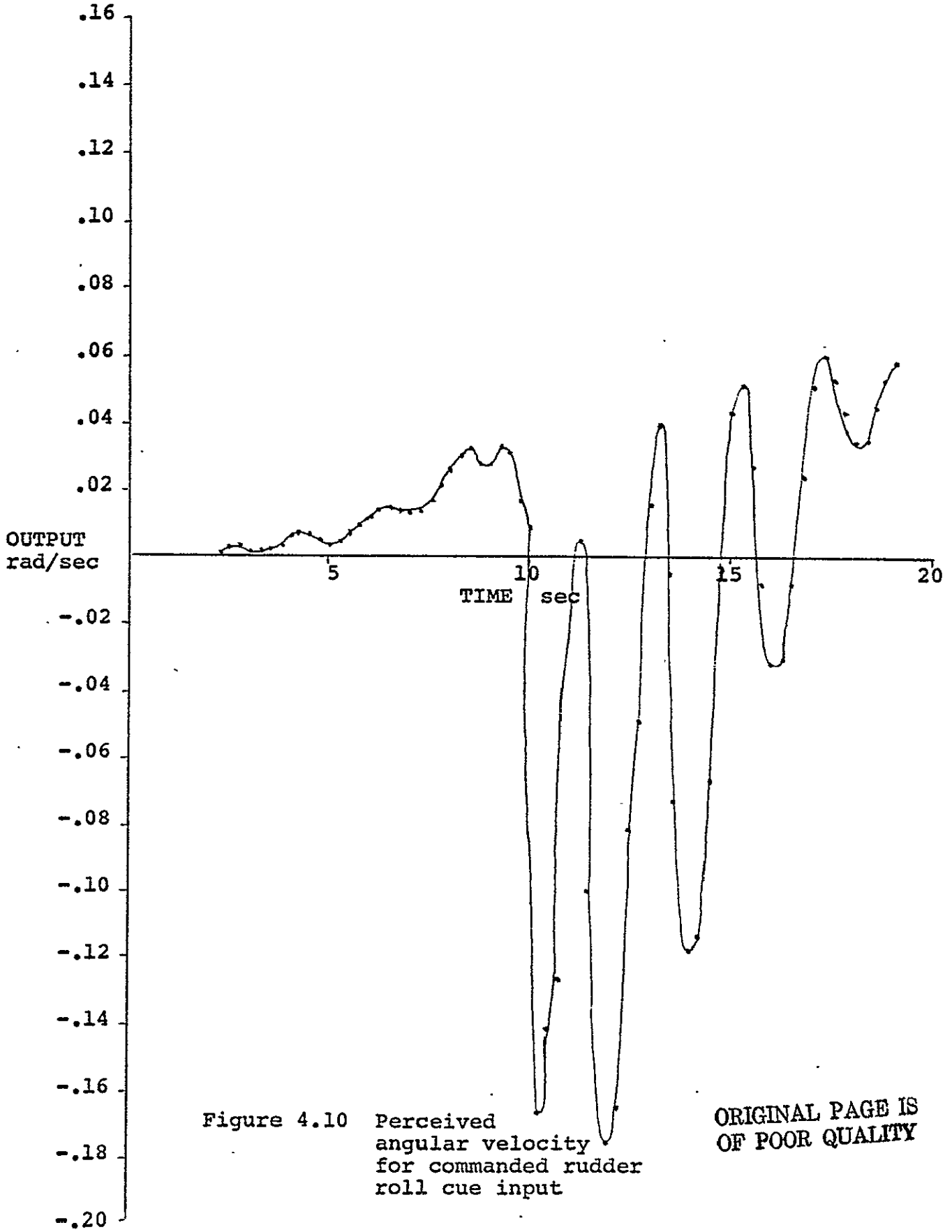

Figure 4.10 Perceived angular velocity for commanded rudder roll cue input

ORIGINAL PAGE IS
OF POOR QUALITY

4.5 Rudder Yaw Cues

Figures 4.11, 4.12 and 4.13 present the final case - the perceived velocities obtained from rudder yaw cues. As in the previous case of rudder roll cues, the motion history is a complicated pulse-like train. But unlike the roll cues, the yaw cues seem to be transferred to the motion base more reliably. This was also true in the case of aileron inputs.

The motion histories for rudder yaw cues are similar for the first ten seconds. This is attributed to the slow rise in angular velocity perception seen previously. The ten second rise time agrees with the rudder roll cue case. The nonlinear filter again does a better job of containing the discontinuous motion than does the linear filter. The commanded case is smoother than the simulated case, but the nonlinear filter does not change the commanded motion very much in the transfer to the motion base.

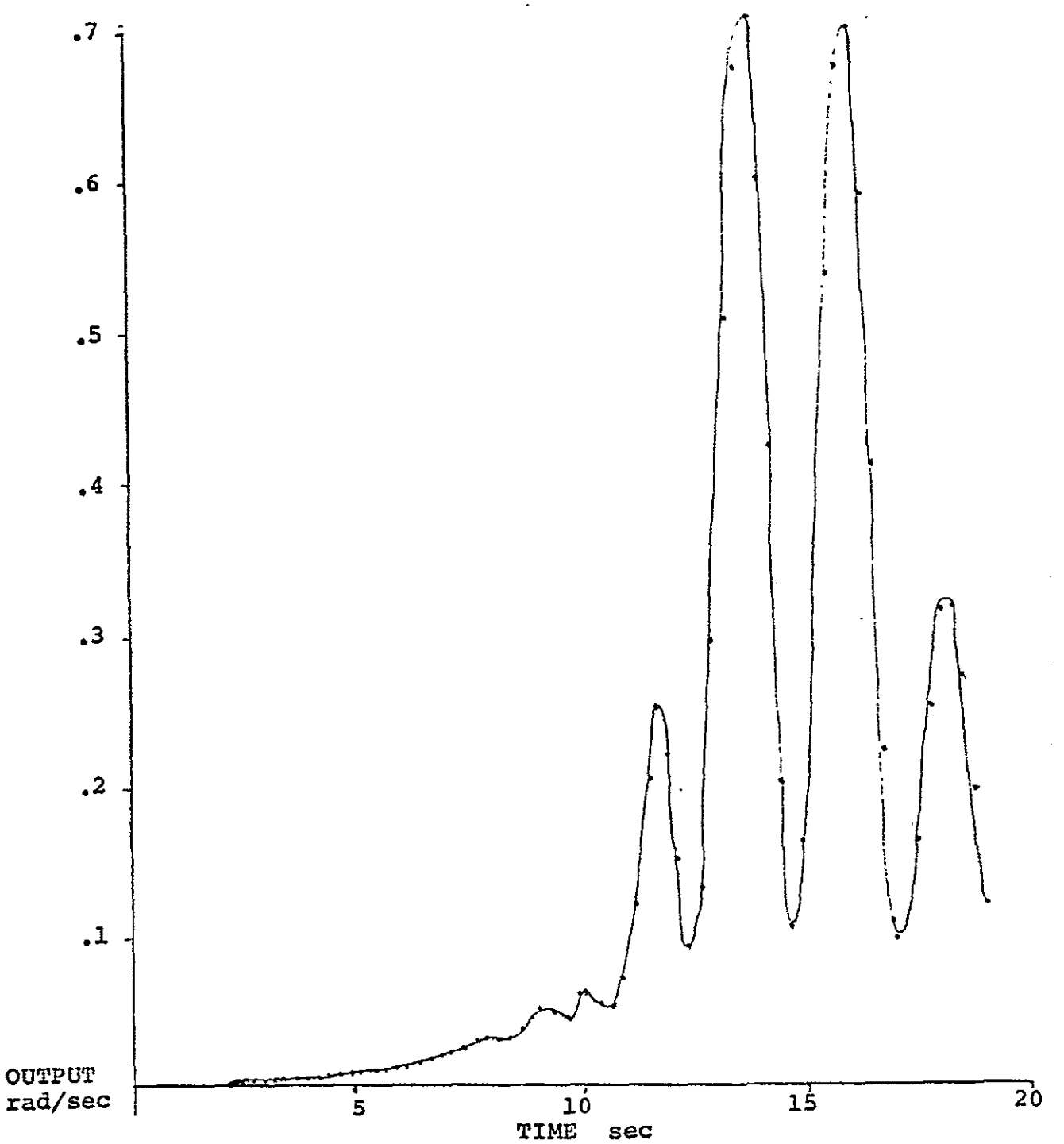

Figure 4.11 Perceived angular velocity for simulated linear rudder yaw cue input

ORIGINAL PAGE IS
OF POOR QUALITY

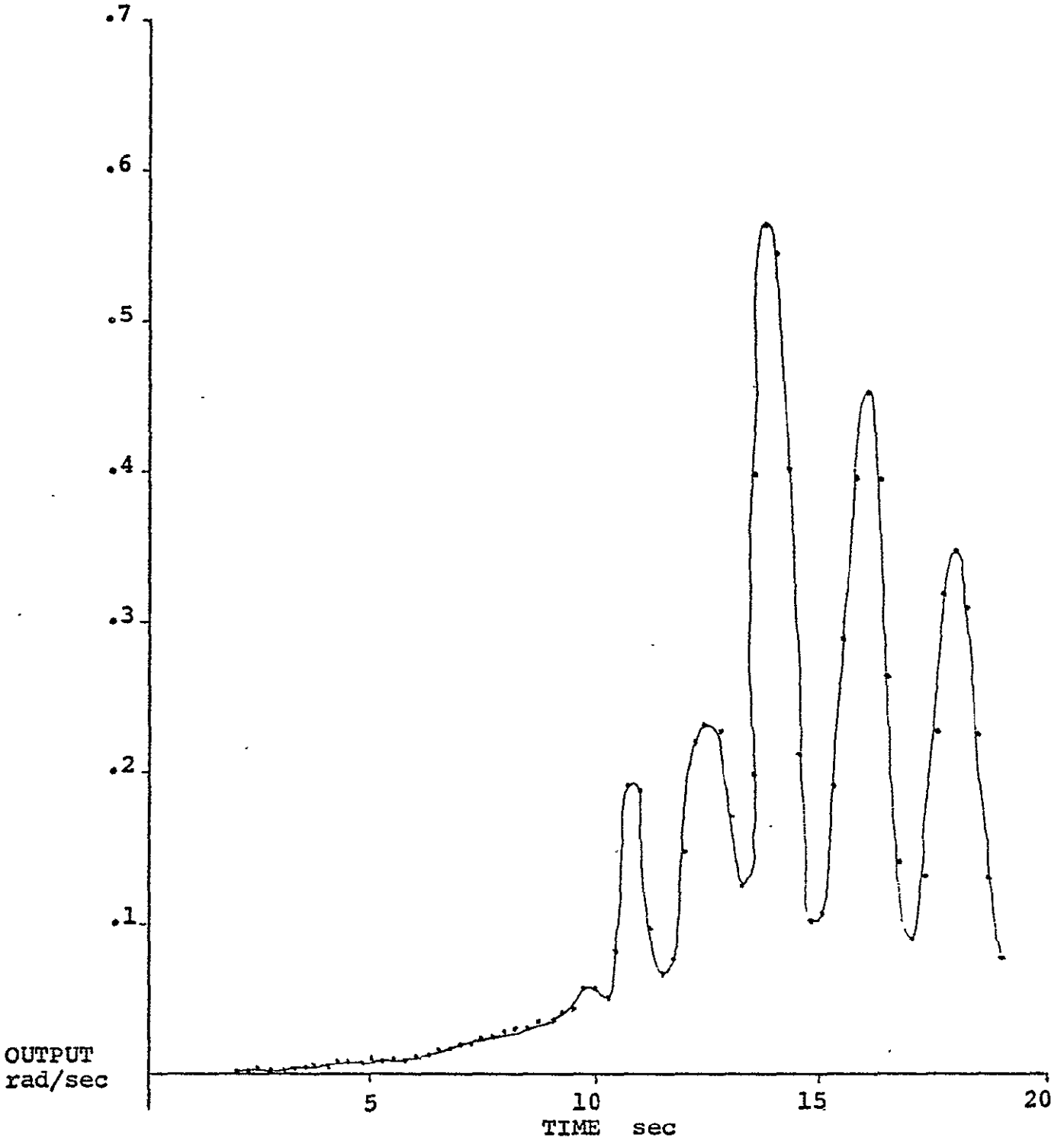

Figure 4.12 Perceived angular velocity for simulated nonlinear rudder yaw cue input

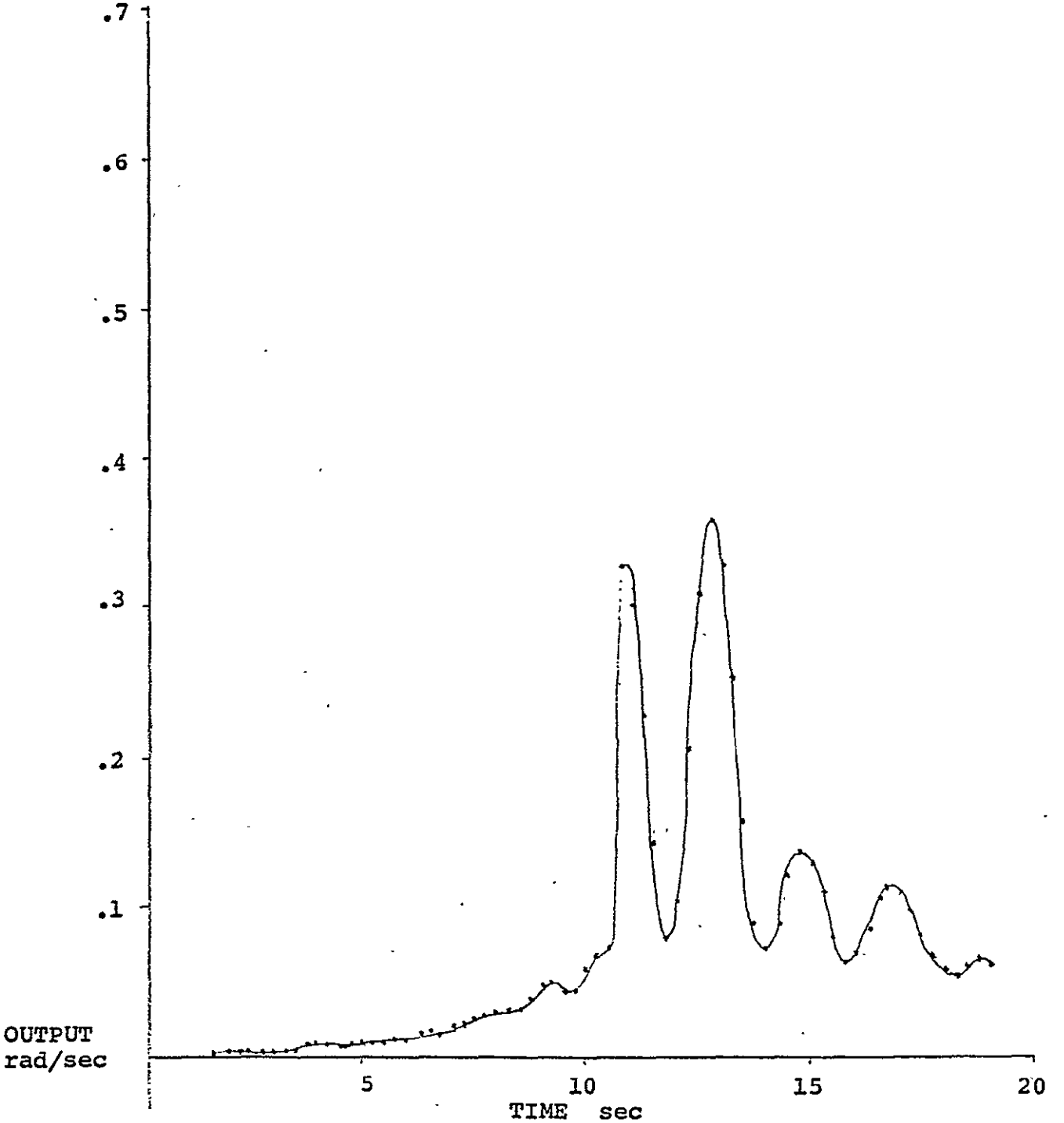

Figure 4.13 Perceived angular velocity for commanded rudder yaw cue input

ORIGINAL PAGE IS
OF POOR QUALITY

4.6 Results

The purpose of this investigation was to determine whether or not there is a vestibular explanation for the results obtained by Parrish and Martin. These results (reported on in Chapter II) indicated that a nonlinear washout scheme provided better simulation fidelity than did the linear washout scheme. This result was not due to the fact that the nonlinear filter presented more of the motion cue; rather, it eliminated the false rate cue which arises in the use of the linear filter.

In order to accomplish the goal of providing a vestibular explanation for the anomalous rate cue, the motion histories from the Parrish and Martin study were input to the Ormsby human dynamic orientation model. Included were aileron and rudder motions with yaw and roll cues, for each of the two washouts. The output from the model is the perceived angular velocity of the pilot during the simulation.

The outputs for each of the motion histories were presented in the preceding sections. Several results can be pointed out:

- The yaw cues provide the most compelling case for a vestibular explanation. In the aileron yaw and the rudder yaw cases, the perceived angular velocities were "smoothed" considerably with the use of a nonlinear washout scheme as opposed to a linear washout scheme. The term

"smooth" refers to the ability of the nonlinear filter to present a continuous motion closely resembling the commanded motion, rather than the discontinuous motion presented by the linear filter. The discontinuity which accompanies the use of the linear filter has previously been described as the fundamental difference between the two filters - the anomalous rate cue. This false cue manifests itself in the form of a jump in the perceived angular velocity of the pilot.

- The results obtained for roll cue inputs were not so corroborative of the Parrish and Martin study as were the results for yaw cue inputs. They did, however, show some of the characteristics exhibited in the yaw cue case. The nonlinear filter contained the discontinuous jumps induced by the pulse train to a greater extent than the linear filter. The nonlinear filter was better able to transfer the commanded input to the motion base than the linear filter. This is evident in comparing Figures 4.11, 4.12 and 4.13.

- The explanation for the differences between the roll cues and the yaw cues most likely could be

found in examining the mechanical differences between motion in the two axes. Intuitively, it can be argued that the yaw motion simulation (twisting about earth vertical) is an easier task mechanically than roll motion simulation (twisting about the horizontal axis). No doubt a careful examination of the simulator base will reveal the cause of the differences observed.

- A comparison between the outputs for aileron and rudder inputs sheds some light on the usefulness of the Ormsby model. The aileron input consisted of two pulses, separated by thirteen seconds, while the rudder input was a train of pulses. The Ormsby model has never been used with a complicated input such as the rudder input. But despite the fact that the output contains large motion discontinuities, even for the commanded case, it is still possible to make a comparison between the linear and nonlinear schemes, and arrive at a conclusion similar to that reached in the aileron input case. Indeed, it does appear that the nonlinear filter contains the discontinuous perceived angular velocity more effectively than

the linear filter.

Thus it is seen that the Ormsby model provides a vestibular explanation for the subjectively acquired difference between the two washout schemes. The linear filter presents an anomalous rate cue as output from a pulse input, which the vestibular system transforms into a discontinuous perceived angular velocity. The nonlinear filter does not present this false cue, and the resulting vestibular transformation provides a much "smoother" perceived angular velocity. In addition, the comparison between the Ormsby model outputs from aileron and rudder cue inputs gives insight to the model's use as a simulator design tool.

CHAPTER V

CONCLUSIONS

This thesis began with a discussion of the importance of motion simulation in general, and went on to examine a particular aspect of simulation - the washout filters used to constrain the motion of the simulator and maintain the fidelity of the simulation. The two washout schemes examined here were a linear washout and a nonlinear washout. They differed in the types of filters used to washout translational cues. The linear washout was seen to present a false rate cue in response to a pulse input. A subjective analysis of these two filters revealed that this false cue causes pilots to rate the fidelity of a simulation using the linear filter much lower than the same simulation using the nonlinear filter.

Examination of physiological models of human dynamic orientation led to the notion that such a model could be useful in comparing simulation schemes. The model used in this work, conceived by Ormsby, draws primarily on knowledge of the orientation information provided by processing information from the vestibular organs. Time histories for different motions were

input to the model in order to evaluate the vestibular reaction to the linear and nonlinear filtering schemes. It was found that indeed the vestibular system reacts differently to the motion histories produced by the two filters.

The next two sections present the conclusions of this work as they relate to the following two questions, first posed in the introduction:

- Can the observed differences in simulation fidelity between the two filters be explained using a physiological model of human dynamic orientation?
- What are the implications for this model as a drawing board tool in simulator design?

The final section suggests avenues for further research in this area.

5.1 The Vestibular Explanation Question

Figures 5.1 and 5.2 present a recapitulation of figures shown in Chapter IV. They are the Ormsby model outputs for aileron yaw and rudder yaw cues, respectively, and they present the best cases for a vestibular explanation of the subjectively observed anomalous rate cues. In each case, the perceived angular velocity shows the expected gradual rise in reaction to the first acceleration in yaw. In the linear case, the second pulse (or pulses) causes discontinuities in the per-

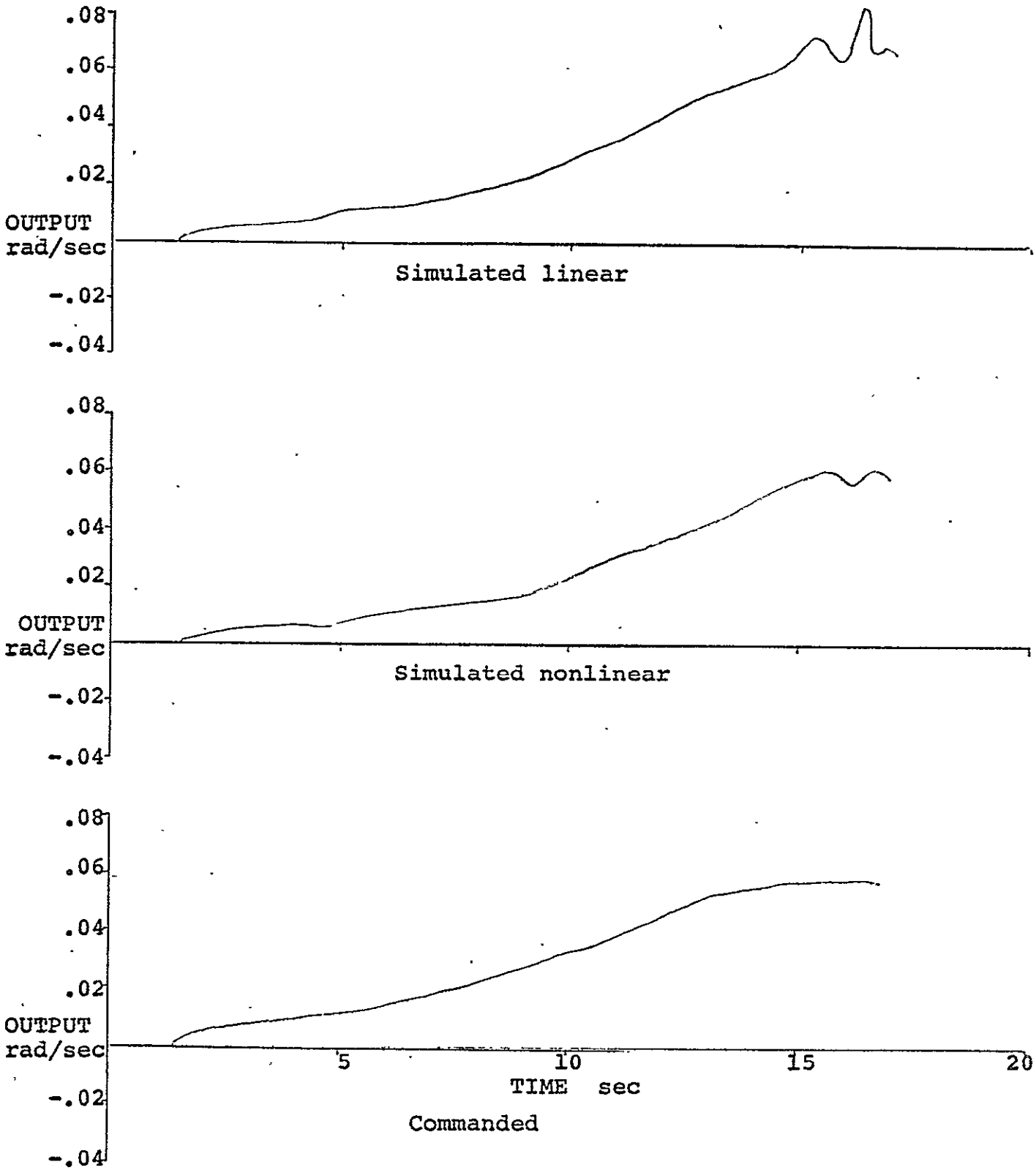

Figure 5.1 Perceived angular velocity for three aileron yaw cue inputs.

ORIGINAL PAGE IS
OF POOR QUALITY

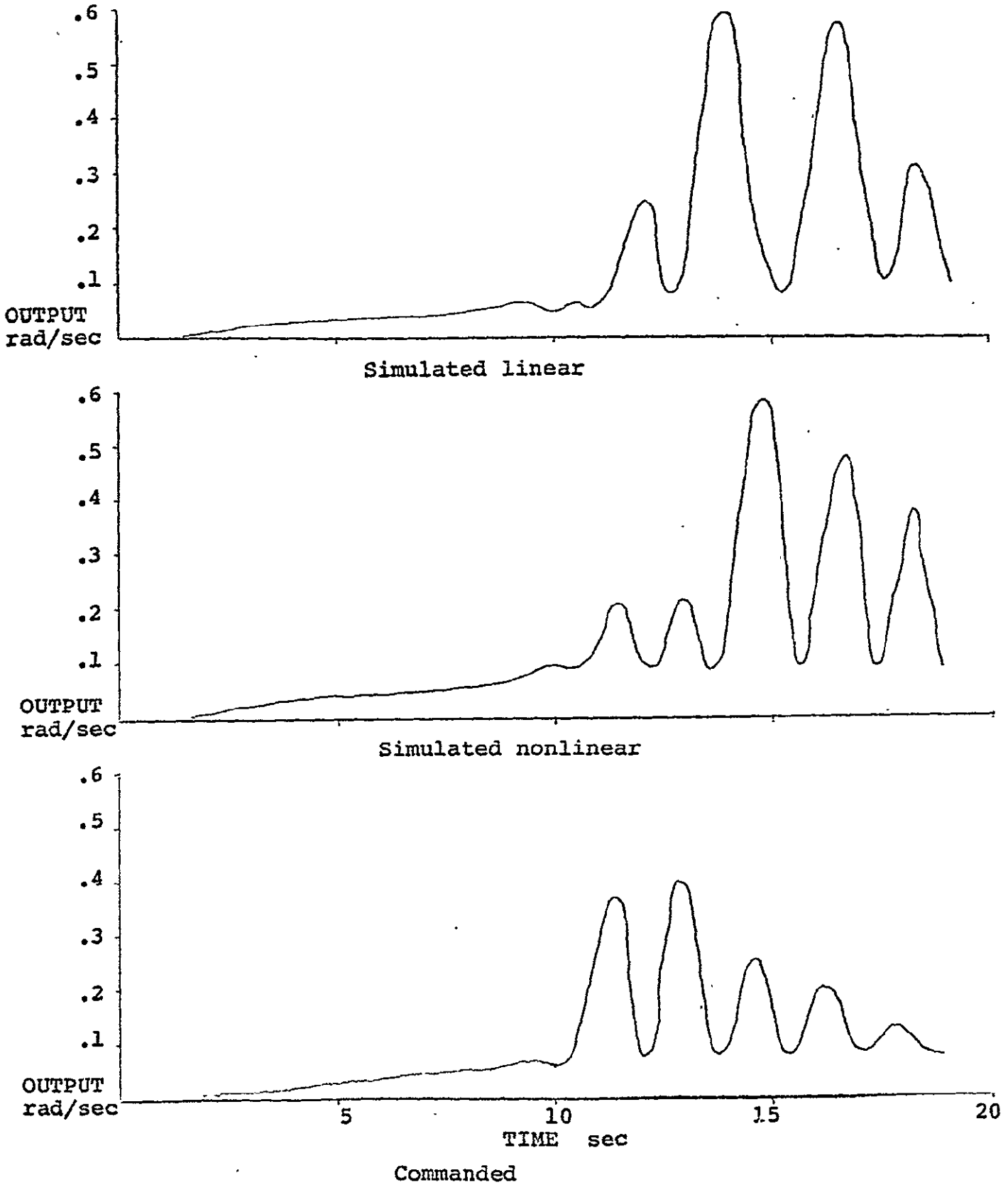

Figure 5.2 Perceived angular velocity for three rudder yaw cue inputs.

ceived velocities. In the nonlinear cases, these disturbances are considerably reduced. This is best seen in comparing the simulated velocities with the commanded velocities. It can be seen that the nonlinear filter is better able to transfer the commanded motions than the linear filter.

So, the physiological model enables a quantitative evaluation of the differences in washout schemes to become a reality. It is now possible to know the outputs from the vestibular sensors and to deduce a reason for the subjective ratings of the two methods. Indeed, there is an anomalous rate cue sensed by the vestibular system - it manifests itself as a discontinuous perceived angular velocity when the linear washout scheme is used, and that discontinuity is lessened considerably when the nonlinear scheme is used.

The physiological model has performed the task demanded of it - it provided a vestibular explanation for the subjectively observed differences between the two washout schemes. That difference was found in the differing perceived angular velocities which are the outputs from the model.

While this was only a limited test of the perceptions involved in the motion simulation, it seems to validate the conclusions reached in the Parrish and Martin study. It is also an additional validation of the model - since the predicted response to a pulse input is a gradual rise in perceived angular velocity to a maximum, and this is what was seen in every case,

the model appears to be functioning at a level consistent with available knowledge of the vestibular output.

5.2 The Suitability as a Design Tool Question

The question of the physiological model's appropriateness for use as a simulator design tool is a more difficult question to answer than the previous one. Certainly one could imagine the usefulness of such a model in simulation design. But the present case is a very limited one, and the small scope of this work should be taken into account in any conclusions which are drawn.

Figures 5.3 and 5.4 present the roll cue input cases, as first presented in Chapter IV. The roll inputs did not propose as compelling a case for a vestibular explanation as the yaw inputs. But these figures are offered so that a comparison between the aileron and rudder cases can be made. It is important to remember that the inputs for the two cases are very different - the aileron input is basically a pulse doublet, but the rudder input is a train of pulses. From this narrow investigation it is hard to say whether the model really gives an accurate picture of the response to a complicated motion history such as the rudder pulse train input.

Assuming the model is proven to accurately portray the vestibular response to a complicated input, it appears that the model is applicable for simulation design purposes. In this

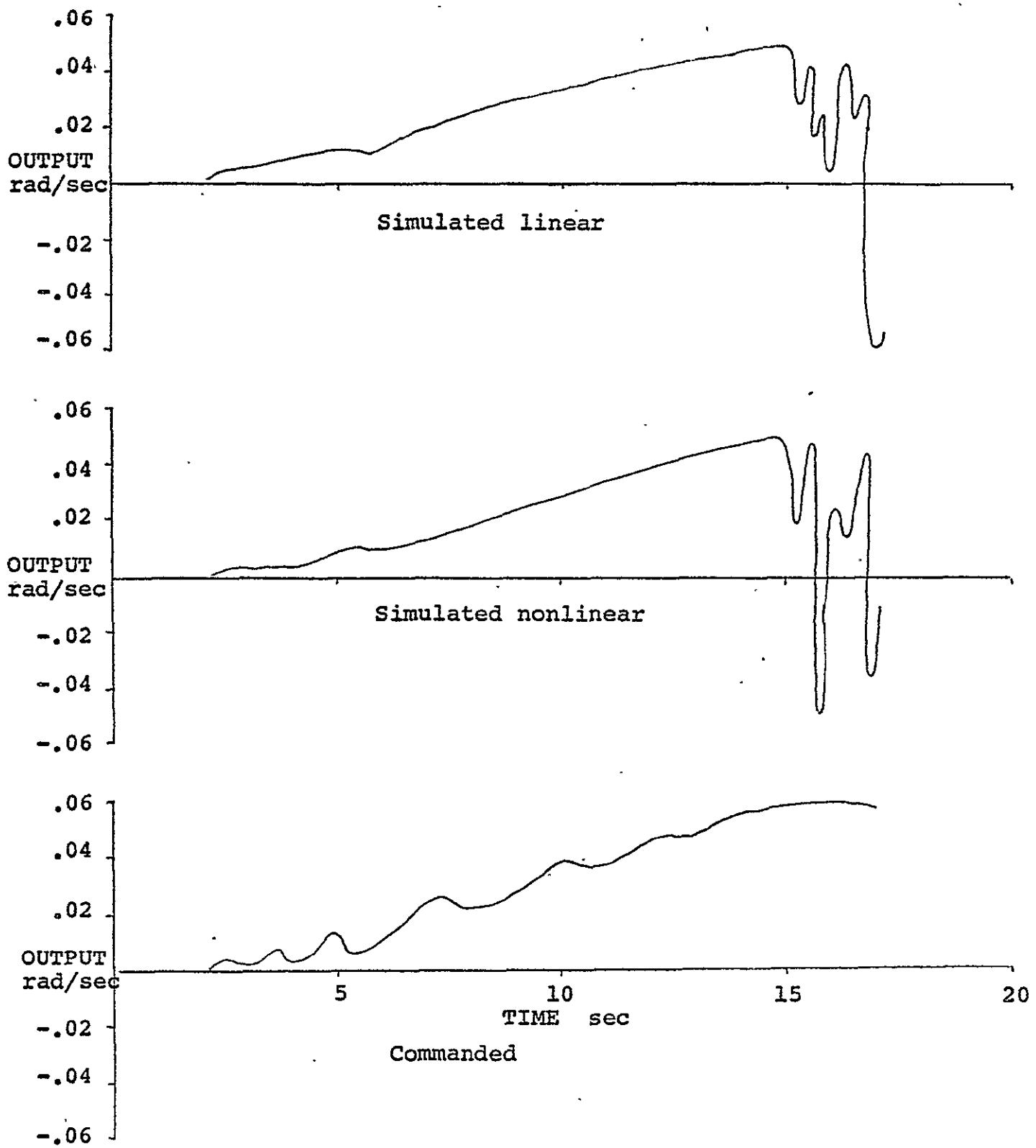

Figure 5.3 Perceived angular velocity for three aileron roll cue inputs.

ORIGINAL PAGE IS
OF POOR QUALITY

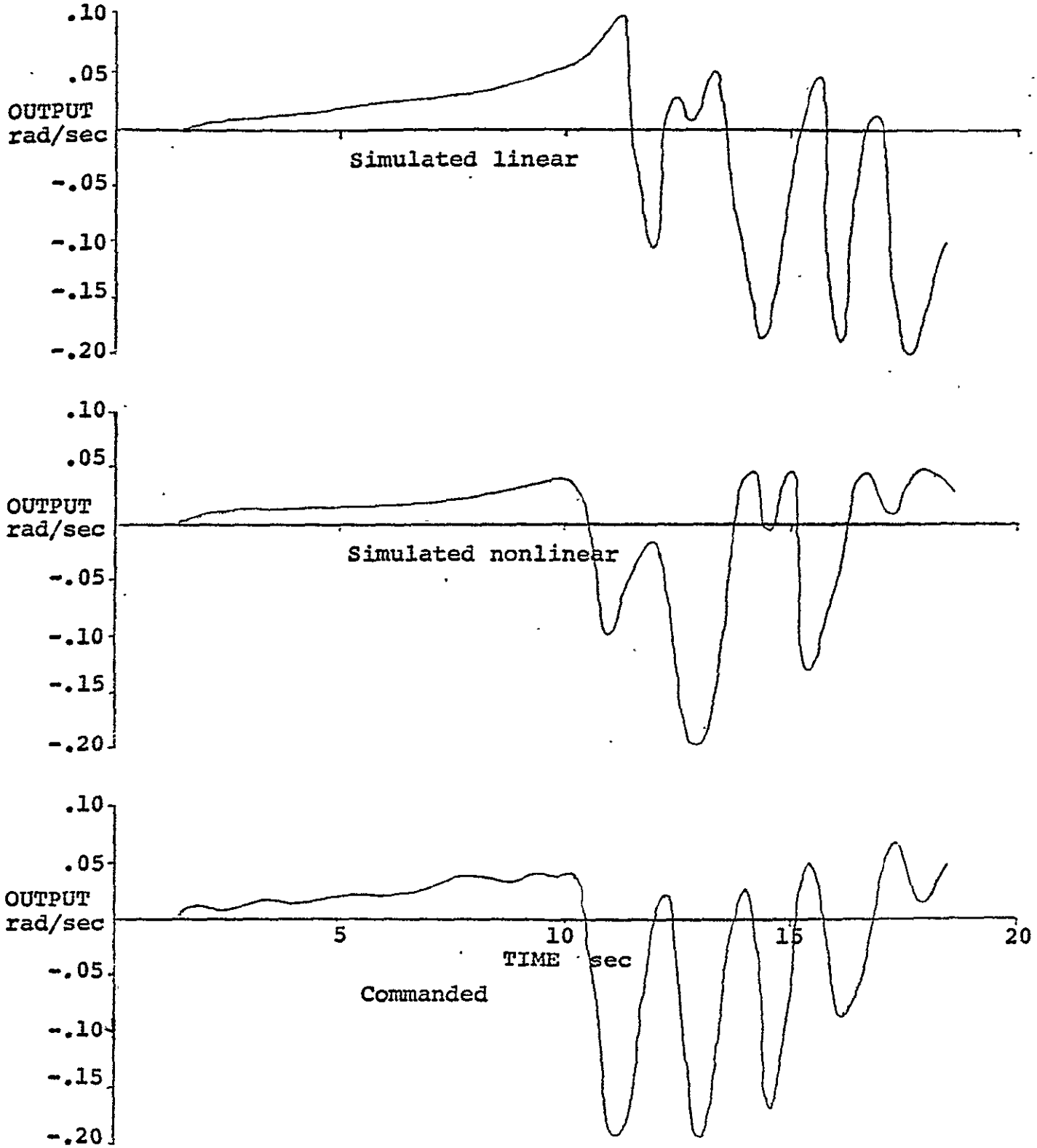

Figure 5.4 Perceived angular velocity for three rudder roll cue inputs.

case, had the washout schemes been simulated on the computer rather than using a computer only to simulate the aircraft which in turn drives the motion base, the same motion histories could have been obtained. Then, without the necessity of setting up an actual motion base, the same time histories could have been procured. Once input to the Ormsby model, the output would have shown the differences in simulation fidelity between the two washout schemes. The same conclusions could have been reached without ever having to use an actual mechanical simulator.

Thus, assuming the motion history of the part of the simulator to be analyzed is sufficiently defined such that a computer simulation program can be written, the Ormsby model can predict pilot perceived angular velocities from that motion simulation. There is no need to use an actual mechanical simulator, and no need to employ pilots for subjective analyses. The model is able to do the comparisons and predictions with confidence.

C-2

5.3 Suggestions for Further Research

This work opens up several areas for further research:

1. It would be useful to understand how certain parameters in each of the washout schemes affects the resulting motions of the simulator base, and the resulting perceived angular velocities of the pilot. By varying different parameters (such as in the preliminary filters or braking acceleration logic) new motion histories could be obtained. These, in turn, when input to the Ormsby model, could provide new insight into the workings of washout schemes.

2. There are several revisions which suggest themselves in regards to the Ormsby model. The necessity for tuning could be eliminated were the Kalman filters to be replaced by continuous Kalman filters, rather than the discrete filters currently in use. Also, more work should be done to verify that the model is indeed capable of handling complex motion histories. Finally, the model might be expanded to include visual and tactile cues, as well as the vestibular cues it now employs.

3. The model should be subjected to more rigorous tests of its ability to be used as a simulator design tool. One way which immediately suggests itself is to take a case such as the one examined here and do the testing in the opposite order. That is, run the motion

histories through the model, and then let the pilots do a subjective analysis. More extensive use of the model will suggest areas for improvement, and begin to perfect it as a simulator design tool.

APPENDIX

This appendix contains programming material used in the work presented in this thesis. The Man-Vehicle Laboratory's PDP 11/34 was the computer used for these FORTRAN programs. Most of the documentation for the main Ormsby programs and associated subroutines is taken from Borah [3].

A.1 Human Dynamic Orientation Model

The listing which follows is the main module which implements the Ormsby model of human dynamic orientation. Several changes have been made to the original program (the first three by Borah):

1. Statements and routines which allowed for varying afferent base rates and additive random noise have been eliminated. Thus, all responses are average responses, and firing rates are those above the spontaneous rate.
2. Statements were added to allow for non-zero long time constant, τ_L (variable TW in the program).
3. Comment cards were added for clarification.

4. Statements were added to calculate state transition matrices for any given update interval, for both canals and otoliths. Vectors TC, TPC, TO and TPO are no longer data entries.

5. DATA statements replace data input cards.

6. Kalman gains GKO and GKS were calculated for a .25 second update interval, rather than the 1.0 second interval used by Ormsby and Borah.

Table A.1 lists the variables found in this program and their definitions. Several subroutines are needed to use this program and they are described in the next sections. Following the listing is a sample page of output. Table A.2 describes the output variables seen on this page.

```
C
C       HUMAN DYNAMIC ORIENTATION PROGRAM
C
      DIMENSION RNP(201),TC(4,4),TO(3,3),TPC(3,3),TPO(2,2),DVC(3),
     1 DVO(2),CC(4),CO(3),THO(6),XCH(4),YCH(4),ZCH(4),CS(3),XOH(3),
     2 WOH(3),YOH(3),ZOH(3),XC(3),YC(3),ZC(3),XO(2),YO(2),GKU(3),
     3 GKS(3),ZO(2),CTC(3,3),CTO(3,3),VBRC(3),VBRO(3),A(3),AC(3),
     4 GKC(4),TWH(3),TAH(3),TOH(3),TWS(3),TAS(3),AO(3),WO(3),Y(3),
     5 DOLD(3),DNEW(3),EWS(3),EWH(3),EAH(3),WPARE(3),WPERP(3),WTOT(3),
     6 EAS(3),WSFU(3),WNCO(3),WNCL(3),FN(3),X(3),VO(3),VG(3),VF(3)
C
C       DATA STATEMENTS
C
      DATA DPR /57.29578/
      DATA DT /.2500000000E 00/
      DATA NITP /8/
      DATA NDT /240/
      DATA DVC /0.22415070E-04,0.47300120E-03,0.49580180E-02/
      DATA CC /-0.23578510E 02,-0.11318880E 04,-0.63718550E 04,
     1         0.63641970E 02/
      DATA GKC /-0.91917720E-03,0.81415620E-05,0.15035120E-03,
     1          0.30559980E-01/
      DATA FSCC /1.57080000E 00/
      DATA TSCC /-0.43633000E 00/
      DATA SSCC /-0.78540000E 00/
      DATA DVO /0.47050430E-03,0.49058940E-02/
      DATA CO /1.80000000E 03,1.80000000E 04,0.00000000E 00/
      DATA GKO /0.6977585E-06,0.5310665E-05,0.10602555E-02/
      DATA GKS /0.1395517E-05,0.1062133E-04,0.2120511E-02/
      DATA FOTO /1.57080E 00/
      DATA TSTO /-0.43633E 00/
      DATA SOTO /-1.57080E 00/
      DATA SACFAC /0.50000E 00/
      DATA OSPG /4.50000E 01/
      DATA DFAC /0.45000E 00/
      DATA XCH /0.00000000E 00,0.00000000E 00,0.00000000E 00,
     1          0.00000000E 00/
      DATA YCH /0.00000000E 00,0.00000000E 00,0.00000000E 00,
     1          0.00000000E 00/
      DATA ZCH /0.00000000E 00,0.00000000E 00,0.00000000E 00,
     1          0.00000000E 00/
      DATA XOH /-0.05280000E-01,-0.06660000E-06,-0.20000000E 00/
      DATA YOH /0.00000000E 00,0.00000000E 00,0.00000000E 00/
      DATA ZOH /-0.11325000E-01,-0.12650000E-06,-0.42000000E 00/
      DATA XC /0.00000000E 00,0.00000000E 00,0.00000000E 00/
      DATA YC /0.00000000E 00,0.00000000E 00,0.00000000E 00/
      DATA ZC /0.00000000E 00,0.00000000E 00,0.00000000E 00/
      DATA WNCO /0.00000000E 00,0.00000000E 00,0.00000000E 00/
      DATA WNCL /0.00000000E 00,0.00000000E 00,0.00000000E 00/
      DATA XO /-0.10533720E 01,-0.15328110E-06/
      DATA YO /0.00000000E 00,0.00000000E 00/
      DATA ZO /-0.2[illegible]E-01, 0.[illegible]460E-06/
```

ORIGINAL PAGE IS
OF POOR QUALITY

```
      DATA DOLD /0.00000000E 00,0.00000000E 00,-1.00000000E 00/
      DATA WSFO /0.00000000E 00,0.00000000E 00,0.00000000E 00/
      DATA WOF /0.00000000E 00,0.00000000E 00,0.00000000E 00/
      DATA TDVEL /3.50000000E 01/
      DATA TDPOS /6.00000000E 01/
      DATA TNC /0.25000000E 00/
      DATA FNOISE /0.00000000E 00/
C
C       SET UP FILE ASSIGNMENTS
C
      CALL ASSIGN(21,'DK1:DBLT.NON')
      CALL ASSIGN(22,'DK1:RESULT.SAR')
      WRITE(22,5)
5     FORMAT(' LINEAR AILERON ROLL 1 ')
C
C
C
      WRITE(22,700) DT,NITP
      WRITE(22,705)
C
C       CANAL SPECIFICATIONS
C
      CALL STMC(DT,NITP,TPC,TC)
      DO 10 I=1,4
10    WRITE(22,710) TC(I,1),TC(I,2),TC(I,3),TC(I,4)
      DO 15 I=1,3
15    WRITE(22,720) TPC(I,1),TPC(I,2),TPC(I,3),DVC(I)
      WRITE(22,730) CC(1),CC(2),CC(3),CC(4)
      WRITE(22,740) GKC(1),GKC(2),GKC(3),GKC(4)
      WRITE(22,750) FSCC,TSCC,SSCC
      CALL EULER(FSCC,TSCC,SSCC,CTC)
      WRITE(22,765)
C
C       OTOLITH SPECIFICATIONS
C
      CALL STMO(DT,NITP,TPO,TO)
      DO 20 I=1,3
20    WRITE(22,770) TO(I,1),TO(I,2),TO(I,3)
      DO 25 I=1,2
25    WRITE(22,780) TPO(I,1),TPO(I,2),DVO(I)
      WRITE(22,790) CO(1),CO(2),CO(3)
      WRITE(22,800) GKO(1),GKO(2),GKO(3),GKS(1),GKS(2),GKS(3)
      WRITE(22,810) FOTO,TOTO,SOTO,SACFAC,OSFG,DFAC
      CALL EULER(FOTO,TOTO,SOTO,CTO)
      DO 27 I=1,3
27    CS(I)=CO(I)*SACFAC
      WRITE(22,825)
C
C       INITIALIZATION
C
      DO 32 I=1,4
32    WRITE(22,830) XCH(I),YCH(I),ZCH(I)
```

```
      A(1)=XCH(4)
      A(2)=YCH(4)
      A(3)=ZCH(4)
      CALL COTRN(A,CTC,1,WO)
      DO 36 I=1,3
36    WRITE(22,836) XOH(I),YOH(I),ZOH(I)
      A(1)=XOH(3)
      A(2)=YOH(3)
      A(3)=ZOH(3)
      CALL COTRN(A,CTO,1,AO)
      DO 45 I=1,3
45    WRITE(22,850) XC(I),YC(I),ZC(I)
      DO 50 I=1,2
50    WRITE(22,855) XO(I),YO(I),ZO(I)
      WRITE(22,875) DOLD(1),DOLD(2),DOLD(3)
      FP=1.0-EXP(-DT/TDPOS)
      FD=TDVEL
      WRITE(22,880) TDVEL,TDPOS,TNC,FP,FNOISE
      FN(1)=EXP(-DT/TNC)
      FN(2)=TNC*(1.-FN(1))/DT-FN(1)
      FN(3)=1.-TNC*(1.-FN(1))/DT
C
C      MAIN PROGRAM CYCLE
C
C      FIND CURRENT STIMULUS IN HEAD COORDINATES
C      (EVERY DT/NITP SEC.):
C        1. ANGULAR ROTATION VECTOR (TWH) AT (TIME).
C        2. SPECIFIC FORCE VECTOR (TAH) AT (TIME+DT/2).
C        3. TRUE DOWN VECTOR AT (TIME+DT/2).
C
      DO 450 ITIME=1,NDT
      DO 100 I=1,NITP
      TIME=(ITIME-1)*DT+I*DT/NITP
      CALL STIM(TIME,TWH,TAH,TDH)
C
C      TRANSFORM TO SENSOR COORDINATES
C
      CALL COTRN(TWH,CTC,0,TWS)
      CALL COTRN(TAH,CTO,0,TAS)
C
C      SENSOR STIMULATION (EVERY DT/NITP SEC.):
C        USING CURRENT STIMULUS VALUES, UPDATE STATE
C        VECTORS FOR 3 CANALS (XC,YC AND ZC), AND
C        3 OTOLITHS (XO,YO AND ZO), AND COMPUTE
C        AFFERENT FIRING RATES (CSX,CSY,CSZ,OSX,OSY,OSZ).
C
      S=TWS(1)
      CALL SVUPD(XC,TPC,DVC,S,CSX,CC,3,4)
      S=TWS(2)
      CALL SVUPD(YC,TPC,DVC,S,CSY,CC,3,4)
      S=TWS(3)
      CALL SVUPD(ZC,TPC,DVC,S,CSZ,CC,3,4)
```

ORIGINAL PAGE IS
OF POOR QUALITY

```
      S=TAS(1)
      CALL SVUPD(XO,TPO,DVO,S,OSX,CO,2,3)
      S=TAS(2)
      CALL SVUPD(YO,TPO,DVO,S,OSY,CO,2,3)
      S=TAS(3)
100   CALL SVUPD(ZO,TPO,DVO,S,OSZ,CS,2,3)
C
C      OPTIMAL ESTIMATOR (UPDATE EVERY DT SEC.):
C        GET CANAL AND OTOLITH SYSTEM STATE ESTIMATES FROM
C        STEADY STATE KALMAN FILTERS.
C
      CALL SSKF(XCH,CSX,TC,CC,GKC,4)
      CALL SSKF(YCH,CSY,TC,CC,GKC,4)
      CALL SSKF(ZCH,CSZ,TC,CC,GKC,4)
      CALL SSKF(XOH,OSX,TO,CO,GKO,3)
      CALL SSKF(YOH,OSY,TO,CO,GKO,3)
      CALL SSKF(ZOH,OSZ,TO,CS,GKS,3)
C
C      ENTER ROTATION RATE ESTIMATE VECTOR (CANAL ESTIMATE).
C
      EWS(1)=XCH(4)
      EWS(2)=YCH(4)
      EWS(3)=ZCH(4)
C
C      ENTER SPECIFIC FORCE ESTIMATE VECTOR (OTOLITH ESTIMATE).
C
      EAS(1)=XOH(3)
      EAS(2)=YOH(3)
C
C      SACCULE NON-LINEARITY
C
      EAS(3)=AMAX1(.6*(ZOH(3)+.4169)-.4169,-.4169)
C
C      RESTORE MAGINITUDE OF OTOLITH ESTIMATE TO VALUE HELD
C      BEFORE CONSIDERATION OF SACCULE NON-LINEARITY.
C      (THEREFORE, NON-LINEARITY EFFECTS ONLY DIRECTION OF
C      OTOLITH ESTIMATE).
C
      CALL NORM(EAS,Y)
      DO 130 I=1,3
      DUMMY=XOH(3)**2+YOH(3)**2+ZOH(3)**2
130   EAS(I)=SQRT(DUMMY)*Y(I)
C
C      TRANSFORM TO HEAD COORDINATES
C
      CALL COTRN(EWS,CTC,1,EWH)
      CALL COTRN(EAS,CTO,1,EAH)
C
C      PRINT STIMULUS,SENSOR AND OPTIMAL ESTIMATOR VALUES.
C
      WRITE(22,900) TIME
      WRITE(22,910) TWH(1),TWS(1),CSX,EWH(1),TAH(1),TAS(1),
```

```
     1              OSX,EAH(1),TDH(1)
      WRITE(22,910) TWH(2),TWS(2),CSY,EWH(2),TAH(2),TAS(2),
     1              OSY,EAH(2),TDH(2)
      WRITE(22,910) TWH(3),TWS(3),CSZ,EWH(3),TAH(3),TAS(3),
     1              OSZ,EAH(3),TDH(3)
      WRITE(22,920)
C
C      DOWN AND W ESTIMATOR (UPDATE EVERY DT SEC.).
C      COMBINE OTOLITH AND CANAL ESTIMATES TO FORM
C      NEW ESTIMATE OF:
C        1. PERCEIVED DOWN (DNEW) AT (TIME+DT/2).
C        2. PERCEIVED ACCELERATION (ACC) AT (TIME+DT/2).
C        3. PERCEIVED ANGULAR VELOCITY (WTOT) AT (TIME).
C
      CALL DOWN(DOLD,EWH,EAH,AO,WSFO,FD,DT,TDPOS,DFAC,WOF,
     1          WNCO,WNCL,FN)
450   CONTINUE
C
C      FORMAT STATEMENTS
C
700   FORMAT( //,'   UPDATE INTERVAL=',F5.2,'SECONDS.   ',
     1        'NUMBER ITERATIONS PER INTERVAL=',I3,//)
705   FORMAT(//,'          SEMI-CIRCULAR CANAL SYSTEM SPECIFICATIONS',/
710   FORMAT( '   CANAL TRANSITION MATRIX=',4E15.8)
720   FORMAT( '   CANAL SYS UPDATE MATRIX=',3E15.8,
     1        '   CANAL DRIVING VECTOR=',E15.8)
730   FORMAT(/,'   CANAL SYS OUTPUT MATRIX=',4E15.8,/)
740   FORMAT( '   CANAL SYS KALMAN GAINS =',4E15.8)
750   FORMAT(/,'   CANAL ORIENTATION WRT HEAD  PHI='E12.5,
     1        '  THETA=',E12.5,'  PSI=',E12.5,/)
765   FORMAT(////,'          OTOLITH SYSTEM SPECIFICATIONS',/)
770   FORMAT( '   OTOLITH TRANSITION MATRIX=',3E15.8)
780   FORMAT( '   OTOLITH SYS UPDATE MATRIX=',2E15.8,
     1        '   OTOLITH DRIVING VECTOR=',E15.8)
790   FORMAT(/,'   OTOLITH SYS OUTPUT MATRIX=',3E15.8)
800   FORMAT(/,'   UTR KAL GAINS=',3E12.5,'  SAC KAL GAINS=',
     1        3E12.5)
810   FORMAT(/,'   OTOLITH ORIENTATION WRT HEAD  PHI=',
     1        E12.5,'  THETA=',E12.5,'  PSI=',E12.5,/,
     2        '    SACFAC=',E12.5,'    O SENS PER G=',
     3        E12.5,'  O SYS GAIN (DFAC)=',E12.5,/)
825   FORMAT('1',///,'   SYSTEM INITIALIZATION',//)
830   FORMAT( '   INITIAL STATE ESTIMATES,  XCH,YCH,ZCH=',
     1        3E15.8)
836   FORMAT( '   INITIAL STATE ESTIMATES,  XOH,YOH,ZOH=',
     1        3E15.8)
850   FORMAT( '   TRUE CANAL STATE VECTORS XC,YC,ZC=',
     1        3E15.8)
855   FORMAT( '   TRUE OTOLITH STATE VECTORS XO,YO,ZO=',3E15.8)
875   FORMAT(/,'   DOLD(1,2,3)=',3E12.5,/)
880   FORMAT(/,'  DOWN RATE T=',E12.5,'  DOWN POS T=',E12.5,
```

ORIGINAL PAGE IS
OF POOR QUALITY

```
     1          '  NON CONF T CONS=',E12.5,'  POS ERROR FAC=',
     2        E12.5,/,'   SIGNAL NOISE FACTOR FNOISE=',E12.5,/,
     3        '1',//,'   SYSTEM SIMULATION',/////)
900    FORMAT(' T=',F6.2,'     W HD        W SENS       C SIG       '
     1        'C EST W HD     SF HD       SF SENS      O SIG
     2        'O EST SF     DOWN HD')
910    FORMAT('            ',9E12.5)
920    FORMAT(' '              RSCC         ROTO         RPOS
     1        'WPARE          WPERP        WTOT         DNEW',
     2        '          ACC')
       STOP
       END
STOP --
```

Table A.1 Variables used in main program

AO(I)	old otolith estimate
CC(I)	canal sensor output
CO(I)	utricle sensor output
CS(I)	saccule sensor output
CSX(I), CSY(I), CSZ(I)	current canal state vectors, sensor coordinates
CTC(I,J)	direction cosine matrix between head and canal, sensor coordinates
CTO(I,J)	direction cosine matrix between head and otolith, sensor coordinates
DFAC	steady-state gain of otolith estimate
DOLD(I)	old DOWN value (=.46)
DPR	degrees per radian (=57.29578)
DT	update interval for DOWN estimator
DVC(I)	canal sensor driving vector
DVO(I)	otolith sensor driving vector
EAH(I)	current otolith specific force estimate, head coordinates
EAS(I)	current otolith specific force estimate, sensor coordinates
EWH(I)	current canal angular velocity estimate, head coordinates
EWS(I)	current canal angular velocity estimate, sensor coordinates
FD	= TDVEL
FN(I)	constants for first-order filter
FNOISE	signal-to-noise factor
FOTO, SOTO, TOTO	Euler angles for head and otolith sensor coordinate transform
FP	position error factor
FSCC, SSCC, TSCC	Euler angles for head and canal sensor coordinate transform
GKC(I)	canal Kalman gains
GKO(I)	otolith (utricle) Kalman gains
GKS(I)	otolith (saccule) Kalman gains

ORIGINAL PAGE IS
OF POOR QUALITY

Table A.1 continued

NDT	length of motion history
NITP	number of sensor updates per DT
OSPG	otolith afferent firing rate per g
OSX(I), OSY(I), OSZ(I)	current otolith state vectors, sensor coordinates
SACFAC	saccule factor (=.5)
TAH(I)	current stimulus specific force, head coordinates
TAS(I)	current stimulus specific force, sensor coordinates
TC(I,J)	state transition matrix for canal Kalman filters
TDH(I)	DOWN
TDPOS	60 second time constant for DOWN position
TDVEL	35 second time constant for DOWN angular velocity
TIME	current time in seconds
TNC	.25 second time constant for unconfirmed canal estimate
TO(I,J)	state transition matrix for otolith Kalman filters
TPC(I,J)	state transition matrix for canal sensor update
TPO(I,J)	state transition matrix for otolith sensor update
TWH(I)	stimulus angular velocity, head coordinates
TWS(I)	stimulus angular velocity, sensor coordinates
WNCL(I)	low frequency portion of WNCO
WNCO(I)	previous unconfirmed canal angular velocity estimate
WO(I)	old otolith estimate
WOF(I)	low frequency portion of otolith angular velocity estimate

Table A.1 concluded

WSFO(I)	previous otolith angular velocity estimate
XC(I), YC(I), ZC(I)	old canal state vectors, sensor coordinates
XCH(I), YCH(I), ZCH(I)	current canal state vectors, sensor coordinates
XO(I), YO(I), ZO(I)	old otolith state vectors, sensor coordinates
XOH(I), YOH(I), ZOH(I)	current otolith state vectors, sensor coordinates

ORIGINAL PAGE IS
OF POOR QUALITY

```
T=  0.25     W HD        W SENS       C SIG      C EST W HD     SF HD       SF SENS       O SIG       O EST SF     DOWN HD
        -0.22990E-03-0.14733E-03-0.46307E-02-0.22082E-03 0.00000E+00-0.42262E+00-0.53976E+02-0.70889E-02 0.00000E+00
         0.00000E+00 0.14733E-03 0.46307E-02 0.50927E-11 0.00000E+00-0.15114E-05-0.12504E-03 0.57664E-06 0.00000E+00
         0.00000E+00 0.97158E-04 0.30537E-02 0.72760E-11-0.10000E+01-0.90631E+00-0.57076E+02-0.47301E+00-0.10000E+01
            RSCC        ROTO        RPOS        WPARE        WPERP        WTOT        DNEW        ACC
         0.34896E-04 0.22366E-08-0.14106E-06-0.55394E-12 0.00000E+00-0.55394E-12-0.10020E-03 0.78428E-02
        -0.80480E-12 0.30599E-04 0.69605E-04 0.19214E-12 0.00000E+00 0.19214E-12 0.34757E-04 0.15412E-04
        -0.53390E-09 0.00000E+00 0.24334E-08-0.11056E-07 0.00000E+00-0.11056E-07-0.10000E+01 0.13806E-01
T=  0.50     W HD        W SENS       C SIG      C EST W HD     SF HD       SF SENS       O SIG       O EST SF     DOWN HD
        -0.13216E-02-0.84697E-03-0.26655E-01-0.11467E-02 0.00000E+00-0.42262E+00-0.50008E+02-0.65646E-02 0.00000E+00
         0.00000E+00 0.84697E-03 0.26655E-01-0.68552E-10 0.00000E+00-0.15114E-05-0.11417E-03 0.48120E-06 0.00000E+00
         0.00000E+00 0.55854E-03 0.17578E-01-0.58208E-10-0.10000E+01-0.90631E+00-0.53622E+02-0.47187E+00-0.10000E+01
            RSCC        ROTO        RPOS        WPARE        WPERP        WTOT        DNEW        ACC
         0.15916E-03-0.12441E-06-0.80650E-06-0.27366E-10 0.00000E+00-0.27366E-10-0.20870E-03 0.64686E-02
         0.12036E-10 0.50930E-04 0.57570E-04 0.20176E-10 0.00000E+00 0.20176E-10 0.19299E-03 0.88294E-04
        -0.20002E-07 0.17827E-08 0.11279E-07-0.17718E-06 0.00000E+00-0.17718E-06-0.10000E+01 0.11875E-01
T=  0.75     W HD        W SENS       C SIG      C EST W HD     SF HD       SF SENS       O SIG       O EST SF     DOWN HD
        -0.81713E-03-0.52366E-03-0.16397E-01-0.33094E-04 0.00000E+00-0.42262E+00-0.46234E+02-0.22724E-02 0.00000E+00
         0.00000E+00 0.52366E-03 0.16397E-01 0.34253E-10 0.00000E+00-0.15114E-05-0.10382E-03 0.41163E-06 0.00000E+00
         0.00000E+00 0.34533E-03 0.10813E-01 0.26375E-10-0.10000E+01-0.90631E+00-0.49575E+02-0.46210E+00-0.10000E+01
            RSCC        ROTO        RPOS        WPARE        WPERP        WTOT        DNEW        ACC
        -0.11744E-03-0.35548E-06-0.30899E-06-0.16374E-11 0.00000E+00-0.16374E-11-0.23696E-03 0.21634E-02
        -0.16900E-10 0.87139E-05 0.19546E-04 0.90417E-12 0.00000E+00 0.98417E-12 0.74086E-04 0.34036E-04
         0.25022E-07 0.17559E-08 0.15369E-08-0.73480E-08 0.00000E+00-0.73480E-08-0.10000E+01 0.20962E-02
T=  1.00     W HD        W SENS       C SIG      C EST W HD     SF HD       SF SENS       O SIG       O EST SF     DOWN HD
         0.13582E+00 0.87039E-01 0.27349E+01 0.13112E+00 0.00000E+00-0.42262E+00-0.42645E+02 0.76289E-03 0.00000E+00
         0.00000E+00-0.87039E-01-0.27349E+01 0.20197E-08 0.00000E+00-0.15114E-05-0.93906E-04 0.35678E-06 0.00000E+00
         0.00000E+00-0.57398E-01-0.18036E+01 0.74506E-08-0.10000E+01-0.90631E+00-0.45726E+02-0.44656E+00-0.10000E+01
            RSCC        ROTO        RPOS        WPARE        WPERP        WTOT        DNEW        ACC
        -0.20769E-01-0.17833E-05 0.85415E-04 0.57505E-08 0.82726E-01 0.82726E-01-0.18209E-03-0.84666E-03
        -0.16061E-06-0.46827E-04-0.78335E-05 0.28216E-06 0.21926E-03 0.21954E-03-0.20609E-01-0.94803E-02
         0.44351E-05-0.30841E-08 0.14592E-06 0.27480E-04-0.19587E-04 0.78934E-05-0.99979E+00-0.13347E-01
T=  1.25     W HD        W SENS       C SIG      C EST W HD     SF HD       SF SENS       O SIG       O EST SF     DOWN HD
         0.63301E+00 0.40567E+00 0.12696E+02 0.53252E+00 0.00000E+00-0.42262E+00-0.39230E+02 0.39591E-02 0.00000E+00
         0.00000E+00-0.40567E+00-0.12696E+02-0.16337E-07 0.00000E+00-0.15114E-05-0.84627E-04 0.31517E-06 0.00000E+00
         0.00000E+00-0.26752E+00-0.83721E+01 0.00000E+00-0.10000E+01-0.90631E+00-0.42064E+02-0.42691E+00-0.10000E+01
            RSCC        ROTO        RPOS        WPARE        WPERP        WTOT        DNEW        ACC
        -0.71074E-01 0.36791E-04 0.37403E-03 0.12625E-07 0.28265E+00 0.28265E+00-0.12567E-03-0.40170E-02
        -0.37924E-06-0.16877E-04-0.38413E-04 0.45845E-05 0.22297E-03 0.22756E-03-0.91146E-01-0.41928E-01
         0.12351E-04 0.34118E-06 0.34687E-05 0.81866E-04-0.56076E-04 0.25790E-04-0.99504E+00-0.31174E-01
T=  1.50     W HD        W SENS       C SIG      C EST W HD     SF HD       SF SENS       O SIG       O EST SF     DOWN HD
         0.65281E+00 0.41836E+00 0.12946E+02 0.25746E+00 0.00000E+00-0.42262E+00-0.35981E+02 0.73046E-02 0.00000E+00
         0.00000E+00-0.41836E+00-0.12946E+02 0.82002E-07 0.00000E+00-0.15114E-05-0.75725E-04 0.28412E-06 0.00000E+00
         0.00000E+00-0.27589E+00-0.85374E+01 0.74506E-08-0.10000E+01-0.90631E+00-0.38581E+02-0.40442E+00-0.10000E+01
            RSCC        ROTO        RPOS        WPARE        WPERP        WTOT        DNEW        ACC
         0.17321E-01 0.29975E-04 0.29762E-03 0.18757E-08-0.70600E-01-0.70600E-01-0.44981E-04-0.74053E-02
        -0.74995E-06-0.60212E-05-0.73862E-04 0.18104E-05 0.32217E-03 0.32398E-03-0.73558E-01-0.33837E-01
        -0.20646E-05 0.54732E-06 0.54345E-05 0.21908E-04-0.20578E-04 0.13295E-05-0.99729E+00-0.54335E-01
```

ORIGINAL PAGE IS
OF POOR QUALITY

Table A.2 Variables output from model

W HD	angular velocity vector, head coordinates
W SENS	angular velocity vector, sensor coordinates
C SIG	canal signal: afferent firing rate from three canals
C EST W HD	canal estimate of angular velocity vector, head coordinates
SF HD	specific force vector, head coordinates
SF SENS	specific force vector, sensor coordinates
O SIG	otolith signal: afferent firing rate from three otoliths
O EST ST	otolith estimate of specific force vector, head coordinates
DOWN HD	unit vector in direction of gravity, head coordinates
RSCC	canal contribution to DOWN, head coordinates
ROTO	otolith contribution to DOWN, head coordinates
RPOS	rotation vector to null difference between SF and DOWN
WPARE	angular velocity perception parallel to DOWN, head coordinates
WPERP	angular velocity perception perpendicular to DOWN, head coordinates
WTOT	total perceived angular velocity, head coordinates
DNEW	perceived DOWN vector, head coordinates
ACC	perceived acceleration vector, head coordinates

A.2 Subroutine STIM

Subroutine STIM is the stimulus routine called by the main program. It is this program which is altered for different applications of the model. The particular subroutine listed here is the one used in this thesis research. Basically, it reads the data from the Langley motion histories from a file on a disk. The desired angular velocities are placed in the proper angular velocity vector locations by this program. Table A.3 lists the filenames, data locations and vector locations for each of the twelve cases examined. Table A.4 lists the variables used in this program,and their definitions.

Note that the STIM routine must return staggered angular velocity and specific force values, as required by the main program. The value of W must correspond to time T, while the values of A and D must correspond to time T+DT/2. This requirement is illustrated in Table A.5, which also gives the printout times for the variables which are output from the main program.

```
      SUBROUTINE STIM(T,W,A,D)
      DIMENSION W(3),A(3),D(3),DATA(6)
      DPR=57.29578
      DO 10 I=1,3
      W(I)=0.0
      D(I)=0.0
10    A(I)=0.0
      A(3)=-1.0
      D(3)=-1.0
      DO 20 I=1,5
      READ(21,15,ERR=16) (DATA(J),J=1,6)
15    FORMAT(1X,6E13.6)
      GO TO 18
16    WRITE(7,15) (DATA(K),K=1,6)
18    IF(I.EQ.2) W(1)=DATA(1)*T/DPR
20    CONTINUE
      RETURN
      END
STOP --
```

ORIGINAL PAGE IS
OF POOR QUALITY

Table A.3 Twelve test cases used by STIM

CASE	FILE NAME	DATA NAME & LOCATION *	ANGULAR VELOCITY VECTOR LOCATION
Simulated aileron linear roll	DBLT.LIN	PDOTM (4,2)	1
Simulated aileron nonlinear roll	DBLT.NON	PDOTM (4,2)	1
Commanded aileron roll	DBLT.LIN	PADOT (2,1)	1
Simulated aileron linear yaw	DBLT.LIN	RDOTM (4,4)	3
Simulated aileron nonlinear yaw	DBLT.NON	RDOTM (4,4)	3
Commanded aileron yaw	DBLT.LIN	RADOT (2,5)	3
Simulated rudder linear roll	RUDDR.LIN	PDOTM (4,2)	1
Simulated rudder nonlinear roll	RUDDR.NON	PDOTM (4,2)	1
Commanded rudder roll	RUDDR.LIN	PADOT (2,1)	1
Simulated rudder linear yaw	RUDDR.LIN	RDOTM (4,4)	3
Simulated rudder nonlinear yaw	RUDDR.NON	RDOTM (4,4)	3
Commanded rudder yaw	RUDDR.LIN	RADOT (2,5)	3

* Data location taken from a 5 X 6 matrix of variables listed in Table 4.1

Table A.4 Variables used in STIM

A(I)	stimulus specific force, head coordinates
D(I)	unit vector aligned with gravity, head coordinates
T	current time in seconds
W(I)	stimulus angular velocity, head coordinates

Table A.5 STIM variables and printout variables [3]

VARIABLE	COORDINATE FRAME	UNITS	STIM - COMPUTE VALUES AT TIMES T+DT/2	STIM - COMPUTE VALUES AT TIMES T	PRINTOUT VALUES AT TIMES T+DT/2	PRINTOUT VALUES AT TIMES T
A	head	g	X			
D	head	g	X			
W	head	rad/sec		X		
W HD	head	rad/sec				X
W SENS	sensor	rad/sec				X
C SIG	sensor	ips				X
C EST W	head	rad/sec				X
SF HD	head	g			X	
SF SENS	sensor	g			X	
O SIG	sensor	ips			X	
O EST SF	head	g			X	
DOWN HD	head	g			X	
RSCC	head	rad				X
ROTO	head	rad				X
RPOS	head	rad				X
WPARE	head	rad/sec				X
WPERP	head	rad/sec				X
WTOT	head	rad/sec				X
DNEW	head	g			X	
ACC	head	g			X	

A.3 Subroutine DOWN

Subroutine DOWN implements the logic for determining the perceived direction of gravity and the perceived angular velocity. Figures 3.7 and 3.8 illustrated this logic, and it was discussed in Chapter III. Table A.6 provides the list of variables used in the subroutine along with their definitions.

```
      SUBROUTINE DOWN(DOLD,WN,SN,SO,WSFO,T,DT,TDPS,
     1                DFAC,WOF,WNCO,WNL,FN)
C
C       DOWN ESTIMATOR AND W ESTIMATOR
C
C         DOWN IS DETERMINED BY RELYING ON LOW FREQUENCY
C         OTOLITH ESTIMATES, CANAL ESTIMATES WHICH ARE
C         CONSISTENT WITH HIGH FREQUENCY OTOLITH ESTIMATES,
C         AND HIGH FREQUENCY PORTION OF CANAL ESTIMATES
C         NOT CONFIRMED BY OTOLITHS.
C
C         W IS DETERMINED BY CANAL ESTIMATES PARALLEL TO
C         DOWN, ROTATION RATE OF DOWN, AND HIGH FREQUENCY
C         PORTION OF CANAL ESTIMATES PERPENDICULAR TO
C         DOWN MINUS ROTATION RATE OF DOWN.
C
      DIMENSION DOLD(3),WN(3),SN(3),SO(3),WSFO(3),F(3),
     1          WSF(3),X(3),WOF(3),RSCC(3),ROTO(3),RTOT(3),
     2          DNEW(3),RPOS(3),WPERP(3),DAVG(3),WPARE(3),
     3          WTOT(3),ACC(3),ANG(3),WOD(3),WODN(3),
     4          WNCO(3),WNL(3),FN(3),WNC(3),WNCH(3),HROTO(3)
C
C
      SFMAG=SQRT(SN(1)**2+SN(2)**2+SN(3)**2)
      FPOS=1.0-EXP(-((SFMAG/DFAC)**(.25))*DT/TDPS)
      TDVEL=T
      F(1)=EXP(-DT/TDVEL)
      F(2)=TDVEL*(1.-F(1))/DT-F(1)
      F(3)=1.-TDVEL*(1.-F(1))/DT
      CALL CROSS(SO,SN,WSF)
      CALL NORM(WSF,X)
      CALL VANG(SO,SN,ANGSF)
      DO 10 I=1,3
      WSF(I)=ANGSF*X(I)
      WOF(I)=F(1)*WOF(I)+F(2)*WSFO(I)+F(3)*WSF(I)
      WOD(I)=WSF(I)-WOF(I)
10    WSFO(I)=WSF(I)
      WODM=SQRT(WOD(1)**2+WOD(2)**2+WOD(3)**2)
      CALL NORM(WOD,WODN)
      WCPWD=WN(1)*WODN(1)+WN(2)*WODN(2)+WN(3)*WODN(3)
      IF(WCPWD) 12,12,11
11    WCPWD=0.0
12    WMAG=-WCPWD*DT
      DO 13 I=1,3
      X(I)=WODN(I)*AMIN1(WMAG,WODM)
      WNC(I)=-WN(I)*DT-X(I)
      WNL(I)=FN(1)*WNL(I)+FN(2)*WNCO(I)+FN(3)*WNC(I)
      WNCO(I)=WNC(I)
      WNCH(I)=WNC(I)-WNL(I)
13    X(I)=X(I)+WNCH(I)
      CALL CROSS(DOLD,SN,ROTO)
      CALL NORM(ROTO,F)
```

ORIGINAL PAGE IS
OF POOR QUALITY

```
      WOPARM=WOF(1)*F(1)+WOF(2)*F(2)+WOF(3)*F(3)
      DO 15 I=1,3
      ROTO(I)=WOPARM*F(I)
15    HROTO(I)=ROTO(I)/2.
      CALL ROTATE(DOLD,HROTO,F)
      WCPARM=X(1)*F(1)+X(2)*F(2)+X(3)*F(3)
      DO 20 I=1,3
      RSCC(I)=(X(I)-WCPARM*F(I))
20    RTOT(I)=RSCC(I)+ROTO(I)
      CALL ROTATE(DOLD,RTOT,DNEW)
      CALL VANG(DNEW,SN,FEE)
      PHI=FPOS*FEE
      CALL CROSS(DNEW,SN,RPOS)
      CALL NORM(RPOS,X)
      DO 30 I=1,3
30    RPOS(I)=PHI*X(I)
      CALL ROTATE(DNEW,RPOS,X)
      CALL NORM(X,DNEW)
      DO 40 I=1,3
40    X(I)=DOLD(I)+DNEW(I)
      CALL NORM(X,DAVG)
      WPARM=WN(1)*DAVG(1)+WN(2)*DAVG(2)+WN(3)*DAVG(3)
      CALL CROSS(DNEW,DOLD,WPERP)
      CALL NORM(WPERP,X)
      CALL VANG(DOLD,DNEW,PHI)
      DO 50 I=1,3
      WPERP(I)=X(I)*PHI/DT
      WPARE(I)=WPARM*DAVG(I)
      DOLD(I)=DNEW(I)
      SO(I)=SN(I)
      WTOT(I)=WPERP(I)+WPARE(I)
      ACC(I)=DFACTOMFW(I)-SN(I)
45    WRITE(32,100) RSCC(I),ROTO(I),RPOS(I),WPARE(I),WPERP(I),
     1              WTOT(I),DNEW(I),ACC(I)
50    CONTINUE
100   FORMAT('          ',8E12.5)
      RETURN
      END
STOP --
```

Table A.6 Variables used in subroutine DOWN

ACC	perceived acceleration vector
ANGSF	angle between SO and SN
DAVG(I)	unit vector in the direction of DOLD + DNEW
DFAC	steady-state gain of otolith estimate
DNEW(I)	current value of DOWN
DOLD(I)	old value of DOWN
DT	update interval for DOWN estimator
FEE	angle between DNEW and SN
FN(I)	constants for first-order filter
FPOS	$e^{-DT/TDPS}$
HROTO(I)	ROTO/2
PHI	FEE*FPOS
ROTO(I)	component of WOF perpendicular to SN and DOLD
RPOS(I)	rotation vector to eliminate integration errors
RSCC(I)	canal contribution to DOWN
RTOT(I)	RSCC+ROTO
SFMAG	specific force magnitude
SN(I)	current otolith specific force estimate
SO(I)	old otolith specific force estimate
T	=TDVEL
TDPS	time constant for DOWN position
TDVEL	time constant for DOWN angular velocity
WCPARM	magnitude of canal angular velocity estimate
WCPWD(I)	canal estimate parallel to high frequency angular velocity otolith estimate
WMAG	angular velocity magnitude
WN(I)	current canal estimate of angular velocity
WNC(I)	current canal estimate of angular velocity not confirmed by otolith estimate
WNCH(I)	high frequency portion of WNC
WNCO(I)	old WNC

Table A.6 concluded

WNL(I)	low frequency portion of WNC
WOD	WSF - WOF
WODM	magnitude of WOD
WOF(I)	low frequency portion of WSF
WOPARM	magnitude of otolith angular velocity estimate
WPARE(I)	canal angular velocity parallel to DNEW
WPARM(I)	canal angular velocity perpendicular to DNEW
WPERP(I)	system angular velocity perpendicular to DNEW
WSF(I)	angular velocity of otolith estimate
WSFO(I)	old WSF
WTOT(I)	WPARM + WPERP

ORIGINAL PAGE IS
OF POOR QUALITY

A.4 Subroutine library

The next listing contains the rest of the subroutines used by the model. They are mostly self-explanatory. Subroutines STMO and STMC are new routines designed to calculate state transition matrices for any given update interval. They implement the equations for the systems described in Tables A.7 and A.8.

```
      SUBROUTINE SVUPD(X,T,D,S,Y,C,N,M)
C
C      STATE VECTOR UPDATE:
C
C        X(NEW)=T*X(OLD + D*S
C        Y(NEW)=C*X(NEW)
C
C      WHERE
C        N IS DIMENSION OF STATE VECTOR
C        X IS STATE VECTOR
C        T IS TRANSITION MATRIX
C        D IS DRIVING VECTOR
C        S IS STIMULUS
C        Y IS OUTPUT (AFFERENT FIRING RATE)
C        C IS OUTPUT MATRIX
C
      DIMENSION X(N),T(N,N),D(N),C(M),R(9)
      DO 5 I=1,N
5     R(I)=X(I)
      DO 10 I=1,N
      X(I)=D(I)*S
      DO 10 J=1,N
10    X(I)=X(I)+T(I,J)*R(J)
      Y=C(M)*S
      DO 20 I=1,N
20    Y=Y+C(I)*X(I)
      RETURN
      END


      SUBROUTINE NORM(A,AN)
C
C      AN = UNIT VECTOR IN DIRECTION OF VECTOR A
C
      DIMENSION A(3),AN(3)
      AM=SQRT(A(1)**2+A(2)**2+A(3)**2)
      IF(AM-1.E-06) 5,5,6
5     AM=1.E-06
6     DO 10 I=1,3
10    AN(I)=A(I)/AM
      RETURN
      END


      SUBROUTINE SSKF(XH,Y,TM,C,GK,N)
C
C      STEADY-STATE KALMAN FILTER (UPDATE EVERY DT SECONDS)
C
C        XH(NEW) = TM*XH(OLD) + GK*(Y-C*TM*XH)
C
C      WHERE
C        XH IS STATE VECTOR ESTIMATE
```

ORIGINAL PAGE IS
OF POOR QUALITY

```
C          TM IS TRANSITION MATRIX
C          GK IS KALMAN GAIN MATRIX
C          Y IS SENSOR SYSTEM OUTPUT
C          C IS OUTPUT MATRIX
C
      DIMENSION XH(N),TM(N,N),C(N),GK(N),S(9)
      DO 40 I=1,N
      S(I)=0.0
      DO 40 J=1,N
40    S(I)=S(I)+TM(I,J)*XH(J)
      EM=0.0
      DO 45 I=1,N
45    EM=EM+S(I)*C(I)
      DO 50 J=1,N
50    XH(J)=S(J)+GK(J)*(Y-EM)
      RETURN
      END
```

```
      SUBROUTINE ROTATE(A,R,AR)
C
C       AR = A ROTATED ABOUT R BY AN ANGLE (RAD)
C            EQUAL TO THE MAGNITUDE OF R
C
      DIMENSION A(3),R(3),AR(3),AP(3),APN(3)
      CALL CROSS(R,A,AP)
      CALL NORM(AP,APN)
      AMAG=SQRT(A(1)**2+A(2)**2+A(3)**2)
      PHI=SQRT(R(1)**2+R(2)**2+R(3)**2)
      DO 10 I=1,3
10    AR(I)=AMAG*SIN(PHI)*APN(I)+COS(PHI)*A(I)
      RETURN
      END
```

```
      SUBROUTINE COTRN(A,B,N,C)
C
C       COORDINATE TRANSFORM:
C         FROM HEAD TO SENSOR IF N=0

C         FROM SENSOR TO HEAD IF N=1
C
C       A = ORIGINAL VECTOR
C       C = TRANSFORMED VECTOR
C       B = TRANSFORMATION MATRIX
C
```

```
      DIMENSION A(3),B(3,3),C(3)
      IF(N) 10,10,20
10    DO 15 I=1,3
15    C(I)=B(I,1)*A(1)+B(I,2)*A(2)+B(I,3)*A(3)
      GO TO 30
20    DO 25 I=1,3
25    C(I)=B(1,I)*A(1)+B(2,I)*A(2)+B(3,I)*A(3)
30    RETURN
      END
```

```
      SUBROUTINE VANG(A,B,PHI)
C
C      PHI = ANGLE BETWEEN A AND B
C
      DIMENSION A(3),B(3),AN(3),BN(3)
      CALL NORM(A,AN)
      CALL NORM(B,BN)
      X=AN(1)*BN(1)+AN(2)*BN(2)+AN(3)*BN(3)
      IF(X.GT.1.0) X=1.0
      Y=SQRT(1.-X**2)
      PHI=ATAN2(Y,X)
      RETURN
      END
```

```
      SUBROUTINE CROSS(A,B,C)
C
C      C = A X B
C
      DIMENSION A(3),B(3),C(3)
      C(1)=A(2)*B(3)-A(3)*B(2)
      C(2)=A(3)*B(1)-A(1)*B(3)
      C(3)=A(1)*B(2)-A(2)*B(1)
      RETURN
      END
```

```
      SUBROUTINE EULER(F,T,S,CT)
C
```

ORIGINAL PAGE IS
OF POOR QUALITY

```
C        PRODUCE DIRECTION COSINE MATRIX (CT) GIVEN
C        EULER ANGLES (F,T AND S).
C
       DIMENSION CT(3,3)
       CT(1,1)=COS(S)*COS(F)-COS(T)*SIN(F)*SIN(S)
       CT(2,1)=-(SIN(S)*COS(F)+COS(T)*SIN(F)*COS(S))
       CT(3,1)=SIN(T)*SIN(F)
       CT(1,2)=COS(S)*SIN(F)+COS(T)*COS(F)*SIN(S)
       CT(2,2)=COS(T)*COS(F)*COS(S)-SIN(S)*SIN(F)
       CT(3,2)=-SIN(T)*COS(F)
       CT(1,3)=SIN(T)*SIN(S)
       CT(2,3)=SIN(T)*COS(S)
       CT(3,3)=COS(T)
       DO 10 I=1,3
10     WRITE(22,100) CT(I,1),CT(I,2),CT(I,3)
100    FORMAT('   CT=',3E15.8)
       RETURN
       END
```

```
       SUBROUTINE STMO(DT,NITP,TPO,TO)
C
C        SUBROUTINE TO CALCULATE OTOLITH STATE
C        TRANSITION MATRICES
C          DT   - UPDATE INTERVAL FOR KALMAN FILTER
C          NITP - NUMBER OF SENSOR UPDATES PER DT
C          TPO  - 2X2 STM FOR OTOLITH SENSOR UPDATE
C          TO   - 3X3 STM FOR OTOLITH KALMAN FILTER SYSTEM
C
       DIMENSION TPO(2,2),TO(3,3)
C        CALCULATE TPO
       T=DT/NITP
       TPO(1,1)=(200.*EXP(-.2*T)-.2*EXP(-200.*T))/199.8
       TPO(2,1)=(EXP(-.2*T)-EXP(-200.*T))/199.8
       TPO(1,2)=40*(EXP(-200.*T)-EXP(-.2*T))/199.8
       TPO(2,2)=(200.*EXP(-200.*T)-.2*EXP(-.2*T))/199.8
C        CALCULATE TO
       T=DT
       TO(1,1)=(200.*EXP(-.2*T)-.2*EXP(-200.*T))/199.8
       TO(2,1)=(EXP(-.2*T)-EXP(-200.*T))/199.8
       TO(3,1)=(EXP(-200.*T))/39760.2+(EXP(-.2*T))/159.84
     1          -(EXP(-T))/159.2
       TO(1,2)=40*(EXP(-200.*T)-EXP(-.2*T))/199.8
       TO(2,2)=(200.*EXP(-200.*T)-.2*EXP(-.2*T))/199.8
       TO(3,2)=(EXP(-T))/159.2-(.2*EXP(-.2*T))/159.84
     1          -(200.*EXP(-200.*T))/39760.2
       TO(1,3)=0.0
       TO(2,3)=0.0
```

```
      TQ(3,3)=EXP(-T)
      RETURN
      END



      SUBROUTINE STMC(DT,NITP,TPC,TC)
C
C       SUBROUTINE TO CALCULATE SEMICIRCULAR CANAL
C       STATE TRANSITION MATRICES
C         DT   - UPDATE INTERVAL FOR KALMAN FILTER
C         NITP - NUMBER OF SENSOR UPDATES PER DT
C         TPC  - 3X3 STM FOR CANAL SENSOR UPDATE
C         TC   - 4X4 STM FOR CANAL KALMAN FILTER SYSTEM
C
      DIMENSION TC(4,4),TPC(3,3)
C       CALCULATE TPC
      T=DT/NITP
      TPC(1,1)=(.05576*EXP(-.03322*T)-.03322*EXP(-.05576*T))/.02254
      TPC(2,1)=-200.033*EXP(-.05576*T)/4.50674
     1          +200.05558*EXP(-.03322*T)/4.50725
     2          +.089*EXP(-199.9998*T)/39982.118
      TPC(3,1)=EXP(-199.9998*T)/39982.118+EXP(-.03322*T)/4.50725
     1          -EXP(-.05576*T)/4.50674
      TPC(1,2)=-.37037*(EXP(-199.9998*T)/39982.118+
     1          EXP(-.03322*T)/4.50725-EXP(-.05576*T)/4.50674)
      TPC(2,2)=2.47492*EXP(-.05576*T)-1.47448*EXP(-.03322*T)
     1          -.0004452*EXP(-199.9998*T)
      TPC(3,2)=.05576*EXP(-.05576*T)/4.50674
     1          -.03322*EXP(-.03322*T)/4.50725
     2          -199.9998*EXP(-199.9998*T)/39982.118
      TPC(1,3)=.37037*(.03322*EXP(-.03322*T)/4.50725
     1          +199.9998*EXP(-199.9998*T)/39982.118
     2          -.05576*EXP(-.05576*T)/4.50674)
      TPC(2,3)=-17.7966*(.03496*EXP(-.05576*T)/4.50674
     1          -.01242*EXP(-.03322*T)/4.50725
     2          -199.979*EXP(-199.9998*T)/39982.118)
      TPC(3,3)=1.000445*EXP(-199.9998*T)+.00024484*EXP(-.03322*T)
     1          -.0006899*EXP(-.05576*T)
C       CALCULATE TC
      T=DT
      TC(1,1)=(.05576*EXP(-.03322*T)-.03322*EXP(-.05576*T))/.02254
      TC(2,1)=-200.033*EXP(-.05576*T)/4.50674
     1         +200.05558*EXP(-.03322*T)/4.50725
     2         +.089*EXP(-199.9998*T)/39982.118
      TC(3,1)=EXP(-199.9998*T)/39982.118+EXP(-.03322*T)/4.50725
     1         -EXP(-.05576*T)/4.50674
      TC(4,1)=EXP(-5.*T)/4788.6+EXP(-.03322*T)/22.3865
     1         -EXP(-199.9998*T)/7796506.55-EXP(-.05576*T)/22.2824
      TC(1,2)=-.37037*(EXP(-199.9998*T)/39982.118+EXP(-.03322*T)/4.5072
     1         -EXP(-.05576*T)/4.50674)
```

ORIGINAL PAGE IS
OF POOR QUALITY

```
      TC(2,2)=2.47492*EXP(-.05576*T)-1.47448*EXP(-.03322*T)
     1        -.0004452*EXP(-199.9998*T)
      TC(3,2)=.05576*EXP(-.05576*T)/4.50674
     1        -.03322*EXP(-.03322*T)/4.50725
     2        -199.9998*EXP(-199.9998*T)/39982.118
      TC(4,2)=.05576*EXP(-.05576*T)/22.2824+
     1        +199.9998*EXP(-199.9998*T)/7796506.55-5.*EXP(-5.*T)/4788.
     2        -.03322*EXP(-.03322*T)/22.3865
      TC(1,3)=.37037*(.03322*EXP(-.03322*T)/4.50725
     1        +199.9998*EXP(-199.9998*T)/39982.118
     2        -.05576*EXP(-.05576*T)/4.50674)
      TC(2,3)=-17.7966*(.03496*EXP(-.05576*T)/4.50674
     1        -.01242*EXP(-.03322*T)/4.50725
     2        -199.9998*EXP(-199.9998*T)/39982.118)
      TC(3,3)=1.000445*EXP(-199.9998*T)+.00024484*EXP(-.03322*T)
     1        -.0006899*EXP(-.05576*T)
      TC(4,3)=25.*EXP(-5.*T)/4788.6+.001104*EXP(-.03322*T)/22.3865
     1        -.00311*EXP(-.05576*T)/22.2824
     2        -39999.92*EXP(-199.9998*T)/7796506.55
      TC(1,4)=0.0
      TC(2,4)=0.0
      TC(3,4)=0.0
      TC(4,4)=EXP(-5.*T)
      RETURN
      END
STOP --
```

Table A.7 Otolith state equations

SENSOR UPDATE

$$\dot{x} = Ax + Bf$$
$$y = Cx + SFR + n$$

where

$$A = \begin{bmatrix} 0 & 0 \\ -40. & -200.2 \end{bmatrix} \quad B = \begin{bmatrix} 0 \\ 1 \end{bmatrix} \quad C = \begin{bmatrix} 1800 & 18000 \end{bmatrix}$$

$$\Phi = \left[sI - A\right]^{-1} = \frac{1}{(s+200)(s+.2)} \begin{bmatrix} s+200.2 & -1 \\ 40 & s \end{bmatrix}$$

KALMAN FILTER UPDATE

$$\dot{x} = Ax + Bf$$
$$y = Cx + SFR + n$$

where

$$A = \begin{bmatrix} 0 & 1 & 0 \\ -40. & -200.2 & 1 \\ 0 & 0 & -1 \end{bmatrix} \quad B = \begin{bmatrix} 0 \\ 0 \\ 1 \end{bmatrix}$$

$$C = \begin{bmatrix} 1800 & 18000 & 0 \end{bmatrix}$$

$$\Phi = \left[sI - A\right]^{-1} = \frac{1}{(s+1)(s+200)(s+.2)} \times$$

$$\begin{bmatrix} (s+1)(s+200.2) & -(s+1) & 1 \\ 40(s+1) & s(s+1) & -s \\ 0 & 0 & (s+200)(s+.2) \end{bmatrix}$$

ORIGINAL PAGE IS
OF POOR QUALITY

Table A.8 Canal state equations

SENSOR UPDATE

$$\dot{x} = Ax + B\omega$$
$$y = Cx + SFR + n$$

where

$$A = \begin{bmatrix} 0 & 1 & 0 \\ 0 & 0 & 1 \\ -.37037 & -.17.7966 & -200.0888 \end{bmatrix} \qquad B = \begin{bmatrix} 0 \\ 0 \\ 1 \end{bmatrix}$$

$$C = \begin{bmatrix} -23.5785 & -1131.89 & -6371.86 \end{bmatrix}$$

$$\Phi = [sI - A]^{-1} = \frac{1}{(s+199.9998)(s+.03322)(s+.05576)} \times$$

$$\begin{bmatrix} (s+199.9998)(s+.08898) & -(s+200.0888) & 1 \\ -.37037 & s(s+200.0888) & -s \\ .37037s & -17.7966(s+.0208) & s^2 \end{bmatrix}$$

KALMAN FILTER UPDATE

$$\dot{x} = Ax + B\omega$$
$$y = Cx + SFR + n$$

where

$$A = \begin{bmatrix} 0 & 1 & 0 & 0 \\ 0 & 0 & 1 & 0 \\ -.37037 & -17.7966 & -200.0888 & 1 \\ 0 & 0 & 0 & -5 \end{bmatrix} \qquad B = \begin{bmatrix} 0 \\ 0 \\ 0 \\ 1 \end{bmatrix}$$

Table A.8 concluded

$$C = \begin{bmatrix} -23.5785 & -1131.89 & -6371.86 & 63.6620 \end{bmatrix}$$

$$\Phi = \left[sI - A\right]^{-1} = \frac{1}{(s+5)(s+199.9998)(s+.03322)(s+.05576)} \times$$

$$\begin{bmatrix} (s+5)(s+199.9998)(s+.08898) & -(s+200.0888)(s+5) & (s+5) & -1 \\ -.37037(s+5) & s(s+5)(s+200.0888) & -s(s+5) & s \\ .37037s(s+5) & -17.7966(s+5)(s+.0208) & s^2(s+5) & -s^2 \\ 0 & 0 & 0 & (s+199.9998)(s+.03322)(s+.05576) \end{bmatrix}$$

ORIGINAL PAGE IS
OF POOR QUALITY

A.5 Kalman gains subroutine

The next listing is a program which calculates Kalman gains for the otolith system. This program calculates only the utricle gains - remember that the saccule gains are twice those of the utricle. This iterative routine makes the following calculations until the Kalman gains reach a steady state:

1. Calculate state estimate.
2. Calculate propagated error covariance.
3. Update state estimate.
4. Update error covariance.
5. Calculate error covariance.

Once steady state gains are obtained (in this case, after 240 iterations), they must be tested in the main program for a known input-output case. This is for the purpose of tuning the model. The following iterative procedure is used:

1. Run main program with Ormsby update intervals of .1 and 1.0 seconds for a known input-output case (for example, a constant yaw acceleration of 1.5°/second for 120 seconds, then a sustained yaw rate of 180°/second for 120 seconds). Plot WTOT for this case.
2. Calculate new Kalman gains for the desired intervals.
3. Run main program with same stimulus for new gains. Plot WTOT.
4. If the plots do not match, vary the input variance,

measurement noise variance and input power (QU, QM and D) to calculate new gains.

5. Continue this process until the WTOT plots are similar.

Note that the gains are changed for the otoliths only. This was done for simplicity, since the Kalman filters for the canals do not change the afferent firing rates appreciably.

Table A.9 lists the variables used in the Kalman gains routine and their definitions.

ORIGINAL PAGE IS
OF POOR QUALITY

```
C          CALCULATES KALMAN GAINS FOR OTOLITH SYSTEM
C
      DIMENSION  PX(3,3),PP(3,3),TM(3,3),TH(9),C(3),GK(3),S(3,3),TT(9)
      DATA  C  /0.18000000E+04,0.18000000E+05,0.00000000E+00/
      DATA  PX /0.10000000E-01,0.00000000E+00,0.00000000E+00,
     1           0.00000000E+00,0.10000000E-01,0.00000000E+00,
     2           0.00000000E+00,0.00000000E+00,0.10000000E-01/
      DATA  D  /.22500000E+00/
      DATA  QU /0.400/
      DATA  QM /12.8000000/
      DATA  DT /.250000000/
      DATA NIT /240/
C
      CALL ASSIGN(30,'DK1:KALMAN.OTO')
C
C          CALCULATE TRANSITION AND COVARIANCE
C          MATRICES
C
      CALL STMO(DT,TM)
      WRITE(30,2) ((TM(I,J),I=1,3),J=1,3)
2     FORMAT(' TRANSITION MATRIX ',3E14.7/19X,3E14.7/19X,3E14.7)
      CALL ICMO(DT,TT)
      DO 3 JTH=1,9
3     TH(JTH)=TT(JTH)*QU*D**2
      WRITE(30,4) (TH(I),I=1,9)
4     FORMAT(' COVARIANCE MATRIX ',3E14.7/19X,3E14.7/19X,3E14.7)
C
      T=0.0
      DO 85 M=1,NIT
C
C          CALCULATION OF S=PX*TM TRANSPOSE
C
      T=M*DT
      DO 10 I=1,3
      DO 10 J=1,3
      S(I,J)=0.0
      DO 5 K=1,3
5     S(I,J)=S(I,J)+PX(I,K)*TM(J,K)
10    CONTINUE
C
C          CALCULATION OF PROPAGATED ERROR COVARIANCE MATRIX
C          PP=TM*S+TH
C
      IC=0
      DO 20 I=1,3
      DO 20 J=1,3
      IF(I.GT.J) GO TO 20
      IC=IC+1
      IF(IC.EQ.7) GO TO 22
      PP(I,J)=TH(IC)
      DO 15 K=1,3
15    PP(I,J)=PP(I,J)+TM(I,K)*S(K,J)
```

```
20      PP(J,I)=PP(I,J)
C
C          CALCULATION OF S(1,1)=(C*PP*C+QM)
C
22      S(1,1)=QM**2
        DO 25 I=1,3
        S(I,2)=PP(I,1)*C(1)+PP(I,2)*C(2)+PP(I,3)*C(3)
25      S(1,1)=S(1,1)+C(I)*S(I,2)
C
C          CALCULATION OF KALMAN GAINS GK=PP*C/S(1,1)
C
        DO 30 I=1,3
30      GK(I)=S(I,2)/S(1,1)
C
C          CALCULATION OF S(I,J)=(I=GK*C)
C
        DO 45 I=1,3
        DO 45 J=1,3
45      S(I,J)=-GK(I)*C(J)
        DO 50 I=1,3
50      S(I,I)=S(I,I)+1.
C
C          CALCULATION OF NEW ERROR COVARIANCE MATRIX
C          PX=S*PP
C
        DO 60 I=1,3
        DO 60 J=1,3
        PX(I,J)=0.0
        DO 55 K=1,3
55      PX(I,J)=S(I,K)*PP(K,J)+PX(I,J)
60      PX(J,I)=PX(I,J)
C
        WRITE(30,70) T,M,GK(1),GK(2),GK(3)
70      FORMAT(' TIME=',F7.2,'  ITERATION NUMBER=',
     1          I3,'  KALMAN GAINS=',3E14.7)
        WRITE(30,75) PX(1,1),PX(1,2),PX(1,3),PX(2,2),PX(2,3),PX(3,3)
75      FORMAT(6E14.7)
85      CONTINUE
        STOP
        END
STOP --
```

ORIGINAL PAGE IS
OF POOR QUALITY

Table A.9 Variables used in Kalman gains programs

C(I)	C matrix (see Table A.7)
D	input power
DT	update interval
GK(I)	Kalman gains
NIT	number of iterations
PP(I,J)	propagated error covariance matrix
PX(I,J)	system covariance matrix
QM	variance of measurement noise
QU	power of input noise
TH(I,J)	$TT*QU*D^2$
TM(I,J)	state transition matrix
TT(I,J)	input covariance matrix

A.6 Kalman gains subroutine library

The last listing is that of the subroutines called by the Kalman gain program. Subroutines STMO and STMC were described in section A.4. Subroutine ICMO calculates the otolith input covariance matrix used by the Kalman gains routine. It implements the following equation:

$$\underline{\Phi}_I = \int_0^{DT} \underline{\Phi}\ \underline{B}\ Q^2\ \underline{B}^T\ \underline{\Phi}^T\ dt$$

where

$\underline{\Phi}_I$ = input covariance matrix

$\underline{\Phi}$ = otolith state transition matrix (see Table A.7)

$\underline{B}$ = otolith B matrix (see Table A.7)

Q = variance of measurement noise

The variables used in these subroutines are defined in the listing.

ORIGINAL PAGE IS
OF POOR QUALITY

```
      SUBROUTINE STMO(DT,TO)
C
C       SUBROUTINE TO CALCULATE OTOLITH STATE
C       TRANSITION MATRICES
C         DT   - UPDATE INTERVAL FOR KALMAN FILTER
C         TO   - 3X3 STM FOR OTOLITH KALMAN FILTER SYSTEM
C
      DIMENSION TO(3,3)
C       CALCULATE TO
      T=DT
      TO(1,1)=(200.*EXP(-.2*T)-.2*EXP(-200.*T))/199.8
      TO(2,1)=(EXP(-.2*T)-EXP(-200.*T))/199.8
      TO(3,1)=(EXP(-200.*T))/39760.2+(EXP(-.2*T))/159.84
     1          -(EXP(-T))/159.2
      TO(1,2)=40*(EXP(-200.*T)-EXP(-.2*T))/199.8
      TO(2,2)=(200.*EXP(-200.*T)-.2*EXP(-.2*T))/199.8
      TO(3,2)=(EXP(-T))/159.2-(.2*EXP(-.2*T))/159.84
     1          -(200.*EXP(-200.*T))/39760.2
      TO(1,3)=0.0
      TO(2,3)=0.0
      TO(3,3)=EXP(-T)
      RETURN
      END



      SUBROUTINE STMC(DT,TC)
C
C       SUBROUTINE TO CALCULATE SEMICIRCULAR CANAL
C       STATE TRANSITION MATRICES
C         DT   - UPDATE INTERVAL FOR KALMAN FILTER
C         TC   - 4X4 STM FOR CANAL KALMAN FILTER SYSTEM
C
      DIMENSION TC(4,4)
C       CALCULATE TC
      T=DT
      TC(1,1)=(.05576*EXP(-.03322*T)-.03322*EXP(-.05576*T))/.02254
      TC(2,1)=-200.033*EXP(-.05576*T)/4.50674
     1          +200.05558*EXP(-.03322*T)/4.50725
     2          +.089*EXP(-199.9998*T)/39982.118
      TC(3,1)=EXP(-199.9998*T)/39982.118+EXP(-.03322*T)/4.50725
     1          -EXP(-.05576*T)/4.50674
      TC(4,1)=EXP(-5.*T)/4788.6+EXP(-.03322*T)/22.3865
     1          -EXP(-199.9998*T)/7796506.55-EXP(-.05576*T)/22.[illegible]
      TC(1,2)=-.37037*(EXP(-199.9998*T)/39982.118+EXP(-.03322*T)/4.5072
     1          -EXP(-.05576*T)/4.50674)
      TC(2,2)=2.47492*EXP(-.05576*T)-1.47448*EXP(-.03322*T)
     1          -.0004452*EXP(-199.9998*T)
      TC(3,2)=.05576*EXP(-.05576*T)/4.50674
     1          -.03322*EXP(-.03322*T)/4.50725
```

ORIGINAL PAGE IS
OF POOR QUALITY

```
2          -199.9998*EXP(-199.9998*T)/39982.118
  TC(4,2)=.05576*EXP(-.05576*T)/22.2824+
1          +199.9998*EXP(-199.9998*T)/7796506.55-5.*EXP(-5.*T)/4788.6
2          -.03322*EXP(-.03322*T)/22.3865
  TC(1,3)=.37037*(.03422*EXP(-.03322*T)/4.50725
1          +199.9998*EXP(-199.9998*T)/39982.118
2          -.05576*EXP(-.05576*T)/4.50674)
  TC(2,3)=-17.7966*(.03496*EXP(-.05576*T)/4.50674
1          -.01242*EXP(-.03322*T)/4.50725
2          -199.9998*EXP(-199.9998*T)/39982.118)
  TC(3,3)=1.000445*EXP(-199.9998*T)+.00024484*EXP(-.03322*T)
1          -.0006899*EXP(-.05576*T)
  TC(4,3)=25.*EXP(-5.*T)/4788.6+.001104*EXP(-.03322*T)/22.3865
1          -.00311*EXP(-.05576*T)/22.2824
2          -39999.92*EXP(-199.9998*T)/7796506.55
  TC(1,4)=0.0
  TC(2,4)=0.0
  TC(3,4)=0.0
  TC(4,4)=EXP(-5.*T)
  RETURN
  END
```

```
      SUBROUTINE ICMO(DT,TT)
C
C       SUBROUTINE TO CALCULATE OTOLITH INPUT
C       COVARIANCE MATRIX
C
C         DT  -  UPDATE INTERVAL FOR KALMAN FILTERS
C         TT  -  INPUT COVARIANCE MATRIX
C
      DIMENSION TT(9)
      T=DT
      TT(1)=-EXP(-.4*T)*9.7851953E-05 + EXP(-1.2*T)*6.5496806E-05
     1      -EXP(-2.0*T)*1.9728037E-05 + 5.2083184E-05
      TT(2)=-EXP(-1.2*T)*3.9098089E-05 + EXP(-.4*T)*1.9570367E-05
     1      +EXP(-2.0*T)*1.9728037E-05 - .0000315E-05
      TT(3)=-EXP(-1.2*T)*5.0135460E-03 + EXP(-2.0*T)*3.1407035E-03
     1      +2.0728433OE-03
      TT(4)=-EXP(-2.0*T)*1.9728037E-05 + EXP(-1.2*T)*1.3099363E-05
     1      -EXP(-.4*T)*3.9140735E-06 + 1.0542747 5E-05
      TT(5)=-EXP(-2.0*T)*3.1407035E-03 + EXP(-1.2*T)*1.0427093E-03
     1      +2.0979942E-03
      TT(6)=-EXP(-2.0*T)*3.1407035E-03 + 1.5
      TT(7)=0.0
      TT(8)=0.0
      TT(9)=0.0
```

ORIGINAL PAGE IS
OF POOR QUALITY

```
                RETURN
                END

STOP --.
```

REFERENCES

1. Ashworth, B.K., and Parrish, R.V., "A visual motion simulator for general aviation compensated with the nonlinear adaptive washout for actuator lag," AIAA Paper Number 76-022, Dayton, Ohio, April 1976.

2. Berthoz, A., Pavard, B., and Young, L.R., "Perception of linear horizontal self-motion induced by peripheral vision (linearvection): Basic characteristics and visual-vestibular interactions," Experimental Brain Research, 23:471-489, 1975.

3. Borah, J.D., Human Dynamic Orientation Model Applied to Motion Simulation, M.S. Thesis, Department of Aeronautics and Astronautics, Massachusetts Institute of Technology, 1976.

4. Gelb, A. (editor), Applied Optimal Estimation, Cambridge: M.I.T. Press, 1974.

5. Held, R., Dichgans, J., and Bauer, J., "Characteristics of moving visual scenes influencing spatial orientation," Vision Research, 15:357-365, 1975.

6. Howard, I.P. and Templeton, W.B., Human Spatial Orientation, New York: John Wiley and Sons, 1966.

7. Jex, H.R., et al, "Effects of simulated surface-effect ship motions on crew habitability," 13th Annual Conference on Manual Control, Cambridge, June 1977.

8. Kalman, R.E. and Bucy, R.S., "New results in linear filtering and prediction theory," Transactions of the American Society of Mechanical Engineers, Journal of Basic Engineering, 83, 1961.

9. Meiry, J.L., The Vestibular System and Human Dynamic Orientation, Sc.D. Thesis, Department of Aeronautics and Astronautics, Massachusetts Institute of Technology, 1965.

10. Ormsby, C.C., Model of Human Dynamic Orientation, Ph.D. Thesis, Department of Aeronautics and Astronautics, Massachusetts Institute of Technology, 1974.

11. Parrish, R.V., Dieudonne, J.E., Martin, D.J., Jr., and Bowles, R.L., "Coordinated adaptive filters for motion simulation," AIAA Paper Number 73-930, Palo Alto, California, September 1973.

12. Parrish, R.V., Dieudonne, J.E. and Martin, D.J., Jr., "Motion software for a synergystic six-degree-of-freedom motion base," NASA TN D-7350, 1973.

13. Parrish, R.V. and Martin, D.J., Jr., "Empirical comparison of a linear and a nonlinear washout for motion

simulators," AIAA Paper Number 75-106, Pasadena, California, January 1975.

14. Parrish, R.V. and Martin, D.J., Jr., "Evaluation of a linear washout for simulating motion cue presentation during landing approach," NASA TN D-8036, 1975.

15. Peters, R.A., "Dynamics of the vestibular system and their relation to motion perception, spatial disorientation and illusions," Systems Technology, Inc., Technical Report Number 168-1, 1968.

16. Schmidt, S.F. and Conrad, B., "Motion drive signals for piloted flight simulators," NASA CR-1601, 1970.

17. Schmidt, S.F. and Conrad, B., "A study of techniques for calculating motion drive signals for flight simulators," Contract NAS2-5816, Analytical Mechanics Associates, Inc., July 1971 (Available as NASA CR-114345).

18. Sinacori, J.B., "A practical approach to motion simulation," AIAA Paper Number 73-931, AIAA Visual and Motion Conference, Palo Alto, California, September 1973.

19. Young, L.R., "Role of the Vestibular System in Posture and Movement," In: Medical Physiology, V.B. Mountcastle (Editor), 13th Edition, Volume I, Chapter 27, St. Louis; C.V. Mosbey and Co., 1974.

20. Young, L.R. and Meiry, J., "A revised dynamic otolith model," Aerospace Medicine, 39:606-608, 1969.